

Introduction to Fluid Mechanics for Groundwater Scientists

Harald Klammmler

Introduction to Fluid Mechanics for Groundwater Scientists

*The Groundwater Project
Guelph, Ontario, Canada
Version 2, November, 2023*

Please Consider Donating

The GW-Project relies on private funding for book production
and management of the Project.

Please consider [making a donation to the Groundwater Project](#) ↗
so books will continue to be freely available.

Harald Klammler

*Visiting Professor
Institute of Geosciences
Federal University of Bahia
Salvador, Bahia, Brazil*

*Introduction to
Fluid Mechanics for
Groundwater Scientists*

*The Groundwater Project
Guelph, Ontario, Canada*

All rights reserved. This publication is protected by copyright. No part of this book may be reproduced in any form or by any means without permission in writing from the authors (to request permission contact: permissions@gw-project.org). Commercial distribution and reproduction are strictly prohibited.

Groundwater Project (the GW-Project) works are copyrighted and can be downloaded for free from gw-project.org. Anyone may use and share gw-project.org links to download the GW-Project's work. It is not permissible to make GW-Project documents available on other websites nor to send copies of the documents directly to others. Kindly honor this source of free knowledge that benefits you and all those who want to learn about groundwater.

Copyright © 2023 Harald Klammler (The Author)

Published by The Groundwater Project, Guelph, Ontario, Canada, 2023.

Klammler, Harald.

Introduction to Fluid Mechanics for Groundwater Scientists / Harald Klammler - Guelph, Ontario, Canada, 2023.

130 pages

ISBN: 978-1-77470-056-3

DOI: <https://doi.org/10.21083/GXAT7083>.

Please consider signing up to the GW-Project mailing list and stay informed about new book releases, events, and ways to participate in the GW-Project. When you sign up to our email list it helps us build a global groundwater community. [Sign up](#).

APA 7th Edition Citation:

Klammler, H. (2023). *Introduction to fluid mechanics for groundwater scientists*. The Groundwater Project. <https://doi.org/10.21083/GXAT7083>.



Domain Editors: Eileen Poeter and John Cherry.

Board: John Cherry, Shafick Adams, Richard Jackson, Ineke Kalwij, Renée Martin-Nagle, Everton de Oliveira, Marco Petitta, and Eileen Poeter.

Cover Image: The Groundwater Project Original, 2023.

Dedication

To all friends, family, and beautiful nature.

Table of Contents

DEDICATION	V
TABLE OF CONTENTS	VI
THE GROUNDWATER PROJECT FOREWORD	VIII
FOREWORD	IX
PREFACE	X
ACKNOWLEDGMENTS	XI
1 INTRODUCTION	1
2 STRAIGHT MOVEMENT OF A RIGID BODY	4
2.1 LOCATION, VELOCITY, AND ACCELERATION	4
2.2 NEWTON'S SECOND LAW OF MOTION, MOMENTUM, AND KINETIC ENERGY	4
2.3 COULOMB FRICTION AND DRAG FORCES.....	6
3 VISCOUS FLOW AND STOKES EQUATION	13
3.1 NEWTONIAN FLUIDS, VISCOSITY, AND STOKES DRAG.....	13
3.2 FLOW BETWEEN TWO PLATES – PLANAR POISEUILLE FLOW	15
3.3 FLOW THROUGH A CIRCULAR PIPE – CYLINDRICAL POISEUILLE FLOW	20
4 INVISCID FLOW AND EULER'S EQUATION	24
5 NAVIER-STOKES EQUATION AND REYNOLDS NUMBER	27
6 FLOW THROUGH POROUS MEDIA AND DARCY'S LAW	31
6.1 NEGLIGIBLE INERTIA AND CONTINUUM PERSPECTIVE	31
6.2 HYDRAULIC HEAD AS DRIVING FORCE POTENTIAL	36
6.3 HYDRAULIC HEAD AS FLUX POTENTIAL	38
6.4 ANISOTROPY	39
7 CONSERVATION OF MASS AND FLOW EQUATIONS	42
8 INITIAL AND BOUNDARY CONDITIONS	49
9 WRAP-UP	52
10 EXERCISES	55
EXERCISE 1 - ACCELERATING BOAT AND RESPONSE-TIME SCALES	55
EXERCISE 2 - STOKES FRICTION AND TERMINAL VELOCITY OF A SINKING SPHERE	56
EXERCISE 3 - IMPLEMENTING THE EULER FORWARD METHOD	56
EXERCISE 4 - EFFECTIVE HYDRAULIC CONDUCTIVITY OF A PIPE AND A FRACTURE	56
EXERCISE 5 - EFFECTIVE HYDRAULIC CONDUCTIVITY OF LAYERED MEDIA.....	57
EXERCISE 6 - FRESHWATER-SALTWATER INTERACTION AND GHYBEN-HERZBERG PRINCIPLE	58
EXERCISE 7 - CONSTANT HEAD <i>K</i> TESTS AND SEEPAGE FORCE	59
EXERCISE 8 - LIQUEFACTION AND QUICKSAND FORMATION.....	60
EXERCISE 9 - UNCONFINED AQUIFER AND DROUGHT	61
EXERCISE 10 - A DYNAMIC AQUIFER MODEL	62
EXERCISE 11 - REDUCED-ORDER AQUIFER MODELS	63
EXERCISE 12 - FALLING HEAD <i>K</i> TEST.....	65
EXERCISE 13 - SLUG TESTS	66
EXERCISE 14 - OSCILLATORY SLUG TEST AND WELL FRICTION.....	68
11 BOXES	72
BOX 1 - ORDER-OF-MAGNITUDE ANALYSIS.....	72

BOX 2 - A SIMPLE NUMERICAL SOLUTION METHOD	74
BOX 3 - EFFECTIVE STRESS, SEEPAGE FORCE AND QUICKSAND FORMATION.....	76
BOX 4 - ANISOTROPY AND NOTATIONAL CONVENTIONS	81
BOX 5 - THE RADIAL FLOW PROBLEM.....	84
BOX 6 - THE WATER TABLE RATIO	87
BOX 7 - UNSATURATED FLOW AND RICHARDS EQUATION.....	89
BOX 8 - MULTI-PHASE FLOW.....	93
11 EXERCISE SOLUTIONS	95
SOLUTION EXERCISE 1 - ACCELERATING BOAT AND RESPONSE-TIME SCALES	95
SOLUTION EXERCISE 2 - STOKES FRICTION AND TERMINAL VELOCITY OF A SINKING SPHERE	97
SOLUTION EXERCISE 3 - IMPLEMENTING THE EULER FORWARD METHOD.....	98
SOLUTION EXERCISE 4 - EFFECTIVE HYDRAULIC CONDUCTIVITY OF A FRACTURE AND A PIPE.....	99
SOLUTION EXERCISE 5 - EFFECTIVE HYDRAULIC CONDUCTIVITY OF LAYERED MEDIA	101
SOLUTION EXERCISE 6 - FRESHWATER-SALTWATER INTERACTION AND GHYBEN-HERZBERG PRINCIPLE	103
SOLUTION EXERCISE 7 - CONSTANT HEAD <i>K</i> TESTS AND SEEPAGE FORCE	105
SOLUTION EXERCISE 8 - LIQUEFACTION AND QUICKSAND FORMATION	106
SOLUTION EXERCISE 9 - UNCONFINED AQUIFER AND DROUGHT.....	107
SOLUTION EXERCISE 10 - A DYNAMIC AQUIFER MODEL.....	109
SOLUTION EXERCISE 11 - REDUCED-ORDER AQUIFER MODELS.....	113
SOLUTION EXERCISE 12 - FALLING HEAD <i>K</i> TEST	115
SOLUTION EXERCISE 13 - SLUG TESTS.....	117
SOLUTION EXERCISE 14 - OSCILLATORY SLUG TEST AND WELL FRICTION	119
12 REFERENCES	123
13 BASIC NOTATIONS.....	126
14 ABOUT THE AUTHOR	129
MODIFICATIONS TO ORIGINAL RELEASE	A

The Groundwater Project Foreword

At the United Nations (UN) Water Summit held on December 2022, delegates agreed that statements from all major groundwater-related events will be unified in 2023 into one comprehensive groundwater message. This message will be released at the UN 2023 Water Conference, a landmark event that will bring attention at the highest international level to the importance of groundwater for the future of humanity and ecosystems. This message will bring clarity to groundwater issues to advance understanding globally of the challenges faced and actions needed to resolve the world's groundwater problems. Groundwater education is key.

The 2023 World Water Day theme *Accelerating Change* is in sync with the goal of the Groundwater Project (GW-Project). The GW-Project is a registered Canadian charity founded in 2018 and committed to the advancement of groundwater education as a means to accelerate action related to our essential groundwater resources. To this end, we create and disseminate knowledge through a unique approach: the democratization of groundwater knowledge. We act on this principle through our website gw-project.org/, a global platform, based on the principle that

“Knowledge should be free, and the best knowledge should be free knowledge.” Anonymous

The mission of the GW-Project is to promote groundwater learning across the globe. This is accomplished by providing accessible, engaging, and high-quality educational materials—free-of-charge online and in many languages—to all who want to learn about groundwater. In short, the GW-Project provides essential knowledge and tools needed to develop groundwater sustainably for the future of humanity and ecosystems. This new type of global educational endeavor is made possible through the contributions of a dedicated international group of volunteer professionals from diverse disciplines. Academics, consultants, and retirees contribute by writing and/or reviewing the books aimed at diverse levels of readers from children to high school, undergraduate and graduate students, or professionals in the groundwater field. More than 1,000 dedicated volunteers from 127 countries and six continents are involved—and participation is growing.

Hundreds of books will be published online over the coming years, first in English and then in other languages. An important tenet of GW-Project books is a strong emphasis on visualization; with clear illustrations to stimulate spatial and critical thinking. In future, the publications will also include videos and other dynamic learning tools. Revised editions of the books are published from time to time. Users are invited to propose revisions.

We thank you for being part of the GW-Project Community. We hope to hear from you about your experience with the project materials, and welcome ideas and volunteers!

The GW-Project Board of Directors

January 2023

Foreword

This book, *Introduction to Fluid Mechanics for Groundwater Scientists*, focuses on the physical mechanisms of groundwater movement. It bridges between 1) what is well known to groundwater scientists as Darcy's empirical law, which is the equation Henry Darcy identified in 1854 from his laboratory experiments using natural granular materials; and 2) the fundamental physics of water in motion as a liquid continuum (known as fluid mechanics) established prior to Darcy's work. The basic concepts needed to establish the theoretical basis for Darcy's empirically developed law preceded its development. The mathematical principles required for its theoretical development lie in the fundamental Navier-Stokes equations that are based on calculus and partial differential equations. The Navier-Stokes equations were developed over a few decades, from 1822 (engineer Claude-Louis Navier, France) to 1850 (physicist George Gabriel Stokes, Ireland). These equations pertain to what are known as Newtonian fluids that are defined using the earliest considerations of fluid physics by Issac Newton in his *Principia Mathematica* (1687). Newton's laws of motion and viscosity underpin the Navier-Stokes equations to provide the theoretical basis for Darcy's law. This theoretical explanation of Darcy's law, beyond the narrow range of the experimental conditions, is why Darcy's empirical equation deserves to be referred to as a 'law' in groundwater science. This book goes well beyond the bridging of Darcy's law to basic physics in that it shows how the basic mathematics are used to develop equations that address many types of practical problems in groundwater hydraulics. Other Groundwater Project books expand on the application of these equations.

The need to understand the introductory level university calculus and partial differential equations in this book will prevent some readers from following the details, however many schematic figures present the basic fluid mechanics, providing valuable visual impressions of the subject matter. Nearly all students in engineering and some in the earth and environmental sciences take courses in calculus and differential equations that are needed to follow the details in this book, however it is rare that the subject matter in the mathematics courses pertains to groundwater. This book offers an opportunity to appreciate how physics and mathematics provide a deeper understanding of groundwater science. In brief, this book reveals the intrinsic scientific beauty in bridging between the empirical and fundamental relations that underpin the functioning of Planet Earth.

The author of this book, Dr. Harald Klammler is a Visiting Professor at the Institute of Geosciences, Federal University of Bahia Salvador, Bahia, Brazil. He has degrees in civil engineering and is the co-author of many papers in which he provides the theoretical basis for empirical relations that are of practical importance.

John Cherry, The Groundwater Project Leader
Guelph, Ontario, Canada, October 2023

Preface

The fundamentals of fluid mechanics are nowadays barely offered as course material to students interested in the field of groundwater science. Instead, one of the fundamental relationships, namely Darcy's law, is most often introduced as a given empirical relationship for computing groundwater fluxes or discharges.

To help overcome this deficiency, [The Groundwater Project \(GW-Project\)](#)[↗] suggested the present book. Upon completing this text, the reader should be able to 1) explain Darcy's law based on forces using Newton's laws of motion and viscosity, 2) understand interconnections among other topics in groundwater science, which are treated more thoroughly in other GW-Project publications, and 3) be able to apply non-dimensionalization and (time) scale analysis across physically different problems.

This book is intended for undergraduate and graduate students as well as professionals in the field of groundwater science and related areas dealing with the mechanics of flow through porous media and its theoretical foundations.

Acknowledgments

I deeply appreciate the thorough and useful reviews of and contributions to this book by the following individuals:

- ❖ David McWhorter, Professor Emeritus, Colorado State University, USA;
- ❖ Wolfgang Kinzelbach, Professor Emeritus, Department of Civil, Environmental, and Geomatic Engineering, ETH Zurich, Switzerland;
- ❖ Garth van der Kamp, Research Associate, Global Institute for Water Security, University of Saskatchewan, Saskatoon, Saskatchewan, Canada (formerly, Research Scientist, Environment Canada);
- ❖ Fred Marinelli, Ensero Solutions, Fort Collins, Colorado, USA;
- ❖ Connie Bryson, Editor, The Groundwater Project, Canada.

I am grateful to Amanda Sills and the Formatting Team of the Groundwater Project for their oversight and copyediting of this book. I thank Eileen Poeter (Colorado School of Mines, Golden, Colorado, USA) for reviewing, editing, and producing this book.

1 Introduction

Groundwater science is concerned with all qualitative and quantitative aspects related to water in Earth's subsurface. As such, it is inherently multidisciplinary and involves physical, chemical, and biological processes with significant socioeconomic and ecological relevance.

This book is primarily concerned with the physical mechanisms of groundwater movement, which is typically slow compared to meteorological or surface water motion. For this reason, groundwater is highly important for sustaining river discharges and well pumping rates by providing stored water during extended droughts, for example. However, groundwater movement is also important as it may cause the spreading of subsurface contaminants towards rivers, lake, and wells.

The fundamental principles for mathematical description of groundwater flow are conservation of mass (the mass of water in a closed environment cannot change) and Darcy's law that stipulates proportionality between hydraulic head gradient and groundwater flux through porous media. Darcy's law is an empirical relationship for the macroscopic *representative-elementary-volume scale* comprising many individual pores and channels. One of the important contributions of fluid mechanics to groundwater science is that it enables us to understand Darcy's law at a fundamental level based on equilibrium between forces that act to drive and resist flow.

Classic textbooks on fluid mechanics, including Bird and others (1960), present a general treatment of transport phenomena, thorough definitions of fluxes, and equations describing change for mass, energy, and momentum. Bear (1972) is particularly dedicated to the processes and mathematical description of the dynamics of flow through porous media, while Freeze and Cherry (1979) focus on more applied aspects of groundwater hydrology. Other classic books by Corey (unpublished manuscript widely distributed in 1977) and Dullien (1979) provide detailed discussions on the nature of pore spaces, their permeability, and the effects of capillary forces when multiple fluid phases are present. These textbooks and a wealth of others are available in their original versions, as cited here, or in many cases as more recent revised editions. Both the [Freeze and Cherry book](#) and the third edition of [Corey's book](#) are available free-of-charge for download on the Groundwater Project website.

In this book, we explain Darcy's law and the underlying concepts embedded in hydraulic head and hydraulic conductivity starting from first physical principles as expressed by Newton's law of motion and fluid viscosity. A complete derivation of the Navier-Stokes equation—which governs fluid movement in most general force balance (or momentum balance) terms and may be found in many textbooks on pure fluid mechanics—is not presented here. However, we present a line of physically based arguments for constructing and presenting a common form of the Navier-Stokes equation, which can be

significantly simplified for typical hydrogeological conditions. These simplifications lead to Darcy's law and are based on the assumptions that friction dominates over inertia in groundwater flow, and that friction may be considered as a distributed body force (as opposed to a surface force) over a representative elementary volume of porous medium.

We further discuss how differences in hydraulic head are directly related to the driving force for groundwater flow, while viscosity provides for the frictional resistant force that is inversely proportional to hydraulic conductivity. More specifically, we identify the hydraulic head as a force potential per unit fluid weight due to effects of fluid pressure and gravity or, alternatively, as the mechanical energy per unit fluid weight available to drive flow. Finally, combination of Darcy's law with mass conservation results in the governing equations for groundwater flow, which are derived for a variety of typical scenarios under saturated flow conditions including transient storage, heterogeneity, and anisotropy.

Overall, this book aims to convey an introductory and progressive (from simpler to more complicated) understanding of the processes underlying the flow of groundwater, and how these can be formulated in mathematical language as (partial) differential equations. As such, we assume that the reader is familiar with the most basic principles of physics and calculus (approximately, at a first-year university level). However, we still attempt to provide relatively detailed derivations starting from a finite difference perspective. We believe this is beneficial because the finite difference method is also the simplest way to numerically solve the resulting equations for the common case where an analytical solution is not available. For the sake of illustrating the physical principles without loss of generality—as well as keeping the formulation of the governing equations and the representation of their solutions as simple as possible—the main discussion is limited to one- and two-dimensional frameworks.

Only a few analytical solutions are presented in this book for the simplest problems, but we provide many graphical representations of conceptual models and solutions. Moreover, we make extensive use of non-dimensionalizing governing equations and order-of-magnitude analysis to extract maximum information from the equations prior to solving them. This allows the estimation of response-time scales (e.g., seconds, days, or years, and so on), over which a system can be expected to react to a change in forcing conditions. Examples include the development of a steady-state laminar flow profile after a change in pressure gradient, and an aquifer providing river baseflow after a recharge period.

When two competing mechanisms act simultaneously, then the ratios of respective response-time scales result in dimensionless numbers quantifying the possible dominance of one mechanism or the other. Smaller response-time scales indicate more efficient mechanisms; examples given here include the Reynolds number (times scales of viscous over advective momentum transport) or the water table ratio (times scales of emptying out

an unconfined aquifer over filling it). In general, the non-dimensionalization of governing equations is very useful: it reduces the number of independent parameters to a minimum, thus simplifies numerical implementation, interpretation of results, and comparison of mathematical models across different scientific areas.

After the main text, this book contains several boxes and solved exercises. The boxes provide complementary information as would be placed in appendixes because they are small excursions from the main focus of the book. This includes the inverse perspective of how the frictional action of the flowing fluid affects the effective stress state of a porous medium. Boxes add details to mathematical derivations such as for flow in the unsaturated zone of an aquifer, where capillary effects become significant, resulting in Richards equation.

The intention of this book is to provide the reader with some fundamental background that may help them identify and explore the many common aspects of different problems related to groundwater flow. As a generalization of the Richard's Equation, we derive the governing equations for simultaneous flow of two immiscible liquid phases, which, for example, can be relevant for the study of contaminant source zones in aquifers. The exercise topics are of practical relevance to groundwater scientists at a variety of spatial and temporal scales, and some are related to recent scientific publications. The solved exercises are substantial in the sense that they are not mere revisions of the book's content; rather, they help the reader derive mathematical models and solutions based on the principles discussed in the main text. A list of basic notations for variables used with respective dimensions is provided at the end of the book.

Citations in the main body of this book refer the reader to classical persons, papers, and textbooks, which are a consequence of the topic being treated. Moreover, links to relevant pages on Wikipedia are provided for easy access to additional information, illustrations, and translations to other languages. As part of [The Groundwater Project \(GW-Project\)](#)  online book series, we also refer extensively to the wealth of further details available in other GW-Project publications.

2 Straight Movement of a Rigid Body

2.1 Location, Velocity, and Acceleration

The movement of a body or a fluid parcel in general can be described by the temporal evolution of its location (where it is, and when). Figure 1 illustrates the simplest example of a body in straight movement without rotation or deformation, where location is represented by coordinate x . Any change in location over time t corresponds to a travel distance of the body, which can be used to express the body *velocity* v in differential form as shown in Equation (1).

$$v = \frac{dx}{dt} \quad (1)$$

where:

x = coordinate of body location (L)

t = time (T)

v = body velocity (LT⁻¹)

dx = small displacement (L), i.e., a change in location during small increment of time dt (T).

Based on Equation (1), we observe that velocity is the first derivative of location with respect to time.



Figure 1 - Body in straight movement at location x , velocity v , and acceleration a . The dashed contours indicate possible locations of the body at different times.

In the same way as the location of a body may change, its velocity may also change. Analogous to Equation (1), the *acceleration* a is defined as the change in velocity per unit time as shown in Equation (2).

$$a = \frac{dv}{dt} = \frac{d^2x}{dt^2} \quad (2)$$

The final term is found by substituting Equation (1) for v . Thus, acceleration is the first derivative of velocity, or the second derivative of location, both with respect to time.

2.2 Newton's Second Law of Motion, Momentum, and Kinetic Energy

Newton's second law of motion [↗] was initially formulated for a mass particle and is written as shown in Equation (3).

$$F = ma \quad (3)$$

where:

F = sum of all forces acting on the particle (MLT^{-2})

m = particle mass (M)

a = particle acceleration (LT^{-2}).

Soon after Newton, Euler in his first law of motion generalized the validity of Equation (3) to the straight movement of rigid bodies, if a is considered as the acceleration of the body's center of mass. Since m is a constant for rigid bodies, this means that at any time t , a body's acceleration is directly proportional to the sum of all forces applied.

In very general terms, we distinguish two fundamental types of forces that can act on a body:

1. *driving forces* (such as gravity on an inclined plane) which attempt to induce movement of the body; and,
2. *resisting forces* (such as friction between a body and the plane) which attempt to hinder the movement.

Considering driving forces as positive and resisting forces as negative, then the (geometric or vector) sum of both types of forces applied becomes the net driving force acting on the body. If the net driving force is not zero, it induces body acceleration in the direction of the net driving force, and is balanced by the respective *inertial force* in the opposite direction. The distinction between driving and resisting forces is of great interest in Section 6.1 when discussing how the movement of groundwater through aquifers can be described by Darcy's law.

Substituting Equation (2) into Equation (3) gives Equation (4).

$$F = m \frac{dv}{dt} \quad (4)$$

Integrating the net driving force F over time from t_0 (at velocity v_0) to t_1 (at velocity v_1) yields Equation (5).

$$\int_{t_0}^{t_1} F dt = m \int_{v_0}^{v_1} \frac{dv}{dt} dt = m \int_{v_0}^{v_1} dv = m(v_1 - v_0) \quad (5)$$

where:

F = sum of all forces acting on the body (MLT^{-2})

t = time (T)

m = body mass (M)

v_0 = initial velocity (LT^{-1})

v_1 = final velocity (LT^{-1})

The first integral in Equation (5) represents the *impulse* of F provided to the body. It is equal to the *change in momentum* M of the body as described by the last part of Equation (5). If F is known as a function of time, then Equation (5) allows us to compute the change

in velocity of a body from initial velocity v_0 to final velocity v_1 . For the particular case where F is constant, and the body starts from rest at time zero (i.e., $t_0 = v_0 = 0$ with $t_1 = t$ and $v_1 = v$), Equation (5) reduces to the well-known equation for linear momentum shown in Equation (6).

$$M = Ft = mv \quad (6)$$

where:

$$M = \text{body momentum (MLT}^{-1}\text{)}$$

In contrast, integrating the net driving force F from Equation (4) over distance from x_0 (at velocity v_0) to x_1 (at velocity v_1) yields Equation (7).

$$\int_{x_0}^{x_1} F dx = m \int_{v_0}^{v_1} \frac{dv}{dt} dx = m \int_{v_0}^{v_1} v dv = \frac{m}{2} (v_1^2 - v_0^2) \quad (7)$$

where $v = dx/dt$ from Equation (1) was used to transition from the second to the third expression. The left-hand side of Equation (7) represents the *work* performed by F on the body and is equal to the *change in kinetic energy* E of the body. For the particular case that F is constant, and the body starts from rest at location zero (i.e., $x_0 = v_0 = 0$ with $x_1 = x$ and $v_1 = v$), Equation (7) reduces to the well-known equation for kinetic energy shown as Equation (8).

$$E = Fx = \frac{mv^2}{2} \quad (8)$$

where:

$$E = \text{body kinetic energy (ML}^2\text{T}^{-2}\text{)}$$

2.3 Coulomb Friction and Drag Forces

Friction is a force that always contributes to resistance against movement. There are many types of friction, and the physical details are complex. Here, we illustrate the strong influence that resisting forces can have on how a body moves according to Newton's second law of motion. For this purpose, we compare two simple examples of:

1. body acceleration opposed by a constant friction force; and,
2. body acceleration opposed by a velocity-dependent friction (drag) force.

For the example of a rigid body of mass m sliding along a horizontal plane as shown in Figure 2, a constant friction force F_f corresponds to the classic case known as Coulomb friction. The Coulomb friction force is equal to the normal force mg multiplied by an empirical dimensionless friction factor f_{col} (i.e., $F_f = mgf_{col}$, with g being acceleration of gravity). The important detail is that f_{col} is a constant (which in practice depends on the material properties of body and plane) and does not depend on where the body is or how fast it moves along the plane.

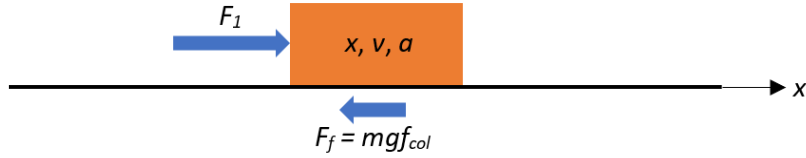


Figure 2 - Illustration of Newton's second law of motion $F = ma$ for a rigid body sliding with variable velocity v in the positive x -direction (i.e., from left to right) over a flat surface. Acting on the body, we consider a driving force F_1 and a resisting Coulomb friction force $F_f = mgf_{col}$ which is proportional to body mass m , acceleration of gravity g , and a constant Coulomb friction factor f_{col} . Thus, F_f does not change in this situation as the body moves.

If we assume further in Figure 2 that the body is being pushed by a force F_1 , then the net driving force to be used in Equation (3) for computing body acceleration is equal to Equation (9).

$$F = F_1 - mgf_{col} \quad (9)$$

This can be substituted into Equation (4) to yield Equation (10).

$$\frac{dv}{dt} = \frac{1}{m}(F_1 - mgf_{col}) \quad (10)$$

where:

$$f_{col} = \text{Coulomb friction factor (-)}$$

Equation (10) is an ordinary differential equation describing the temporal evolution of body velocity v as a function of a possibly variable force F_1 . The left-hand side represents the temporal change in velocity (i.e., the acceleration), which is equal to the expression on the right-hand side. To solve Equation (10), an initial condition must be defined. Here we stipulate that the velocity at some initial time t_0 be equal to an arbitrary value v_0 leading to Equation (11).

$$\int_{v_0}^{v_1} dv = \int_{t_0}^{t_1} \left(\frac{F_1}{m} - gf_{col} \right) dt \quad (11)$$

Along the lines of Equation (5), i.e., assuming a constant F_1 and integrating on both sides using $t_0 = 0$, gives the solution shown by Equation (12).

$$v_1 = v_0 + \left(\frac{F_1}{m} - gf_{col} \right) t_1 \quad (12)$$

This is graphically illustrated by the red lines in Figure 3 for different values of v_0 and a positive (accelerating) value of $F_1/m - gf_{col} = 0.54 \text{ m/s}^2$ (e.g., $F_1 = 5 \text{ N}$, $m = 2 \text{ kg}$, $g = 9.81 \text{ m/s}^2$, $f_{col} = 0.2$). As to be expected, the solutions correspond to straight lines indicating that the body accelerates uniformly without ever reaching a steady (constant) velocity, except for the trivial case of $F_1 = F_f$ leading to $F = 0$.

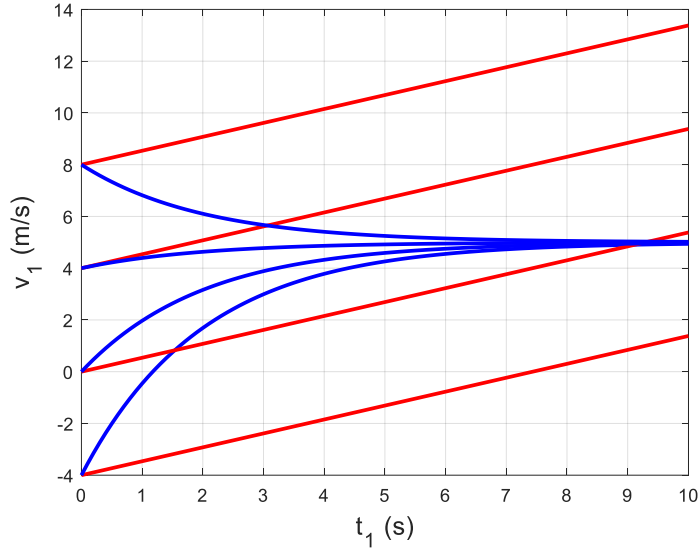


Figure 3 - Example solutions of body velocity v_1 as a function of time t_1 for constant Coulomb friction (Equation (12); red lines) and, as discussed next, velocity proportional drag friction (Equation (16); blue lines). While the red lines do not converge to a steady state, the blue lines asymptotically approach a single terminal velocity, regardless of the initial velocity.

For comparison, Figure 4 represents the example of a *velocity dependent drag force* F_f opposing acceleration by driving force F_1 . Drag forces occur in the presence of relative motion between a solid body and a fluid. They are due to frictional (i.e., viscous) effects inside the fluid as it must flow around the body. In the simplest case of a well-defined flow field (i.e., in the absence of turbulent wakes behind the body), Stokes' law states that in an otherwise stagnant fluid, the drag force on a moving solid body is proportional to the body velocity v and some drag coefficient f_{sto} (i.e., $F_f = v f_{sto}$). Thus, in analogy to Equations (9), (10), and (11), we find Equations (13), (14), and (15).

$$F = F_1 - v f_{sto} \quad (13)$$

$$\frac{dv}{dt} = \frac{1}{m} (F_1 - v f_{sto}) \quad (14)$$

$$\int_{v_0}^{v_1} \frac{dv}{F_1 - v f_{sto}} = \frac{1}{m} \int_{t_0}^{t_1} dt \quad (15)$$

where:

$$f_{sto} = \text{drag coefficient (MT}^{-1}\text{)}$$

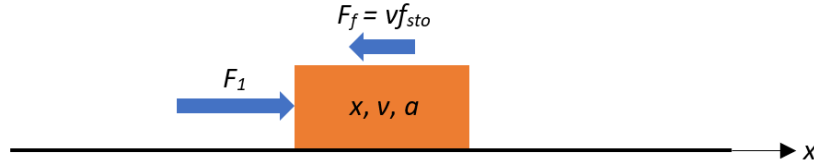


Figure 4 - Velocity-dependent friction (drag) force. This is the exact same scenario as shown in Figure 2, except for assuming a Stokes friction force $F_f = v f_{sto}$, where f_{sto} is a constant Stokes friction factor. Thus, F_f is proportional to velocity v and will grow as the body accelerates.

To keep the example simple, we assume that the density of the fluid (e.g., air) is much smaller than that of the solid body, such that the inertia (technically termed *added mass*) of the fluid as it locally accelerates around the body may be neglected in Equation (14). Equation (15) is written to separate the variables t and v on either side of the equation, and integrating with $t_0 = 0$ gives Equation (16) and (17).

$$-\frac{1}{f_{sto}} \ln \frac{F_1 - v_1 f_{sto}}{F_1 - v_0 f_{sto}} = \frac{t_1}{m} \quad (16)$$

$$v_1 = \frac{F_1}{f_{sto}} \left[1 - \left(1 - \frac{v_0 f_{sto}}{F_1} \right) \exp \left(-\frac{f_{sto}}{m} t_1 \right) \right] \quad (17)$$

This is illustrated by the blue lines in Figure 3 for different values of v_0 with example values of $F_1/f_{sto} = 5$ m/s and $m/f_{sto} = 2$ s (e.g., $F_1 = 5$ N, $m = 2$ kg, $f_{sto} = 1$ Ns/m). In strong contrast to the red lines corresponding to Coulomb friction and Equation (12), the velocity now converges exponentially to a single value for large enough times, regardless of the initial velocity at time zero.

For very large times (i.e., $t_1 \rightarrow \infty$), the exponential term in Equation (17) approaches zero and we arrive at the steady-state velocity (or *terminal velocity*) v_∞ as shown by Equation (18).

$$v_\infty = \frac{F_1}{f_{sto}} \quad (18)$$

This constant terminal velocity is reached when the drag force F_f becomes equal to the applied force F_1 such that the net force F becomes zero. Thus, Equation (17) can be reformulated as Equation (19).

$$\frac{v_1}{v_\infty} = 1 - \left(1 - \frac{v_0}{v_\infty} \right) \exp \left(-\frac{f_{sto}}{m} t_1 \right) \quad (19)$$

Equation (19) is an equivalent normalized form where all individual terms are dimensionless. This is the case for v_1/v_∞ and v_0/v_∞ being the ratios of velocities. It is also the case for $t_1 f_{sto}/m$, which can be determined by inspecting Equation (13) while recognizing the dimensions of f_{sto} as mass per time. In fact, the ratio m/f_{sto} has dimensions of time and it can be interpreted as the dynamic response time (or *response-time scale*) T of the body movement when subjected to a step change in accelerating force, for example, as shown in Equation (20).

$$T = \frac{m}{f_{sto}} \quad (20)$$

Given Equation (20), Equation (19) can be further simplified to Equation (21).

$$\frac{v_1}{v_\infty} = 1 - \left(1 - \frac{v_0}{v_\infty}\right) \exp\left(-\frac{t_1}{T}\right) \quad (21)$$

Equation (21) is graphically represented in Figure 5 for different values of v_0/v_∞ showing a consistent asymptotic convergence to $v_1 = v_\infty$ for large enough times.

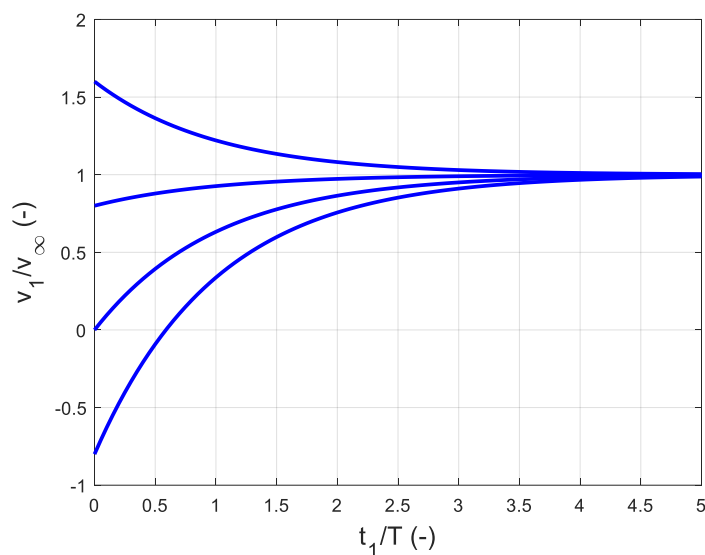


Figure 5 - Graphs of Equation (21) for different values of v_0/v_∞ showing asymptotic convergence and significant (with respect to $v_\infty - v_0$) changes in velocity for times t_1 being on the same order-of-magnitude as the response-time scale T (i.e., $t_1/T \approx 1$). The first and second lines from the top show deceleration and acceleration toward $v_0/v_\infty = 1$, respectively. The third line corresponds to acceleration from rest ($v_1 = 0$) and the fourth line to acceleration from a movement in the opposite direction ($v_1 < 0$).

The asymptotic nature of the response implies that the steady-state is never exactly reached, which is a common characteristic of many processes. However, Figure 5 also illustrates that at $t_1 \approx T$ the changes in velocity are already quite substantial or significant with respect to the full asymptotic change of $v_\infty - v_0$. In practice, if the response-time scale T of a problem is known to be on the order of either seconds, days, or decades, for example, then one may expect to observe a significant system response due to a change in forcing conditions only after a period of either seconds, days, or decades, respectively. This is very approximate information, but it can be extremely useful in many situations where more detailed information and/or solutions are not available.

[Box 1](#) discusses how order-of-magnitude analysis of a governing equation can be a useful shortcut to simplifying a problem by non-dimensionalization and to estimating T without the need for deriving an explicit solution as shown above. [Exercise 1](#) provides an

example of a boat being accelerated on a lake with focus on response-time scales as a function of boat mass.

Some additional, interesting observations of general validity can be made. These observations are pertinent for subsequent sections of this book that are more directly related to fluid flow.

1. The convenience of working with dimensionless terms becomes clear when observing that Equation (19) and (21) express the dimensionless velocity v_1/v_∞ as a function of dimensionless time t_1/T with a single dimensionless parameter v_0/v_∞ . This is much more efficient than the dimensional Equation (17), where v_1 is regarded as a function of t_1 , requiring three independent parameters: v_0 , F_1/f_{sto} and m/f_{sto} .
2. Generally, different forms of normalization are possible, and the best option needs to be chosen depending on the situation. For the case of $F_1 = 0$, for example, we know that $v_\infty = 0$ (because the only acting force is drag) and division by v_∞ would not make sense. In such a case it would be useful to simplify Equation (17) accordingly to $v_1 = v_0 \exp\left(-\frac{f_{sto}}{m} t_1\right)$ and normalize by the initial velocity v_0 instead.
3. Equation (18) reflects that terminal velocity v_∞ does not depend on the initial velocity v_0 . In other words, there is only a single steady-state of $v_1 = v_\infty$ that the system can converge to in this example, regardless of its past trajectory or initial condition.
4. By orienting the positive direction of the x -axis in Figure 4 downward and regarding F_1 as the force of gravity on the body, the problem becomes that of a solid body (or particle) sinking in a viscous liquid as discussed in Section 3.1.
5. Equation (20) shows that the response time T is a pure system property, as it does not depend on the driving force F_1 nor the initial velocity v_0 . Intuitively speaking, this is because larger changes in F_1 not only imply the competing effects of larger initial acceleration but also larger changes in terminal velocity.
6. As illustrated by Figure 5, the dimensionless time t_1/T allows for a rough but quick assessment of whether the system is near its initial state ($t_1/T \ll 1$ and $v_1 \approx v_0$), passing through the transient stage ($t_1/T \approx 1$ and $v_0 < v_1 < v_\infty$), or near steady state ($t_1/T \gg 1$ and $v_1 \approx v_\infty$).
7. While we consider T as the time scale of system response (i.e., how long it takes for the body to approach steady-state movement), t_1 may represent a time scale of interest (e.g., a temporal resolution of observations or predictions). For example, if we are interested in a system's daily response and T is on the order of seconds or minutes, then $t_1/T \gg 1$ and the *near (or quasi) steady-state assumption* can be invoked. This assumption neglects the transient phase because it is negligibly short and, thus, significantly simplifies the modeling effort by reducing Equation (17) to $v_1 = F_1/f_{sto} = v_\infty$. That is, v_1 can be regarded as directly proportional to F_1 . In other

words, the quasi-steady-state assumption considers the transient phase of system response as a succession of steady states. Exercise 1 demonstrates this concept.

8. As discussed further in Section 6.1 in relation with Darcy's law, observation (3) and (7) in this list are fundamental for groundwater movement in aquifers, in that a given force (associated with a hydraulic gradient) can only establish a single steady-state response (flow velocity), and that the transient (accelerating) flow stages can be safely neglected.

3 Viscous Flow and Stokes Equation

3.1 Newtonian Fluids, Viscosity, and Stokes Drag

Fluids are fundamentally different from rigid bodies in that individual fluid parcels may deform in arbitrary ways. At this point, however, we assume the simple case of straight laminar and incompressible fluid movement⁷. Here fluid laminae are defined as illustrated by the spaces between the dashed lines in Figure 6. We imagine flow channels that fluid parcels strictly follow without ever crossing over to another lamina. In the case of straight flow, the velocity is the same everywhere in the flow direction s along the flow channel, but it may vary from one lamina to the next in the normal direction n . Newton found that the frictional force F between adjacent fluid lamina of thickness Δn is proportional to the relative difference in flow velocities $\Delta v/\Delta n$ multiplied by the area of contact Δs . A third coordinate oriented normal to the plane shown in the diagram can be taken to be 1 unit thick with no variation from the illustrated conditions, but it is not relevant to the discussion here. Figure 6 illustrates this situation for two rectangular fluid parcels shown in yellow and orange.

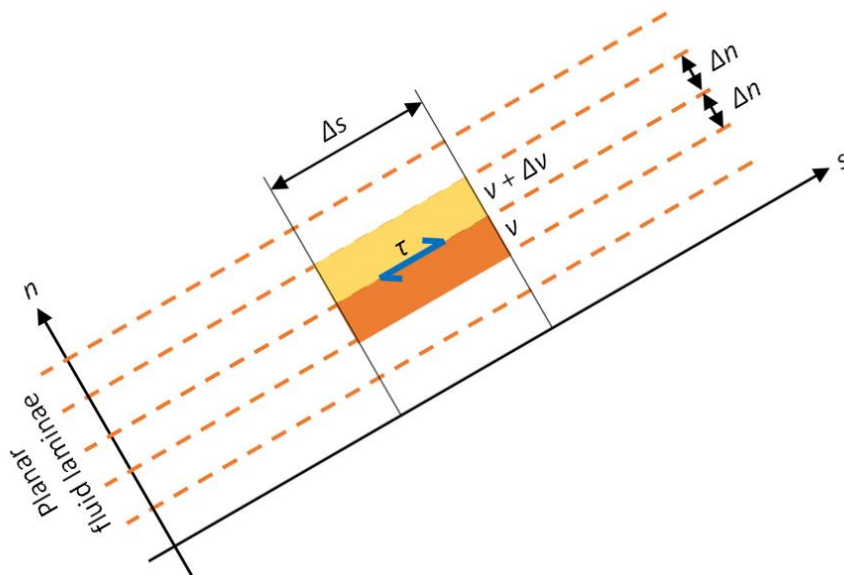


Figure 6 - Two adjacent rectangular fluid parcels traveling in the s -direction along planar fluid laminae of width Δn (delimited by dashed lines) at different velocities v and $v + \Delta v$. For Newtonian fluids of dynamic viscosity μ , the shear stress τ between the parcels, is equal to $\mu\Delta v/\Delta n$.

As the proportionality constant—or, in other words, the relevant *friction factor* for fluids—Newton introduced the dynamic viscosity μ ⁷, which is a fundamental property of a fluid (e.g., small for gases like air and much larger for thick liquids like honey). Thus, the frictional force along the contact surface between two adjacent fluid laminae results as $F_f = \mu\Delta s\Delta v/\Delta n$. Since fluid laminae can be imagined as infinitely thin and arbitrarily long, it

is convenient to reformulate this relationship in terms of the *shear stress* $\tau = F_f/\Delta s$ and the differential operator dv/dn instead of $\Delta v/\Delta n$, as shown by Equation (22).

$$\tau = \mu \frac{dv}{dn} \quad (22)$$

where:

τ = shear stress on the interface between adjacent fluid laminae ($\text{ML}^{-1}\text{T}^{-2}$)

μ = dynamic viscosity ($\text{ML}^{-1}\text{T}^{-1}$)

v = fluid velocity in s -direction as a function of n (LT^{-1})

n = coordinate perpendicular to laminar flow direction (L)

The above relationship states that the shear stress in the s -direction is equal to the dynamic viscosity of the fluid multiplied by the velocity gradient in the n -direction (i.e., perpendicular to the flow direction). The existence of a velocity gradient implies that neighboring fluid parcels move at different velocities such that the entire fluid suffers internal deformation by shearing and the velocity gradient may also be called the *strain rate*. This contrasts with elasticity, where stress is proportional to strain, not strain rate. Fluids described by Equation (22) are called *Newtonian fluids*, and this concept generally represents an excellent approximation for practical situations in groundwater science. However, there are exceptions beyond the scope of this book when fluids may be non-Newtonian and shear stresses depend on additional factors—such as pressure or strain history—that cannot be described by a constant fluid viscosity.

A solid body moving through a stagnant fluid locally disturbs the fluid depending on its shape. If the body motion is slow enough for all inertial (i.e., acceleration) effects to be negligible, then we speak of Stokes (or creeping) flow around the body. In this case, the fluid laminae near the body are no longer completely straight, but all shear stresses and normal pressures on the body surface due to the movement (i.e., except for the normal pressures due to hydrostatic buoyancy) are proportional to the fluid viscosity μ and the velocity v of the body relative to the fluid. Integration over the total surface area of the solid body thus results in a drag force due to friction $F_f \approx \mu v$ against the direction of body movement. For a spherical object, for example, Stokes derived a law for the frictional force, or drag force as shown by Equation (23).

$$F_f = 6\pi R\mu v \quad (23)$$

where:

F_f = frictional (Stokes drag) force against the direction of body movement
(MLT^{-2})

R = radius of the sphere (L)

v = velocity of the sphere relative to the fluid (LT^{-1})

This relates back to observation 8 in Section 2.3 and motivated the use of $F_f = f_{sto}v$ in the introductory example of Figure 4 as well as the term Stokes drag coefficient for f_{sto} (which in Equation (23) would be equal to $6\pi R\mu$). [Exercise 2](#) gives an example of how the terminal falling velocity of a spherical particle in water depends on the particle radius and fluid viscosity.

3.2 Flow Between Two Plates – Planar Poiseuille Flow

Now we assume that all fluid laminae are perfectly straight and parallel again, while contained between two stationary surfaces ([fixed plates](#)). Such approaches are also called *shell models* and they are an important idealization for groundwater flow along rock fractures, for example. In analogy to Section 3.1 and as illustrated in Figure 7, we select a rectangular fluid parcel of length Δs and height Δn . The depth or width in the third dimension can again be set to *unity* and is not explicitly needed here.

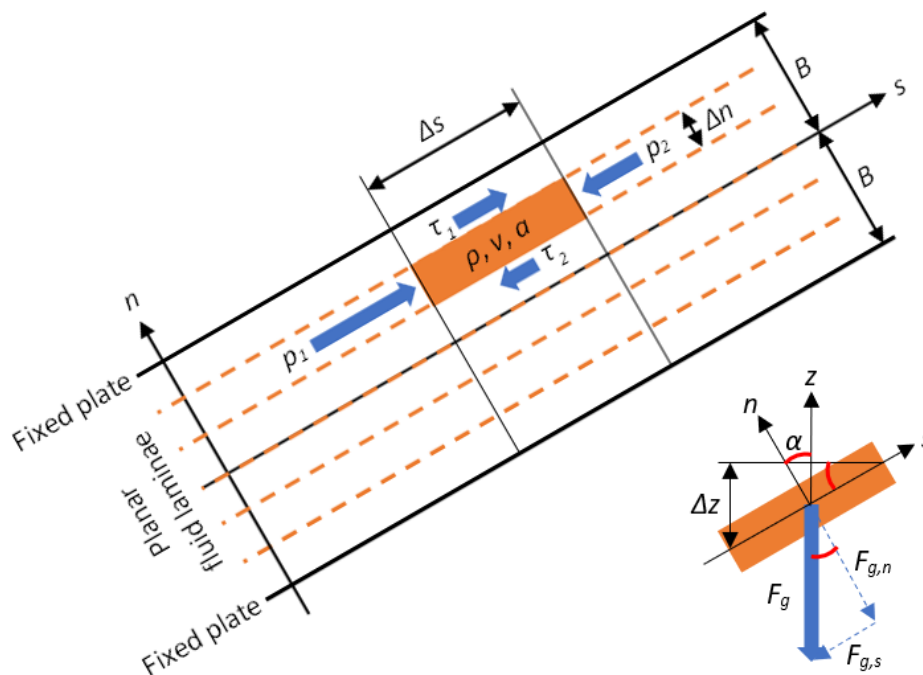


Figure 7 - Schematic representation of planar Poiseuille flow with pressures p and shear stresses τ acting on a rectangular fluid parcel of length Δs traveling along a lamina of width Δn . Moreover, the force of gravity F_g acts on the parcel with components $F_{g,s}$ and $F_{g,n}$ as shown in the separate inset on the bottom right for an inclination angle α indicated by the red arcs.

For flow to initiate, there must be a driving force along the s -direction, which is then opposed by a resisting force in the opposite direction. In general, the forces that may act on a fluid (parcel) can either be surface forces or body forces. *Surface forces* require physical contact over a surface and may be due to pressure and friction. While pressures always act in the direction normal to a surface, frictional or viscous effects may induce both normal

and tangential stresses. In contrast, *body forces* such as gravity do not require physical contact and act uniformly distributed over all elements inside a fluid parcel on a per volume or per mass basis.

The blue arrows in Figure 7 indicate the forces on a fluid parcel for developing a force balance in the direction of a flow lamina to evaluate a net driving force that may cause changes in velocity. Pressures p_1 and p_2 act over the front and rear surfaces of area Δn , while tangential shear stresses τ_1 and τ_2 against adjacent laminae apply over the lateral surfaces of area Δs . For graphical clarity, the body force F_g on the parcel due to gravity is shown in the separate inset with individual components $F_{g,s}$ and $F_{g,n}$ in the directions of flow and normal to it, respectively.

The net driving force in the positive s -direction (and again per unit width in the third dimension) on the fluid parcel is shown by Equation (24).

$$F = (p_1 - p_2)\Delta n + (\tau_1 - \tau_2)\Delta s - F_{g,s} \quad (24)$$

The parcel mass is $m = \rho\Delta s\Delta n$, where ρ is the fluid density. Furthermore, $F_g = mg$ where g is the acceleration of gravity, and we can write $F_{g,s} = F_g \sin\alpha = \rho\Delta s\Delta n g \sin\alpha$. Then, from the identical angles α indicated by the red arcs in the inset of Figure 7, we infer $\sin\alpha = \Delta z/\Delta s$. Finally, Equation (4) is invoked to express $dv/dt = F/m$, and we arrive at Equation (25).

$$\frac{dv}{dt} = \frac{F}{m} \approx \frac{1}{\rho} \left[\frac{p_1 - p_2}{\Delta s} + \frac{\tau_1 - \tau_2}{\Delta n} - \rho g \frac{\Delta z}{\Delta s} \right] \quad (25)$$

Recognizing that $p_1 = p(s)$ and $p_2 = p(s + \Delta s)$, then $(p_1 - p_2)/\Delta s$ becomes $-dp/ds$ in differential form, i.e., for Δs becoming very small. Similarly, $\tau_1 = \tau(n + \Delta n)$ and $\tau_2 = \tau(n)$, such that $(\tau_1 - \tau_2)/\Delta n$ becomes $d\tau/dn$, while $\Delta z/\Delta s$ becomes dz/ds . This leads to Equation (26).

$$\frac{\partial v}{\partial t} = \frac{1}{\rho} \left[-\frac{\partial p}{\partial s} + \frac{\partial \tau}{\partial n} - \rho g \frac{\partial z}{\partial s} \right] \quad (26)$$

In Equation (26), $\partial()/\partial()$ is written instead of $d()/d()$ to emphasize that we use *partial derivatives* because there is more than one independent variable (s , n , and t). In this simple case, which can be described by an incompressible shell model, there is only one velocity component that is not zero (here in the s -direction) and, for a given fluid lamina, this velocity may only change with time (called *local acceleration*, $\partial v/\partial t$), while being constant along the flow path. That is, *convective acceleration* is zero because $\partial v/\partial s = 0$. Equation (26) reflects the fact that there are contributions to a driving force in the positive s -direction when the pressure gradient $\partial p/\partial s$ is negative (i.e., larger pressures on the left) and when $\partial z/\partial s$ is negative (i.e., negative α and downward flow).

Substituting Equation (22) into Equation (26) results in the *one-dimensional unsteady Stokes equation* shown as Equation (27).

$$\frac{\partial v}{\partial t} = \frac{\mu}{\rho} \frac{\partial^2 v}{\partial n^2} - g \frac{\partial \left(\frac{p}{\rho g} + z \right)}{\partial s} = \frac{\mu}{\rho} \frac{\partial^2 v}{\partial n^2} - g \frac{\partial h}{\partial s} \quad (27)$$

In this equation, the partial derivatives along s are combined into a single term by considering ρ and g to be constants. The ratio μ/ρ is known as *kinematic viscosity* or *momentum dispersivity*. The new variable $h = p/\rho g + z$ is the *hydraulic head*, which combines effects of pressure and gravity into a single variable of great interest for groundwater scientists. Equation (27) is the governing partial differential equation for the velocity $v(n,t)$ as a function of *hydraulic (head) gradient* $J = \partial h/\partial s$, and it is a special case of the more general *Navier-Stokes equation*. Further details on the Navier-Stokes equation and hydraulic head are discussed in Sections 5 and 6.

Assuming a constant hydraulic gradient $J = \partial h/\partial s$ and steady state (i.e., $\partial v/\partial t = 0$), Equation (27) yields Equation (28).

$$J = \frac{\mu}{\rho g} \frac{\partial^2 v}{\partial n^2} \quad (28)$$

Integrating twice over n leads to Equation (29).

$$v = \frac{\rho g J}{2\mu} n^2 + C_1 n + C_2 \quad (29)$$

where:

C_1 and C_2 = integration constants

Assuming the stationary plates are centered about the s -axis and separated by a distance $2B$ as shown in Figure 7, we may apply the boundary conditions of $v(n = B) = v(n = -B) = 0$. This is called the “*no-slip*” *boundary condition* and imposes the requirement that the velocity of the fluid at a solid surface boundary is equal to the velocity of the surface (here, zero). Substituting both boundary conditions into Equation (29) gives the following:

$$\begin{aligned} 0 &= \frac{\rho g J}{2\mu} B^2 + C_1 B + C_2 \\ 0 &= \frac{\rho g J}{2\mu} B^2 - C_1 B + C_2 \end{aligned}$$

This leads to $C_2 = -\rho g J B^2/(2\mu)$ and $C_1 = 0$, such that Equation (29) becomes Equation (30).

$$v = -\frac{\rho g}{2\mu} (B^2 - n^2) J \quad (30)$$

In Equation (30) the negative sign again indicates that the flow velocity is against the direction of the head gradient (i.e., from points of larger to smaller hydraulic head). The velocity profile is parabolic (quadratic in n) and has a maximum value v_{max} at $n = 0$ as determined by Equation (31).

$$v_{max} = -\frac{\rho g}{2\mu} B^2 J \quad (31)$$

Integrating Equation (30) over n from $-B$ to B results in the volumetric flow rate (discharge) Q per unit width in the third dimension as shown by Equation (32).

$$Q = -\frac{2\rho g}{3\mu} B^3 J \quad (32)$$

The mean flow velocity $v_{mean} = Q/(2B)$ is shown by Equation (33).

$$v_{mean} = -\frac{\rho g}{3\mu} B^2 J \quad (33)$$

Ignoring the negative sign in Equation (32) by using the absolute value $|J|$ of the hydraulic gradient and identifying the term $2B$ as a fracture width (or aperture), we arrive at the famous “cubic law” for fracture flow (Snow, 1969) in the form shown by Equation (34).

$$Q = \frac{\rho g}{12\mu} (2B)^3 |J| \quad (34)$$

Equation (34) states that the flow rate along a fracture plane, when idealized as the space between two parallel and perfectly flat surfaces, is proportional to the cube of the fracture aperture. We assumed a *unitary* extent of the flow laminae in the third dimension such that Equation (34) represents a flow rate per unit fracture extent transverse to the flow direction. Multiplication by some value of fracture width in the third dimension which is perpendicular to both s and n would result in a true volumetric flow rate in dimensions of L^3T^{-1} , or for example units of m^3/s .

At steady state, the driving force over all laminae due to pressure differences and gravity as expressed by the hydraulic gradient must be equal to the resisting friction force that the stationary plates exert on the fluid in the form of shear stress. This may be verified by applying Equation (24) with $\Delta n = 2B$ showing that the driving force per unit flow length Δs is equal to $2\rho gBJ$. At the same time, the resisting shear stress between the fluid and the plates may be computed from the velocity gradients at the plate surfaces resulting from the first derivative of Equation (30) as shown by Equation (35).

$$\frac{dv}{dn} = \frac{\rho g}{\mu} nJ \quad (35)$$

This gives $\tau_1 = \rho gBJ$ for $n = B$ and $\tau_2 = -\rho gBJ$ for $n = -B$ from Equation (22). Overall, this confirms that the fluid acts with a force gradient (i.e., force per unit flow length Δs) equal to $2\rho gBJ$ on the plates, while the plates provide the respective resisting force gradient of the same magnitude acting onto the fluid (all per unit width in the third dimension).

Exact solutions of Equation (27) exist but are complicated, such that we proceed with an order-of-magnitude analysis of the governing equation as explained in Box 1. The final expression of Equation (27) may be written in non-dimensional form by adopting the dimensionless variables $v^* = v/v_{max}$, $t^* = t/T$, and $n^* = n/B$. Using Equation (31) to relate v_{max} to J , both variables drop out and we arrive at Equation (36).

$$\frac{\rho B^2}{\mu T} \frac{\partial v^*}{\partial t^*} = 2 + \frac{\partial^2 v^*}{\partial n^{*2}} \quad (36)$$

Since the right-hand side is of unit order-of-magnitude, the left-hand side must also be of unit order-of-magnitude, which may be achieved by adopting Equation (37).

$$T = \frac{\rho B^2}{\mu} \quad (37)$$

This eliminates the leading factor on the left and means that T is the response-time scale of the problem, that is, the approximate time (corresponding to one dimensionless time unit) after which the velocity profile has approached the steady-state shape to a significant degree. The temporal evolution of the velocity profile is shown in Figure 8. The solutions are computed by the method of finite differences as outlined in [A Simple Numerical Solution Method](#) and applied in [Exercise 3](#). For plates of finite extent (i.e., in physical—rather than mathematical—situations), there are also entrance and exit effects, with an associated flow development over certain distances, where $\partial v/\partial s \neq 0$. These effects are not discussed in this book.

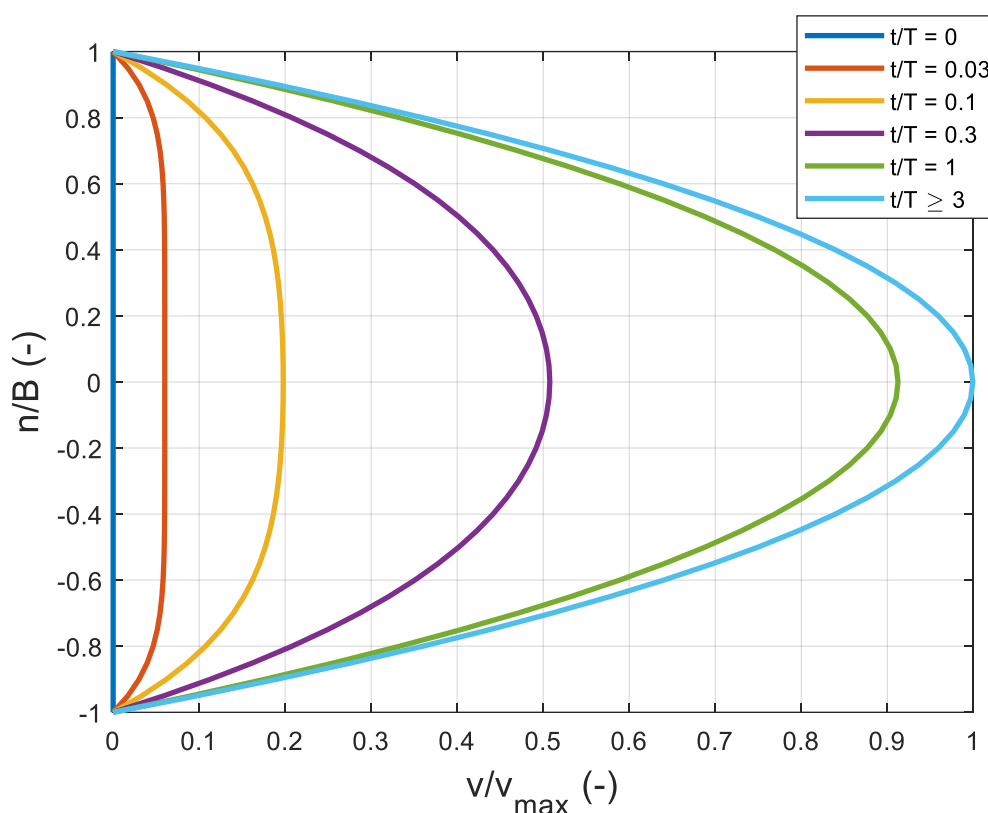


Figure 8 - Solutions of the velocity profile from Equation (36) by the method of finite differences (as described in Box 2) with T from Equation (37) for different non-dimensional times t/T after starting from rest at $t = 0$. The effects of shear stresses develop first in the form of velocity gradients near the stationary plates at $n = \pm B$ and then propagate inward. At $t \approx T$, the velocity profile has significantly approached its steady-state shape; after $t \approx 3T$, for all practical purposes it no longer changes.

3.3 Flow Through a Circular Pipe – Cylindrical Poiseuille Flow

In the case of laminar flow through a straight circular pipe, the flow laminae are no longer plane surfaces as in Section 3.2, rather they are cylindrical as illustrated in Figure 9.

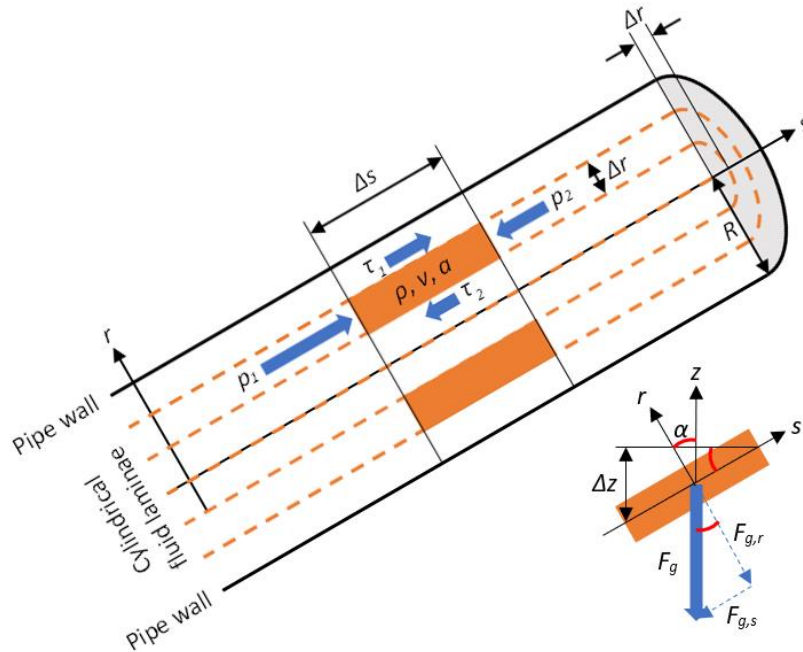


Figure 9 - Schematic representation of cylindrical Poiseuille flow along a circular pipe (half cross-section shaded in gray) with pressures p and shear stresses τ acting on a fluid parcel of length Δs traveling along a cylindrical lamina of width Δr . Moreover, the force of gravity F_g acts on the parcel with components $F_{g,s}$ and $F_{g,r}$ as shown in the separate inset on the bottom right for an inclination angle α indicated by the red arcs.

The forces acting on a fluid parcel of length Δs and thickness Δr are again indicated by the blue arrows and are due to the driving pressure gradient (p_1 and p_2) as well as the viscous shear stresses against adjacent laminae (τ_1 and τ_2). The annular surface area over which the pressure gradient acts is equal to $\pi[(r + \Delta r)^2 - r^2] \approx 2\pi r \Delta r$, where the approximation is justified by anticipating that $\Delta r \ll r$. The shear stresses τ_1 and τ_2 act over the cylindrical surface areas $2\pi(r + \Delta r)\Delta s$ and $2\pi r \Delta s$, respectively. Thus, the net driving force on the cylindrical fluid parcel is shown by Equation (38).

$$F = 2(p_1 - p_2)\pi r \Delta r + 2\tau_1\pi(r + \Delta r)\Delta s - 2\tau_2\pi r \Delta s - F_{g,s} \quad (38)$$

With parcel mass $m = 2\pi r \Delta r \Delta s \rho$ and $F_g = mg$, the component of the gravity force in the opposite direction is $F_{g,s} = F_g \sin \alpha = 2\pi \rho g r \Delta r \Delta s \Delta z / \Delta s$. Analogous to Equation (25), we invoke Equation (4) to obtain Equation (39).

$$\frac{dv}{dt} \approx \frac{1}{\rho} \left[\frac{p_1 - p_2}{\Delta s} + \frac{1}{r} \frac{\tau_1(r + \Delta r) - \tau_2 r}{\Delta r} - \rho g \frac{\Delta z}{\Delta s} \right] \quad (39)$$

Recognizing that $p_1 = p(s)$ and $p_2 = p(s + \Delta s)$, $(p_1 - p_2)/\Delta s$ becomes $-\partial p/\partial s$ in differential form. Similarly, $\tau_1 = \tau\{r + \Delta r\}$ and $\tau_2 = \tau(r)$, thus $[\tau_1(r + \Delta r) - \tau_2 r]/\Delta r$ becomes $\partial(\tau r)/\partial r$. Here we use $\tau\{r + \Delta r\}$ to denote τ at radius $r + \Delta r$, while $\tau_1(r + \Delta r)$ is the product of τ_1 and $(r + \Delta r)$. This leads to the partial differential equation shown as Equation (40).

$$\frac{\partial v}{\partial t} = \frac{1}{\rho} \left[-\frac{\partial p}{\partial s} + \frac{1}{r} \frac{\partial(r\tau)}{\partial r} - \rho g \frac{\partial z}{\partial s} \right] \quad (40)$$

Substituting Equation (22) with $n = r$ to eliminate τ from Equation (40) gives Equation (41).

$$\frac{\partial v}{\partial t} = \frac{\mu}{\rho} \frac{1}{r} \frac{\partial}{\partial r} \left(r \frac{\partial v}{\partial r} \right) - g \frac{\partial \left(\frac{p}{\rho g} + z \right)}{\partial s} = \frac{\mu}{\rho} \frac{1}{r} \frac{\partial}{\partial r} \left(r \frac{\partial v}{\partial r} \right) - g \frac{\partial h}{\partial s} \quad (41)$$

As in Equation (27) $h = p/\rho g + z$ represents hydraulic head. This partial differential equation is again a special case of the Navier-Stokes equation and the same as Equation (27), except that Equation (41) uses cylindrical coordinates s and r instead of cartesian coordinates s and n .

At steady state, $\partial v/\partial t = 0$ and using a constant hydraulic gradient $J = \partial h/\partial s$ yields Equation (42).

$$J = \frac{\mu}{\rho g} \frac{1}{r} \frac{\partial}{\partial r} \left(r \frac{\partial v}{\partial r} \right) \quad (42)$$

Multiplication by $\rho g r/\mu$ and integration over r yields

$$\frac{\rho g J}{2\mu} r^2 + C_1 = r \frac{\partial v}{\partial r}$$

then, division by r and integrating once more over r leads to

$$v = \frac{\rho g J}{4\mu} r^2 + C_1 \ln r + C_2$$

with integration constants C_1 and C_2 . Since the flow velocity for $r = 0$ at the center of the pipe cannot be infinitely large, C_1 must equal zero. Further assuming that the pipe is of radius R as shown in Figure 9, we apply the no-slip boundary condition of $v(r = R) = 0$, yielding $C_2 = -\rho g J R^2/(4\mu)$ and Equation (43).

$$v = -\frac{\rho g}{4\mu} (R^2 - r^2) J \quad (43)$$

As for parallel plates in Equation (30), the steady-state velocity profile is parabolic. However, in this case the maximum value at $r = 0$ equals Equation (44).

$$v_{max} = -\frac{\rho g}{4\mu} R^2 J \quad (44)$$

This is half the magnitude of Equation (31) for planar flow and reflects the fact that for pipe flow there is a larger influence of nearby frictional (no-slip) boundaries, which are present in all radial directions and not only in one dimension as in plane flow (n -direction in Figure 7). Integrating Equation (43) over the cross-sectional area of the pipe gives the fluid discharge Q as shown by Equation (45).

$$Q = 2\pi \int_0^R vr dr = -\frac{\rho g \pi}{8\mu} R^4 J \quad (45)$$

This also yields a mean flow velocity $v_{mean} = Q/(\pi R^2)$ as shown by Equation (46).

$$v_{mean} = -\frac{\rho g}{8\mu} R^2 J \quad (46)$$

This is exactly half the maximum velocity of Equation (44).

From Equation (38), the driving force gradient (i.e., force per total cross-sectional flow area and unit flow length Δs) can be expressed as $\pi \rho g R^2 J$. This is the sum of the pressure component $\pi R^2(p_1 - p_2)/\Delta s$ and the gravity component $\pi R^2 \rho g \Delta z/\Delta s$. For comparison, the resisting frictional stress at the pipe wall may be found from the velocity gradient shown by Equation (47).

$$\frac{dv}{dr} = \frac{\rho g}{2\mu} r J \quad (47)$$

This was achieved by taking the derivative of Equation (43). Using this derivative in Equation (22) with $r = R$ and multiplying by the pipe circumference $2\pi R$ gives a resisting force gradient of $\pi \rho g R^2 J$. This is exactly equal to the driving force gradient, which confirms the force balance between the pipe and the flowing fluid at steady state, that is, at $\partial v/\partial t = 0$.

In the same way as in Section 3.2 and outlined in Box 1, the final expression in (41) may be written in non-dimensional form by adopting the dimensionless variables $v^* = v/v_{max}$, $t^* = t/T$, and $r^* = r/R$. Equation (44) relates v_{max} and J , which drop out after substitution, leading to Equation (48).

$$\frac{\rho R^2}{\mu T} \frac{\partial v^*}{\partial t^*} = 4 + \frac{1}{r^*} \frac{\partial}{\partial r^*} \left(r^* \frac{\partial v^*}{\partial r^*} \right) \quad (48)$$

By setting the leading factor on the left-hand side to unity, we identify the response-time scale as shown by Equation (49).

$$T = \frac{\rho R^2}{\mu} \quad (49)$$

This is the same as for flow between two flat plates in Equation (37), except for containing the radius (half-diameter) R instead of plate half-distance B . Solutions of the temporal evolution of velocity profiles from Equation (48) are depicted in Figure 10.

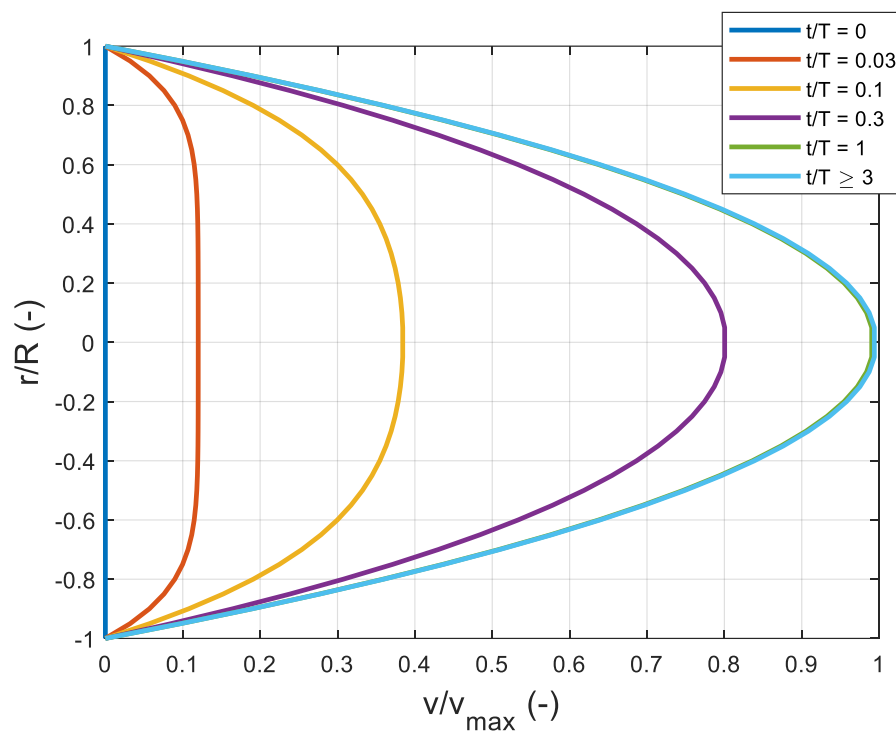


Figure 10 - Solutions of the velocity profile from Equation (48) with T from Equation (49) for different non-dimensional times t/T after starting from rest at $t=0$. The effects of shear stresses develop first in the form of velocity gradients near the pipe walls at $r = \pm R$ and then propagate inward. At $t \approx T$, the velocity profile has practically reached its steady state shape (green line under light blue line for $t \geq 3T$).

4 Inviscid Flow and Euler's Equation

In Sections 3.2 and 3.3, we considered fluid flowing in the form of laminae, where velocity could change over time or between laminae, but otherwise was bound to be uniform along laminae. This provides a relatively simple means to illustrate the effects of viscous frictional forces (shear stresses) between laminae and the associated transient flow regime, where inertial forces due to local acceleration (i.e., $\partial v/\partial t$) are relevant before steady-state velocity profiles are established.

In this section, we change the perspective, assuming zero viscosity (i.e., inviscid flow) where *inertial forces due to convective acceleration* (i.e., $\partial v/\partial s \neq 0$, where bulk flow is in the s -direction) may also be significant. As in Section 3, we maintain the condition of a homogeneous and incompressible fluid, meaning that ρ is constant in space and time. In practice, such conditions are relevant for the (subsonic) flow of air or water around objects like airplanes, hydrofoils, or bridge piers. For example, within a domain that includes neither (1) the viscous boundary layer immediately at the solid surface in contact with the flowing fluid, where the viscous no-slip condition applies, nor (2) possible turbulent wakes down-stream of the object.

The respective force balance on a fluid parcel in its direction s of movement is illustrated in Figure 11 resulting in a net driving force as shown by Equation (50).

$$F = (p_1 - p_2)\Delta A - F_{g,s} = (p_1 - p_2)\Delta A - \rho g \Delta z \Delta A \quad (50)$$

In this equation, we use $F_{g,s} = F_g \sin \alpha = \rho g \Delta z \Delta A$, since $F_g = mg$, $m = \rho \Delta s \Delta A$, and $\sin \alpha = \Delta z/\Delta s$ from the identical angles α indicated by the red arcs in Figure 11.

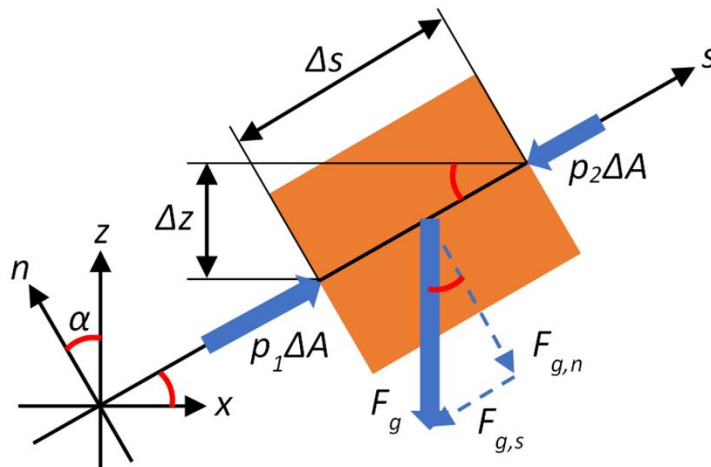


Figure 11 – An inviscid fluid parcel (orange patch) of length Δs and cross-sectional area ΔA moving in direction s with forces (blue arrows) acting due to pressure and gravity. In contrast to Figure 7 and Figure 9, there are no shear stresses, because flow is inviscid, but flow velocity and direction may change along the flow path.

Newton's law of motion from Equation (4) states that this net driving force must be balanced by the inertial force mdv/dt . However, velocity $v(s,t)$ is now both a function of time t as well as location s . This means that it can be uniform in space while changing with time, which is called local acceleration $\partial v/\partial t$ (where the partial derivative $\partial/\partial t$ is used to indicate that v is a function of more than one variable).

In contrast, flow velocity may not change in time (steady state), but it may change with location, which is called convective acceleration due to $\partial v/\partial s \neq 0$. This can be imagined by considering flow that converges as it passes through a tapered nozzle, where v increases along the flow path, but does not change with time at any location. Of course, both local and convective accelerations may occur simultaneously and by the chain rule of differentiation the *total (or material) derivative* $dv(s,t)/dt$ of velocity with respect to time is shown by Equation (51).

$$\frac{dv}{dt} = \frac{\partial v}{\partial t} \frac{\partial t}{\partial t} + \frac{\partial v}{\partial s} \frac{\partial s}{\partial t} = \frac{\partial v}{\partial t} + v \frac{\partial v}{\partial s} \quad (51)$$

This recognizes that s is also a function of t through the respective partial derivative in the center expression, while substituting $v = \partial v/\partial t$ in the final expression. As opposed to the local acceleration $\partial v/\partial t$, the convective acceleration is expressed by the term $v\partial v/\partial s$, and the total acceleration is the sum of both. Thus, we rewrite Equation (4) as Equation (52).

$$\frac{\partial v}{\partial t} + v \frac{\partial v}{\partial s} = \frac{F}{m} \quad (52)$$

With F from Equation (50), and parcel mass $m = \rho \Delta s \Delta A$, we arrive at Equations (53) and (54) after converting the right-hand side to differential form.

$$\frac{\partial v}{\partial t} + v \frac{\partial v}{\partial s} \approx \frac{1}{\rho} \left[\frac{(p_1 - p_2)}{\Delta s} - \rho g \frac{\Delta z}{\Delta s} \right] \quad (53)$$

$$\frac{\partial v}{\partial t} + v \frac{\partial v}{\partial s} = -\frac{1}{\rho} \left[\frac{\partial p}{\partial s} + \rho g \frac{\partial z}{\partial s} \right] \quad (54)$$

Equation (54) is known as Euler's equation [↗](#) for the direction aligned with flow, as opposed to perpendicular. At steady state when $\partial v/\partial t = 0$ and knowing $dv^2/ds = 2v dv/ds$ from the chain rule of differentiation, Equation (54) may also be written in the well-known form shown by Equation (55).

$$\frac{\rho}{2} \frac{dv^2}{ds} + \frac{dp}{ds} + \rho g \frac{dz}{ds} = 0 \quad (55)$$

When the hydraulic head $h = p/\rho g + z$ is introduced as was done for Equations (27) and (41), then Equation (55) becomes Equation (56).

$$\frac{\partial v}{\partial t} + v \frac{\partial v}{\partial s} = -g \frac{\partial \left(\frac{p}{\rho g} + z \right)}{\partial s} = -g \frac{\partial h}{\partial s} \quad (56)$$

In general, the direction s of flow is unknown and velocity $v(x,z,t)$ has to be considered as a general function of spatial coordinates x and z (for two-dimensional flow in a vertical plane) and time t . After expanding Equation (52) to involve two convective

acceleration terms (for accommodating two-dimensional flow in not only the s direction but in both the x and z directions), the force balance of Figure 11 remains applicable. With this, Equation (54) becomes Equation (57) and (58) for $s = x$ ($\alpha = \pi/2$) and $s = z$ ($\alpha = 0$), respectively.

$$\frac{\partial v_x}{\partial t} + v_x \frac{\partial v_x}{\partial x} + v_z \frac{\partial v_x}{\partial z} = -\frac{1}{\rho} \left[\frac{\partial p}{\partial x} + \rho g \frac{\partial z}{\partial x} \right] \quad (57)$$

$$\frac{\partial v_z}{\partial t} + v_x \frac{\partial v_z}{\partial x} + v_z \frac{\partial v_z}{\partial z} = -\frac{1}{\rho} \left[\frac{\partial p}{\partial z} + \rho g \frac{\partial z}{\partial z} \right] \quad (58)$$

These are Euler's equations in two-dimensional cartesian coordinates, which could be simplified by using $\partial z/\partial x = 0$ because elevation z does not change in the horizontal direction x , and $\partial z/\partial z = 1$. But not doing so, we may again use the hydraulic head h to write Equation (59) and (60).

$$\frac{\partial v_x}{\partial t} + v_x \frac{\partial v_x}{\partial x} + v_z \frac{\partial v_x}{\partial z} = -g \frac{\partial h}{\partial x} \quad (59)$$

$$\frac{\partial v_z}{\partial t} + v_x \frac{\partial v_z}{\partial x} + v_z \frac{\partial v_z}{\partial z} = -g \frac{\partial h}{\partial z} \quad (60)$$

These are two equations that result from applying the force (momentum) balance based on Newton's second law of motion containing three unknown variables v_x , v_z , and h . The system may be solved after also including a third equation establishing mass balance. This is discussed further in Section 7 related to groundwater flow.

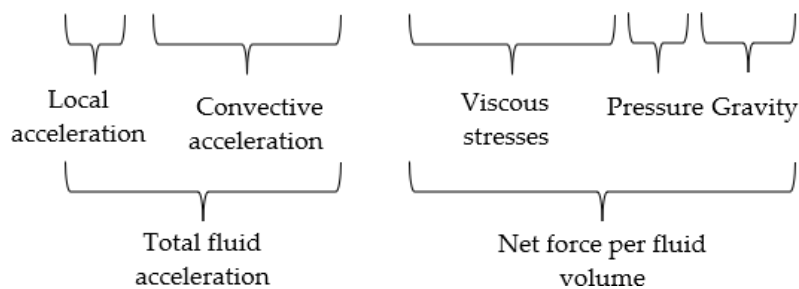
5 Navier-Stokes Equation and Reynolds Number

As discussed at the beginning of Section 3.2, the forces that may act on a fluid (parcel) may be due to pressure and viscous stress as surface forces, as well as gravity as the relevant body force in groundwater science. These driving and resisting forces result in a net force that must be balanced by inertial forces due to local and/or convective acceleration according to Newton's second law of motion.

All of Section 3 was dedicated to viscous flow, where convective acceleration was either negligible (flow around sphere) or zero (straight Poiseuille flow). Section 4 discussed the opposite situation of zero viscosity and, hence, no shear stresses, while accounting for convective acceleration (i.e., spatial changes in flow velocity). Combining all mechanisms leads to the Navier-Stokes equations as the most general formulation of momentum balance in a fluid. Based on Equation (57) and (58), we achieve this by including viscosity and second derivative viscous stress terms analogous to Equation (27), resulting in Equations (61) and (62).

$$\frac{\partial v_x}{\partial t} + v_x \frac{\partial v_x}{\partial x} + v_z \frac{\partial v_x}{\partial z} = \frac{1}{\rho} \left[\mu \left(\frac{\partial^2 v_x}{\partial x^2} + \frac{\partial^2 v_x}{\partial z^2} \right) - \frac{\partial p}{\partial x} - \rho g \frac{\partial z}{\partial x} \right] \quad (61)$$

$$\frac{\partial v_z}{\partial t} + v_x \frac{\partial v_z}{\partial x} + v_z \frac{\partial v_z}{\partial z} = \frac{1}{\rho} \left[\mu \left(\frac{\partial^2 v_z}{\partial x^2} + \frac{\partial^2 v_z}{\partial z^2} \right) - \frac{\partial p}{\partial z} - \rho g \frac{\partial z}{\partial z} \right] \quad (62)$$



For these equations, attention has been limited to the incompressible flow of a homogeneous fluid (i.e., density is constant both in time and space) in a two-dimensional vertical plane. In the general three-dimensional case including a velocity component v_y , Equations (61) and (62) would be complemented by a respective third equation, as well as first- and second-order derivative terms in y for v_x and v_z .

This is not a rigorous derivation, especially of the viscous term, which contains rather complex physical and mathematical aspects. However, presenting and discussing Equations (61) and (62) is instructive for several reasons. First, we identify the overall form of Newton's second law of motion of Equation (3) or (4) in that the left-hand sides of Equations (61) and (62) represent the total fluid acceleration $a = dv/dt$, while the bracketed term on the right-hand side represents the net effect F of all driving and resisting forces per unit fluid volume. The bracketed term is divided by density ρ which is mass per unit fluid

volume, so fluid volume cancels out leaving force per fluid mass equal to acceleration, which is again Newton's second law of motion.

Second, the term for viscous stresses containing second-order derivatives is also known as the Laplace operator and describes the diffusive transport of momentum. As such, its mathematical effect is to bring the velocity at a location toward the mean velocity of its immediate surroundings. Equations (61) and (62) could be reformulated in a coordinate system that is aligned with the local direction of flow as was done with Equation (54). However, this is not very useful because in general—and especially when turbulence occurs—the flow field is unknown. Moreover, due to the Laplace operator, there always remains a second derivative in the direction(s) perpendicular to flow.

Third, under hydrostatic conditions (i.e., when all velocities are zero), then Equations (61) and (62) reduce to $\partial p/\partial x = 0$ and $\partial p/\partial z = -\rho g$, correctly reflecting that p is constant in the horizontal direction, while $p = -\rho g z$ in the vertical direction. Finally, we again introduce the hydraulic head $h = p/\rho g + z$ to arrive at Equations (63) and (64).

$$\frac{\partial v_x}{\partial t} + v_x \frac{\partial v_x}{\partial x} + v_z \frac{\partial v_x}{\partial z} = \frac{\mu}{\rho} \left(\frac{\partial^2 v_x}{\partial x^2} + \frac{\partial^2 v_x}{\partial z^2} \right) - g \frac{\partial h}{\partial x} \quad (63)$$

$$\frac{\partial v_z}{\partial t} + v_x \frac{\partial v_z}{\partial x} + v_z \frac{\partial v_z}{\partial z} = \frac{\mu}{\rho} \left(\frac{\partial^2 v_z}{\partial x^2} + \frac{\partial^2 v_z}{\partial z^2} \right) - g \frac{\partial h}{\partial z} \quad (64)$$

Equation (63)—and, similarly, Equation (64)—may be rewritten by adopting the dimensionless variables $v_x^* = v_x/v$, $t^* = t/T$, $x^* = x/L$, $z^* = z/L$, and $h^* = h/h_0$, where v , T , L , and h_0 are characteristic velocity, time, length, and head scales for a given problem, yielding Equation (65).

$$\frac{v}{T} \frac{\partial v_x^*}{\partial t^*} + \frac{v^2}{L} \left(v_x^* \frac{\partial v_x^*}{\partial x^*} + v_z^* \frac{\partial v_x^*}{\partial z^*} \right) = \frac{\mu v}{\rho L^2} \left(\frac{\partial^2 v_x^*}{\partial x^{*2}} + \frac{\partial^2 v_x^*}{\partial z^{*2}} \right) - \frac{g h_0}{L} \frac{\partial h^*}{\partial x^*} \quad (65)$$

This shows that for a fluid with a hydraulic head distribution h^* , the dynamics (i.e., temporal changes $\partial v_x^*/\partial t$) of flow depends on the contributions of the convective acceleration and viscous stress terms. The importance of each mechanism is expressed by the coefficients before the parenthetical terms, which are both dimensionless and of unit order-of-magnitude. Quantification of this relative importance is achieved by dividing the coefficient v^2/L by the coefficient $\mu v/(\rho L^2)$, resulting in a dimensionless magnitude known as Reynolds number Re as shown by Equation (66).

$$Re = \frac{\rho v L}{\mu} \quad (66)$$

For $Re = 0$, we return to the situation of viscous flow described by Stokes' equation as considered in Section 3, whereas in the opposite case of $Re = \infty$, Euler's equations for inviscid flow from Section 4 are recovered. The non-linearity of the convective acceleration term also introduces significant complexity and, for large enough values of Re , turbulence may arise as an expression of highly chaotic flow behavior. Thus, solutions of the Navier-Stokes equation include the well-organized laminar flow for small values of Re , and

also the chaotic movement of fluid parcels in turbulent flow for large values of Re . The Reynolds number is a simple and important mathematical tool to distinguish between laminar and turbulent flow regimes with schematic illustrations of both cases shown in Figure 12.

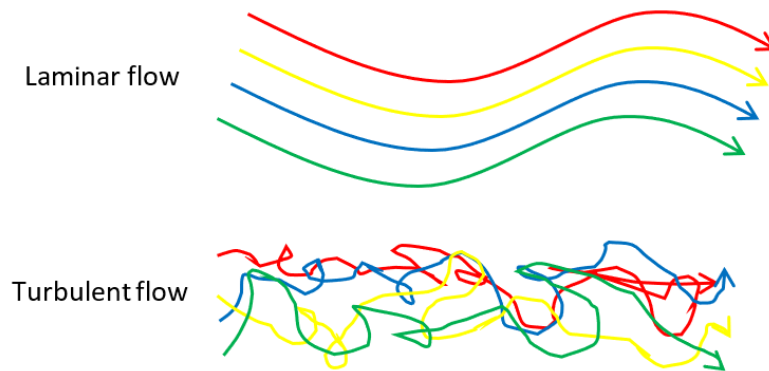


Figure 12 - Schematic examples of trajectories for well-ordered, but not necessarily straight, laminar flow (top) and chaotic turbulent flow (bottom). For a video of turbulent pipe flow, see <https://youtu.be/6VRgKIPhwng>. For further illustrations of fluid flow in general, see <https://qfm.aps.org/> and <http://www.flowillustrator.com> where you can also create your own simulations.

To provide an alternative—and perhaps more intuitive—perspective on the meaning of the Reynolds number, we return to Equation (65) and assume that inertial effects due to convective acceleration are dominant. After dividing the equation by a correspondingly large value of v^2/L , we arrive at Equation (67).

$$\frac{L}{vT} \frac{\partial v_x^*}{\partial t^*} + v_x^* \frac{\partial v_x^*}{\partial x^*} + v_z^* \frac{\partial v_x^*}{\partial z^*} \approx 0 \quad (67)$$

This order-of-magnitude equality can only be true if the leading coefficient $L/(vT)$ is of unit order-of-magnitude resulting in an inertial response-time scale T_{in} as shown by Equation (68).

$$T_{in} = \frac{L}{v} \quad (68)$$

This inertial response-time scale may also be regarded as the time scale of convective momentum transport. In rather simplistic terms, recall Equation (6) defined the linear momentum M of a body of mass m at velocity v as $M = mv$. Since the body moves at velocity v with momentum M , the rate of momentum transport (or momentum flux) is $Mv = mv^2$. From this, the convective transport of momentum M occurs at a velocity v , such that the transport time scale over some length scale L becomes T_{in} from Equation (68).

Assuming that viscous effects are dominant in Equation (65) and dividing the equation by a correspondingly large value of $\mu\nu/(\rho L^2)$ yields Equation (69).

$$\frac{\rho L^2}{\mu T} \frac{\partial v_x^*}{\partial t^*} \approx \frac{\partial^2 v_x^*}{\partial x^{*2}} + \frac{\partial^2 v_x^*}{\partial z^{*2}} \quad (69)$$

Again, this order-of-magnitude equality can only hold if the leading coefficient $\rho L^2/(\mu T)$ is of unit order-of-magnitude resulting in a viscous response-time scale T_{vis} as shown by Equation (70).

$$T_{vis} = \frac{\rho L^2}{\mu} \quad (70)$$

This agrees with Equation (37) and Equation (49) if L is considered either as the half-width B between plates or as the pipe radius R .

Using Equations (68) and (70), we now see that the Reynolds number of Equation (66) is also equal to $Re = T_{vis}/T_{in}$ (i.e., the ratio of viscous to inertial response-time scales). This relates back to the relative efficiency of each mechanism. For small Reynolds numbers, $T_{vis} < T_{con}$ meaning that the viscous effects work much faster to establish the well-ordered flow paths of laminar flow than any perturbations can propagate by convection. In contrast, for large Reynolds numbers, $T_{vis} > T_{con}$, and the opposite is the case. Random inertial perturbations to the flow field arise and propagate much faster than they can be dissipated by viscous friction, leading to the chaotic flow patterns of turbulence.

6 Flow Through Porous Media and Darcy's Law

6.1 Negligible Inertia and Continuum Perspective

Flow through porous media is a highly important topic in groundwater science because it allows describing the movement of water through the subsurface. The principles of flow culminating in the Navier-Stokes equation discussed in Section 5 remain applicable, but it is generally not possible to directly use it in practice. The boundary conditions of flow at the microscopic pore scale—that is, the exact geometric properties of the solid-fluid interface—are extremely complex and unknown. To acquire an appreciation of this unknown complexity, it is helpful to imagine the complicated pore space geometry in a granular aquifer and the variable nature of the grain surfaces. Luckily, when applied to slow flow through porous media, the Navier-Stokes equation is amenable to significant simplifications by neglecting effects of inertia. Moreover, the complex pore structure may be regarded from a macroscopic (spatial average) perspective over many pore scales, where both the porous medium and the fluid behave as continua occupying the same space.

A *macroscopic fluid parcel* moving through a porous medium of porosity θ is illustrated in Figure 13. Comparison of Figure 13 with Figure 11 that portrays inviscid flow shows a friction force F_f acting throughout the fluid parcel to resist flow. Thus, F_f may be considered as a body force per unit fluid volume, which represents the average macroscopic effect of the complex frictional surface forces acting at the microscopic scale throughout the pore network. With this, Equation (61) may be rewritten for a general flow direction s as indicated in Figure 13, while substituting the viscous stress term by F_f to arrive at Equation (71).

$$\frac{\partial v}{\partial t} + v \frac{\partial v}{\partial s} = \frac{1}{\rho} \left[F_f - \frac{\partial p}{\partial s} - \rho g \frac{\partial z}{\partial s} \right] \quad (71)$$

This equation is also a direct extension of Equation (54) where F_f is added to the other forces per unit fluid volume of density ρ in brackets. By regarding everything in terms of unitary fluid volume, porosity θ drops out.

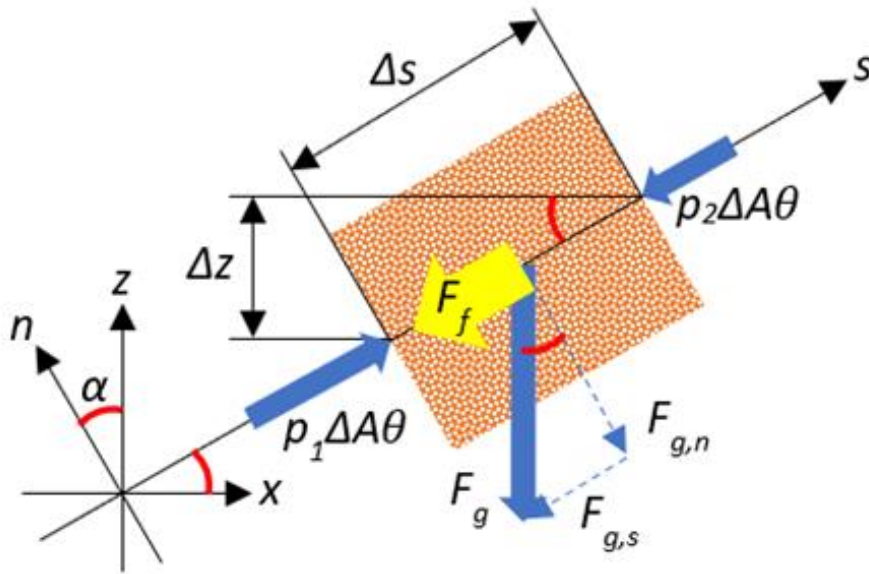


Figure 13 - Extension of Figure 11 to consider a macroscopic (Darcy scale) fluid parcel (orange) traveling through a porous medium (white dots) of porosity θ , where friction acts as an additional resisting body force F_f (yellow arrow) on the fluid parcel besides pressure and gravity. Although friction is a surface force in principle, it is considered to be an effective body force per unit fluid volume by assuming that the fluid parcel is much larger than the grains of the stationary matrix, and that friction against individual grains is spatially distributed over the fluid volume.

Flow through the interconnected pore space of a porous matrix may be imagined as the movement of a fluid along a network of narrow tortuous conduits of variable cross-sectional shapes and sizes that typically do not exceed the millimeter scale, that is, $< 10^{-3}$ m. Laboratory and field experience also tells us that groundwater flow velocities are generally on the order of centimeters per day or smaller and very rarely reach meters per day (i.e., $v < 10^{-5}$ m/s). Knowing $\rho = 10^3$ kg/m³ and $\mu = 10^{-3}$ kg/(ms) for water, Equation (66) delivers $Re < 10^{-2}$, which indicates that viscous effects strongly dominate over inertial effects and laminar (as opposed to turbulent) flow prevails. Mathematically, this implies that the *convective acceleration term becomes negligible* (i.e., $v\partial v/\partial s \approx 0$), simplifying Equation (71) into Equation (72).

$$\frac{\partial v}{\partial t} = \frac{1}{\rho} \left[F_f - \frac{\partial p}{\partial s} - \rho g \frac{\partial z}{\partial s} \right] \quad (72)$$

Based on the typical parameter values above and Equation (70), we further arrive at $T_{vis} < 1$ s as the time scale for transient flow effects to dissipate and steady-state laminar flow velocity profiles to establish at the microscale. This is much shorter than typical time scales of interest to hydrogeologists (like days, months, years or more) and indicates that the *quasi-steady-state assumption* is an appropriate simplification (i.e., $\partial v/\partial t \approx 0$). This means that any changes in hydraulic driving forces “immediately” propagate into corresponding changes in flow velocity. In both Figure 8 and Figure 10, this corresponds to $t/T \gg 1$, also

showing that effects of transient changes in the flow profiles across the pores can be neglected. Exercise 1 also provides an example of applying the quasi-steady-state assumption. Hence, Equation (72) becomes Equation (73) representing the frictional force per unit fluid volume.

$$F_f = \frac{dp}{ds} + \rho g \frac{dz}{ds} \quad (73)$$

When density ρ and acceleration of gravity g are constants, this may be reformulated by combining the derivatives as shown by Equation (74).

$$\frac{F_f}{\rho g} = \frac{d\left(\frac{p}{\rho g} + z\right)}{ds} = \frac{dh}{ds} = J \quad (74)$$

In Equation (74) the *hydraulic head* h in dimensions of length, and the dimensionless *hydraulic gradient* J are defined by Equations (75) and (76).

$$h = \frac{p}{\rho g} + z \quad (75)$$

$$J = \frac{dh}{ds} \quad (76)$$

Since F_f is a force per unit fluid volume and ρg is the force of gravity (i.e., weight) per unit fluid volume, Equation (74) shows that J represents a driving force per unit fluid weight.

To further analyze the nature of the porous frictional force F_f , we recall results in Section 3.2 and Section 3.3 for the two extremely regular conduit shapes delimited by flat plates and along a circular pipe. By substituting Equation (74) for J in Equation (33) and Equation (46), we find $F_f = -3v_{mean}\mu/B^2$ and $F_f = -8v_{mean}\mu/R^2$, respectively, where the negative sign indicates that F_f acts in the direction opposite to flow velocity v_{mean} . Using L as a characteristic length scale (i.e., for B and R here) and N as a proportionality constant depending on the flow geometry (e.g., planar versus circular, or any irregular shape in a porous medium), results in Equation (77).

$$F_f = -\frac{N\mu}{L^2} q \quad (77)$$

In Equation (77), porosity θ is embedded in N , and the volumetric flux shown in Equation (78) is introduced.

$$q = \theta v_{mean} = \frac{Q}{A} \quad (78)$$

While v_{mean} represents the average linear seepage velocity through the pore space, q expresses the velocity calculated as if the fluid discharge Q (fluid volume per time) passed through a unit cross-sectional area A of the bulk porous medium (i.e., including pores and solids). Sometimes q is called *Darcy flux* or *specific discharge*. For many more details on the meaning, importance, and measurement of seepage velocity, see the GW-Project book [Groundwater Velocity](#) (Devlin, 2020).

Alternatively, if the fluid parcel in Figure 13 is assumed to be stationary, then identical flow conditions could be imagined by moving the solid grains at a velocity v_{mean} against the fluid. For a single spherical particle moving through a fluid in the laminar flow regime, the frictional force is given by Equation (23). Using a length scale L for diameter $2R$, and after division by volume L^3 , we find $F_f = -3\pi v_{mean}\mu/L^2$ as the frictional force per volume, which further corroborates Equation (77).

The coefficient $N\mu/L^2$ of Equation (77) may be regarded as a Stokes (drag) friction factor f_{sto} described in Section 2, but here it is per unit fluid volume. As derived from first principles and the Navier-Stokes equation by Hubbert (1940, 1957), it is interesting to observe that this frictional term contains the dynamic viscosity μ as purely a fluid property, and intrinsic permeability k as a property pertaining only to the porous medium. This is presented in Equation (79).

$$k = \frac{L^2}{N} \quad (79)$$

The dimensionless coefficient N describes the geometric properties of the pore space, such as pore cross-sectional shapes, tortuosity, and spacing/interconnectivity, while L^2 accounts for the geometric scaling. In other words, if a porous medium of perfect spheres with 1 mm diameter were rebuilt with spheres of 1 cm diameter in an identical packing arrangement, then N would not change, while L would increase by a factor of 10 (i.e., L^2 would increase by a factor of 100).

Thus, Equation (77) may be substituted into Equation (74) to arrive at the differential form of Darcy's law as shown by Equation (80).

$$q = -\frac{\rho g k}{\mu} \frac{dh}{ds} = -K \frac{dh}{ds} = -KJ \quad (80)$$

Here, K is hydraulic conductivity used in the general expression of Darcy's law ($q = -KJ$) as defined by Equation (81).

$$K = \frac{\rho g k}{\mu} \quad (81)$$

Conductivity K has dimensions of length per time and is inversely proportional to a Stokes friction factor per unit fluid weight, thus it represents the facility for flow to occur in response to a given hydraulic gradient J .

Further details on this topic are provided in other GW-Project books Conceptual and Visual Understanding of Hydraulic Head and Groundwater Flow (Cohen & Cherry, 2020) and Hydrogeologic Properties of Earth Materials and Principles of Groundwater Flow (Woessner & Poeter, 2020; in particular their Box 3). Moreover, Bear (1972) gives an overview of different derivations of Darcy's law. Here we present only a few additional remarks:

1. For one-dimensional flow in the direction of coordinate s , Equations (78) and (80) may be combined into Equation (82).

$$Q = -AK \frac{dh}{ds} \quad (82)$$

Multiplying Equation (82) by $ds/(AK)$ and integrating between two locations s_1 and s_2 along a flow path of constant discharge Q , but possibly variable cross-sectional area A and conductivity K , gives Equation (83).

$$Q = -\frac{\Delta h}{R_K} \quad (83)$$

Equation (83) involves the head difference $\Delta h = h(s_2) - h(s_1)$, and a hydraulic resistance R_K presented as Equation (84).

$$R_K = \int_{s_1}^{s_2} \frac{1}{AK} ds \quad (84)$$

Considering the special case of a porous column of length ΔL with constant A and K , then $R_K = \Delta L/(AK)$ and Equation (70) becomes Equation (85).

$$Q = -AK \frac{\Delta h}{\Delta L} \quad (85)$$

This is the form that was initially inferred from laboratory column experiments by Darcy. [Exercise 4](#) and [Exercise 5](#) relate to hydraulic conductivity and its effective values under different idealized conditions.

2. The minimum volume of a fluid parcel for frictional force F_f to be considered a body (rather than surface) force exerted by many distributed grains as shown in Figure 13 is also called the *representative elementary volume* (REV) or the minimum *Darcy scale*. For porous media like sand, the REV is typically on the order of cubic centimeters, reflecting that Darcy's law is a macroscopic law with respect to individual (microscopic) grains and pore spaces.
3. Turbulence—particularly the transitions between laminar and turbulent flow regimes—are very complex processes. When dealing with granular media, it is natural to adopt an average grain or pore size diameter to represent the length scale L as in Equation (66). Based on this, experience has shown that Darcy's law is accurate for $Re < 1$, while for larger values, inertial effects may become significant, even when flow is not yet turbulent. High Reynolds numbers and exceptions to laminar flow may naturally occur in large karst flow conduits, where, for example, L can be on the order of meters for cave cross-sections. Turbulent flow conditions may also be induced near pumping wells due to flow convergence and large flow velocities. Inside pumping well casings, both L (well cross-section) and velocity along the axis of the well bore are larger than under ambient conditions in aquifers, where L is on the order of grain size and flow area is distributed over the surface of the well screen resulting in lower velocity than along the casing inside the bore. While F_f is proportional to q in the Darcy flow regime (Equation (77)) friction losses are larger in the case of turbulent flow and may be approximated by including a

quadratic friction term $-bq^2$ with the coefficient b depending on the specific setting, geometry, and completion of each pumping well. Thus, Equation (80) becomes $J = q/K + bq^2$. This was first suggested based on empirical observations by Forchheimer (1901).

4. Large transient time scales T_{vis} and significant effects of local acceleration $\partial v/\partial t$ may also occur in wellbore casings where L is on the order of centimeters and the time scale of interest may be short—on the order of tens of seconds—for example due to quickly changing flow velocities during oscillatory slug tests. This is explored in Exercise 14 though knowledge of elements in Section 7 are needed for this exercise, so we defer linking to Exercise 14 until those elements are discussed.
5. The introduction of hydraulic head h in Equation (74) required the assumption that density ρ and acceleration of gravity g are constant. In contrast, Equation (73) is the general force balance shown in Figure 13 and not limited by these restrictions, such that a generalized form of Darcy's law with respect to Equation (80) can be written as shown by Equation (86).

$$q = -\frac{k}{\mu} \left(\frac{dp}{ds} + \rho g \frac{dz}{ds} \right) \quad (86)$$

While it is reasonable to regard the acceleration of gravity g as constant in groundwater science, ρ may vary due to pressure changes (compressibility), variability of solute concentration, or temperature differences. In hydrogeology, compressibility is generally not relevant for force (or momentum) balances as considered here. However, compressibility may be important for mass balances, that is, for changes in groundwater storage, such as discussed in Section 7 and in the GW-Project book [Groundwater Storage in Confined Aquifers](#) (Wang, 2020). Thus, the main factors influencing ρ in Equation (86) are solute concentration and temperature when they vary in space and time. This scenario is treated in detail by the GW-Project book [Variable-Density Groundwater Flow](#) (Post & Simmons, 2022). [Exercise 6](#) presents a simplified hydrostatic example of the interaction between freshwater and denser saltwater that is relevant to coastal aquifers.

6.2 Hydraulic Head as Driving Force Potential

The *hydraulic head* h as defined in Equation (75) for constant fluid density is a fundamental variable in groundwater science for quantifying the combined effects of pressure and gravity as driving mechanisms for fluid movement. From a classical mechanics perspective, h may be viewed more specifically as the scalar potential of the driving force acting on the fluid per unit weight. This becomes clear by inspection of Equations (61) and (62) where pressure gradient and gravity appear as forces per unit volume, which become forces per unit weight after division by specific fluid weight, ρg (i.e., force of gravity per fluid volume), to arrive at h in Equation (74).

Being a scalar potential means that h has a single (scalar) value at each location and taking its spatial derivative in any direction results in a force per weight component for that location in that same direction. Consequently, the spatial gradient of h results in a force per weight vector that is aligned with the direction of largest change in h at a location and the vector's magnitude is equal to the (negative) steepness of that change in h . These forces per unit fluid weight are reflected by the terms $\partial h/\partial s$, $\partial h/\partial x$, and $\partial h/\partial z$ in Equations (27), (41), (56), (59), (60), (63), and (64), for example. Since h has the dimension of length, the spatial derivatives are dimensionless, which is consistent with the resulting driving force per weight field also being dimensionless.

All the other terms in Equations (27), (41), (56), (59), (60), (63), and (64) are related to viscosity and inertia, which are mechanisms resisting fluid movement. In the case of inviscid flow, Equation (56) shows that the driving force due to $\partial h/\partial s$ is balanced only by inertial forces such that a force on a fluid parcel causes its acceleration (Euler's second law of motion). In strong contrast, for flow-through porous media, Equation (74) reflects that the driving force on a macroscopic fluid parcel is purely balanced by frictional resistance. Since this frictional resistance is directly proportional to flow velocity, a given driving force on fluid in porous media results in a certain flow rate (Darcy's law) and not acceleration.

By *Newton's third law of motion*, the frictional force F_f that the stationary matrix exerts on the flowing fluid must be balanced by an opposite force of the same magnitude that the fluid exerts on the matrix. Depending on the flow direction, this counterforce may increase or decrease the compressional stress between solid grains due to gravity, thus affecting the *pore pressure distribution* and *effective stress* state of the solid matrix. This is discussed in detail in [Box 3](#). [Exercise 7](#) provides an opportunity to explore Darcy's law, gradient, and seepage force. [Exercise 8](#) is an extension of Exercise 7 that considers upward instead of downward flow through a sand column and determines the minimum density of sand grains required to avoid quicksand conditions.

In the case of fluid flow that is not within a porous medium as treated in Section 5, both friction and inertia may be relevant to forces on a water parcel, but hydraulic head, h , retains its significance as a scalar potential of a vector field representing driving force per fluid weight.

The seepage forces generated by upward flow of groundwater in discharge areas are an important factor in the development of landscape morphology due to enhanced erodibility at points of groundwater discharge. These forces are also of importance where construction alters the earth surface or the groundwater flow field such as at the toe of slopes in open pit mines or dams. When the upward force begins to move sediment particles, the flow path becomes shorter which raises the gradient, further increasing the seepage force. This negative feedback mechanism can result in a phenomenon called piping where groundwater flow erodes sediment and causes failure of the slope or dam.

In more intuitive terms beyond the considerations in Box 3, Equation (75) can be multiplied by ρg to arrive at the dynamic pressure for conditions where water is in motion (i.e., $p_{dynamic} = p - p_{hydrostatic}$) where $p_{dynamic} = \rho g h$ and $p_{hydrostatic} = -\rho g z$. When considering this, it is helpful to remember that z is positive upward. This shows that the hydraulic head h is proportional to the *dynamic* portion $p_{dynamic}$ of pressure p , which is sometimes called *excess pore pressure* and does not include the hydrostatic contribution to pressure $p_{hydrostatic}$. Hence, the hydraulic head is a useful concept in fluid mechanics because it relates to the forces within a fluid, which exist beyond the hydrostatic forces and are, hence, responsible for driving flow. Under hydrostatic conditions when $p = -\rho g z$, this expression demonstrates once more that $p_{dynamic} = 0$ (i.e., there is no driving gradient) because effects of pressure and gravity are opposite and fully cancel.

Since the hydraulic head gradient is a force per unit fluid weight, its integral along a flow path must represent some work or energy per unit fluid weight, for example as shown by Equation (7). For inviscid flow at steady state (i.e., $\partial v/\partial t = 0$), and knowing $2vdv/ds = dv^2/ds$, Equation (56) becomes $dv^2/(2g) = dh$. This shows that the change in hydraulic head is equal to the change in kinetic energy per unit weight of a fluid parcel traveling an infinitesimal distance ds .

This relationship between hydraulic head and kinetic energy per unit weight of a fluid parcel is further clarified by inspecting the expression for kinetic energy in Equation (8) after dividing by weight $V\rho g$. Moreover, for flow through porous media, multiplying Equation (74) by ds leads to $F_f ds/(\rho g) = dh$, showing that the change in hydraulic head in this case is equal to the frictional work per unit weight of fluid performed along ds .

This frictional work in the flow of groundwater is converted into thermal energy and is sometimes called *hydraulic loss*. Hydraulic loss causes an increase in temperature, which is too small to be measurable in typical situations of groundwater science. In any case, since the hydraulic head is a potential for force per unit fluid weight, its spatial derivative (gradient) is a force per unit fluid weight. Consequently, the gradient's path integral is hydraulic head and is equal to mechanical energy per unit weight of fluid that drives fluid flow and is converted into frictional and/or kinetic energy.

6.3 Hydraulic Head as Flux Potential

Under homogeneous (i.e., hydraulic conductivity K is constant in space) and isotropic (i.e., hydraulic conductivity is the same in all directions) conditions, Equation (80) may be written as shown by Equation (87).

$$q = -\frac{d(Kh)}{ds} \quad (87)$$

Equation (87) shows that hydraulic head h , or more specifically the product Kh , is a scalar potential for a vector field of Darcy fluxes q . This means that the spatial derivative of Kh in any direction equals the flux component at a location in that same direction. To illustrate

this graphically, consider flow of magnitude q_{s1} along a direction s_1 as shown in Figure 14, then the flux q_{s2} along an arbitrary direction s_2 at angle α to direction s_1 is equal to the expression in Equation (88).

$$q_{s2} = q_{s1} \cos \alpha = -K \frac{\Delta h}{\Delta s_1} \cos \alpha \quad (88)$$

In this equation, $\Delta h = h_2 - h_1$ and Δs_1 is the respective flow distance along s_1 . Figure 14 also indicates what is shown by Equation (89).

$$\Delta s_1 = \Delta s_2 \cos \alpha \quad (89)$$

This may be substituted into Equation (88) to find what is shown by Equation (90).

$$q_{s2} = -K \frac{\Delta h}{\Delta s_2} \quad (90)$$

This reaffirms that the flux q_{s2} in an arbitrary direction s_2 may be found from Darcy's law by simply using the hydraulic gradient dh/ds_2 in that same direction.

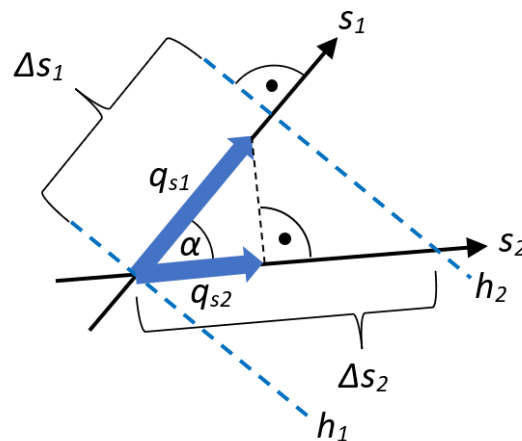


Figure 14 - Relationship between flux q_{s1} along direction s_1 to flux q_{s2} along direction s_2 at an arbitrary angle α . Constant hydraulic heads h_1 and h_2 are indicated by the blue dashed lines. The hydraulic gradient along the direction of flow perpendicular to the lines of constant heads is the largest, and it decreases to zero as α approaches 90° .

6.4 Anisotropy

Hydraulic conductivity K may be homogeneous, as considered in Section 6.3, or vary as a function of location under heterogeneous conditions. Moreover, K may also vary as a function of direction at a single location, which is known as *anisotropy*. In the latter case, K takes so-called principal values along mutually perpendicular principal directions, which may be imagined as the axes of an ellipsoid in three dimensions, or the axes of an ellipse in two dimensions. As illustrated in Figure 15, we focus on two dimensions and assume that the principal directions are aligned with the x and z -axes, along which hydraulic conductivities are equal to K_{xx} and K_{zz} , respectively. Given a hydraulic gradient J

as shown by Equation (91) in the direction s of orientation α , its components along the x and z -axes are expressed by Equations (92) and (93), respectively.

$$J = \frac{h_2 - h_1}{\Delta s} \quad (91)$$

$$J_x = J \cos \alpha \quad (92)$$

$$J_z = J \sin \alpha \quad (93)$$

The respective fluxes from Darcy's law result as shown by Equations (94) and (95).

$$q_x = -K_{xx}J_x = -K_{xx}J \cos \alpha \quad (94)$$

$$q_z = -K_{zz}J_z = -K_{zz}J \sin \alpha \quad (95)$$

With this, the orientation β and magnitude q of groundwater flux may be found from Equations (96) and (97).

$$\tan \beta = \frac{q_z}{q_x} = \frac{K_{zz}}{K_{xx}} \tan \alpha \quad (96)$$

$$q = \sqrt{q_x^2 + q_z^2} = K_{xx}J \sqrt{\cos^2 \alpha + \left(\frac{K_{zz}}{K_{xx}}\right)^2 \sin^2 \alpha} \quad (97)$$

where K_{zz}/K_{xx} is called the *anisotropy ratio*. Equation (96) shows that for $K_{zz}/K_{xx} \neq 1$, the directions of hydraulic gradient and groundwater flux no longer coincide as it is the case under isotropic conditions when $K_{zz}/K_{xx} = 1$. Also, using $K = K_{xx} = K_{zz}$ in Equation (97) shows that Darcy's law for isotropic conditions in Equation (80) is recovered given that $\cos^2 \alpha + \sin^2 \alpha = 1$.

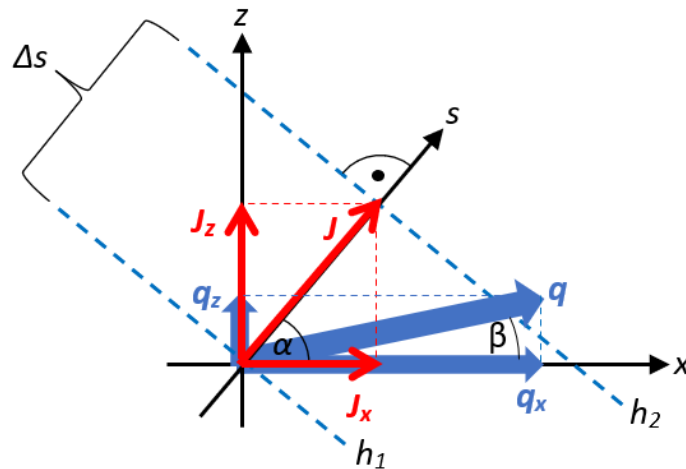


Figure 15 - Geometric decomposition of hydraulic gradient J (red arrows) in direction s into components J_x and J_z in the directions of the hydraulic conductivity anisotropy axes (here aligned with x and z). The corresponding flux components, q_x and q_z , constitute the flux vector q (blue arrows), which is not aligned with J under anisotropic conditions.

The principal axes of hydraulic conductivity do not necessarily have to be aligned with the coordinate axes as assumed here. However, the underlying principle remains the same, while the trigonometric operations become more cumbersome resulting in a hydraulic conductivity tensor (a two-by-two matrix). This tensor is symmetric containing values for K_{xx} and K_{zz} on its diagonal, with non-zero but equal values for $K_{xz} = K_{zx}$ otherwise. The latter account for the contributions of J_x to q_z and of J_z to q_x . The same applies to the extension for three dimensions, where operations of vector algebra become efficient tools as shown in [Box 4](#) ↓.

7 Conservation of Mass and Flow Equations

Section 6.1 demonstrated that Darcy's law is a force balance for flow through porous media, which implements the principle of conserving momentum by a series of simplifications to the Navier-Stokes equation. Besides momentum conservation, there is also the physical principle of mass conservation⁷, of which some ancient cultures were aware and was later tested and formulated more rigorously by the chemists Lomonosov and Lavoisier in the eighteenth century.

Within the realm of classical mechanics, the law of mass conservation postulates that *matter cannot be created or destroyed*. For fluids with a constant density and as illustrated in Figure 16, this implies the very simple concept that the volume of fluid stored in a reservoir must grow as fluid is added (inflow) and decrease as fluid is taken away (outflow). If volumetric changes are not permitted, this means that inflow must equal outflow. Mathematically, the law of mass conservation for fluids of constant density may be written as Equation (98).

$$\Delta V = (Q_{in} - Q_{out})\Delta t \quad (98)$$

where:

ΔV = change in fluid volume stored (L^3)

Q_{in} = inflow (L^3T^{-1})

Q_{out} = outflow (L^3T^{-1})

Δt = time interval (T)

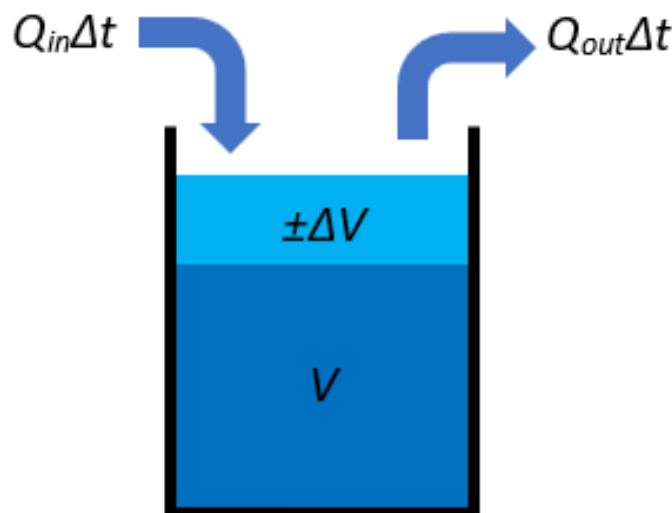


Figure 16 - Law of mass conservation (Equation (98)) for a fluid of constant density, postulating that the volumetric change ΔV of fluid stored in a reservoir is equal to the difference between inflow Q_{in} and outflow Q_{out} during a time period Δt .

Now consider a reservoir such as presented in Figure 16 that is connected to four other reservoirs as depicted in Figure 17. Each reservoir has its hydraulic head (e.g., water level) h and the reservoirs exchange fluxes q across their common sides. For the center reservoir, Equation (98) then becomes Equation (99).

$$\frac{\Delta V}{\Delta t} = (q_{x1}\Delta z_{x1} - q_{x2}\Delta z_{x2})\Delta y + (q_{y1}\Delta z_{y1} - q_{y2}\Delta z_{y2})\Delta x \quad (99)$$

where:

Δz = height of the reservoir interfaces in the third dimension, over which flow occurs between neighboring reservoirs (L)

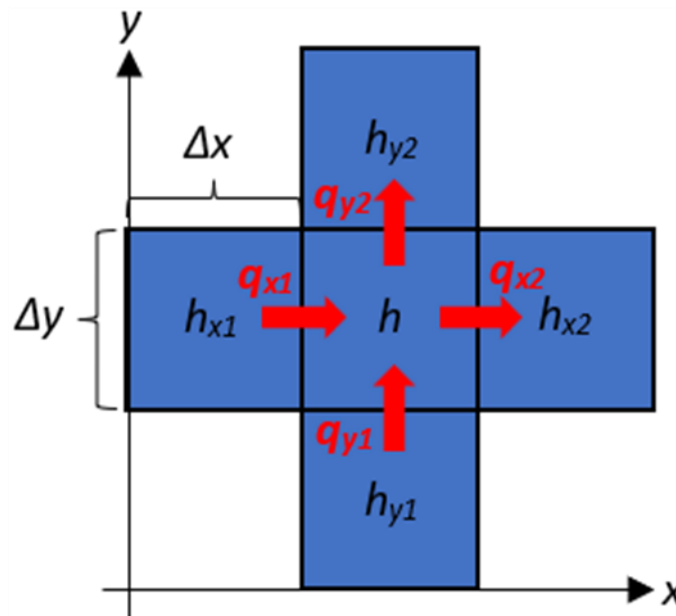


Figure 17 - Five interacting reservoirs of size $\Delta x\Delta y$ in the horizontal plane at hydraulic heads h and exchanging fluxes q (red arrows).

The volumetric change ΔV may be related to respective changes in head Δh as shown by Equation (100).

$$\Delta V = S_y \Delta h \Delta x \Delta y \quad (100)$$

where:

S_y = specific yield (dimensionless)

Specific yield quantifies the volumetric change in fluid storage per unit change in head (i.e., per unit change in water table elevation in an unconfined aquifer) for a unit horizontal area of aquifer. For a reservoir as in Figure 16, S_y would be one. If the reservoir were filled with a porous material (e.g., sand) extending above any change in water level, S_y would be equal to the drainable porosity of the porous material.

If the reservoir in Figure 16 had a lid on its top at a constant elevation Δz above its bottom, then changes in water level elevation for storing or releasing water would not be possible. Still, changes in fluid pressure, and hence hydraulic head, lead to elastic deformation (i.e., compression and expansion) of both the fluid and, if present, the porous matrix. This results in small changes in fluid density and matrix porosity such that the change in fluid volume (for the fluid considered at some reference pressure, often atmospheric pressure) relates to a respective change in head as shown in Equation (101). Wang (2020) discusses this in detail in the GW-Project book [Groundwater Storage in Confined Aquifers](#).

$$\Delta V = S_s \Delta h \Delta x \Delta y \Delta z \quad (101)$$

where:

$$S_s = \text{specific storage (L}^{-1}\text{)}$$

Specific storage quantifies the volumetric change in fluid storage per unit change in head (i.e., for a change in pore pressure in a confined aquifer) per unit volume of aquifer. Within the saturated domains of three-dimensional flow problems, S_s is the only relevant storage parameter.

Under unconfined conditions, changes in groundwater storage may simultaneously occur due to both water table fluctuations and elastic deformation such that the right-hand sides of Equations (100) and (101) may be summed to arrive at what is presented in Equation (102).

$$\Delta V = S \Delta h \Delta x \Delta y \quad (102)$$

where:

$$S = S_y + S_s \Delta z, \text{ the storativity or storage coefficient (dimensionless)}$$

In practice, $S_y \gg S_s \Delta z$ and $S = S_y$ is a reasonable approximation for unconfined aquifers. Under confined conditions, however, S_y does not exist—leaving a much smaller value of $S = S_s \Delta z$ as the relevant storage coefficient.

For confined conditions where Δz is a constant (or unconfined conditions, where changes in Δz are small compared to the average saturated aquifer thickness), substituting Equation (102) into Equation (99) and dividing by $\Delta x \Delta y$ gives Equation (103).

$$S \frac{\Delta h}{\Delta t} = \left(\frac{q_{x1} - q_{x2}}{\Delta x} + \frac{q_{y1} - q_{y2}}{\Delta y} \right) \Delta z \quad (103)$$

This corresponds to Equation (104) in differential form, where subscripts x and y with q indicate direction of the fluxes.

$$S \frac{\partial h}{\partial t} = - \left(\frac{\partial q_x}{\partial x} + \frac{\partial q_y}{\partial y} \right) \Delta z \quad (104)$$

Finally, assuming homogeneous conditions with constant hydraulic conductivity K and constant thickness Δz , and substituting Equation (80) for directions x and y into Equation (104), then dividing by the constant value of $K\Delta z$, leads to Equation (105).

$$\frac{S}{T_K} \frac{\partial h}{\partial t} = \frac{\partial^2 h}{\partial x^2} + \frac{\partial^2 h}{\partial y^2} \quad (105)$$

where:

$T_K = K\Delta z$ is the *hydraulic transmissivity* (L^2T^{-1}) of an aquifer with hydraulic conductivity K and thickness Δz

Box 5 provides an analogous derivation in radial coordinates that is relevant to flow toward a well.

The following short list of remarks relevant to aquifer dynamics also provides links to exercises that discuss additional simplified examples. Further details are discussed in the GW-Project book *Hydrogeologic Properties of Earth Materials and Principles of Groundwater Flow* by Woessner & Poeter (2020).

1. At *steady state*, changes in storage vanish such that $\partial h/\partial t = 0$ and Equation (105) for two-dimensional groundwater flow under confined, homogeneous and isotropic conditions becomes Equation (106).

$$\frac{\partial^2 h}{\partial x^2} + \frac{\partial^2 h}{\partial y^2} = 0 \quad (106)$$

This is also known as the *Laplace equation* governing *potential flow*. A simulator for potential flow as well as further definitions and derivations are available at <https://potentialflow.com>. The Laplace equation appears in many scientific fields, and many analytical solutions are available for specific boundary conditions. The extension to three dimensions is straightforward by adding a term in the z -direction (i.e., $\partial^2 h/\partial z^2$). Box 4 presents different mathematical formats for writing the Laplace equation.

2. As shown in Figure 18, Equation (105) can be generalized by including *groundwater extraction* q_{ex} (e.g., due to pumping) and *recharge* q_{re} (e.g., due to infiltration of precipitation) as additional terms in the mass balance of Equation (99), yielding Equation (107).

$$S \frac{\partial h}{\partial t} = T_K \left(\frac{\partial^2 h}{\partial x^2} + \frac{\partial^2 h}{\partial y^2} \right) + q_{re} - q_{ex} \quad (107)$$

In this equation, we emphasize that both q_{re} and q_{ex} appear in the dimensions of length per time (i.e., a discharge per unit surface area of the aquifer) and may vary in both space and time (like hydraulic head h can vary).

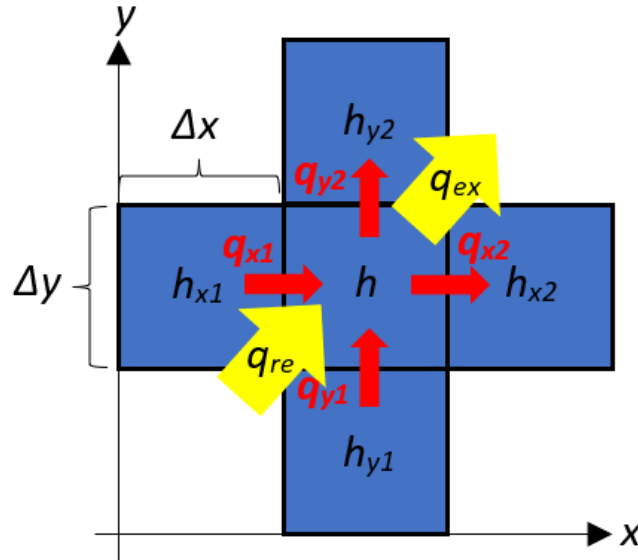


Figure 18 - Five interacting reservoirs as in Figure 17 of size $\Delta x \Delta y$ at hydraulic heads h and exchanging fluxes q (red arrows), while being exposed to recharge q_{re} and groundwater extraction q_{ex} (yellow arrows).

3. Under homogeneous but *anisotropic conditions*, K varies with direction such that $q_x = -K_{xx} \partial h / \partial x$ and $q_y = -K_{yy} \partial h / \partial y$, if the principal hydraulic conductivity directions with values K_{xx} and K_{yy} align with the respective coordinate axes (as discussed in Section 6.4). Thus, Equation (105) becomes Equation (108).

$$S \frac{\partial h}{\partial t} = T_{K,xx} \frac{\partial^2 h}{\partial x^2} + T_{K,yy} \frac{\partial^2 h}{\partial y^2} \quad (108)$$

where:

$$\begin{aligned} T_{K,xx} &= K_{xx} \Delta z \\ T_{K,yy} &= K_{yy} \Delta z \end{aligned} = \text{the respective magnitudes of anisotropic transmissivity}$$

4. Under *heterogeneous conditions*, K and/or Δz and hence, T_K may vary in space and cannot be taken out of the second derivative for being constants as is done in Equations (107) and (108). Equation (105) then becomes Equation (109).

$$S \frac{\partial h}{\partial t} = \frac{\partial}{\partial x} \left(T_K \frac{\partial h}{\partial x} \right) + \frac{\partial}{\partial y} \left(T_K \frac{\partial h}{\partial y} \right) \quad (109)$$

5. Under *unconfined conditions*, the water table in the aquifer is a free surface. Its elevation changes in the direction of flow such that the thickness Δz contributing to flow varies. When defining the head h as the vertical distance of the water table above a horizontal aquifer bottom and neglecting the vertical flow components (Dupuit-Forchheimer assumption ↗), then this may be accounted for by setting $T_K = Kh$ in Equation (109) leading to Equation (110).

$$S \frac{\partial h}{\partial t} = \frac{\partial}{\partial x} \left(Kh \frac{\partial h}{\partial x} \right) + \frac{\partial}{\partial y} \left(Kh \frac{\partial h}{\partial y} \right) \quad (110)$$

This renders a non-linear equation in h . However, knowing $\partial h^2/\partial x = 2h\partial h/\partial x$ by the chain rule of differentiation, the squared head h^2 may be regarded as a *discharge potential* since its spatial derivative $\partial h^2/\partial x$ is proportional to the depth integrated flux $hq_x = -Kh\partial h/\partial x$. Substituting for $h\partial h/\partial x$ in Equation (110), while assuming steady state and constant K , we arrive at Equation (111).

$$\frac{\partial^2 h^2}{\partial x^2} + \frac{\partial^2 h^2}{\partial y^2} = 0 \quad (111)$$

This is convenient, because available solutions to the Laplace equation (Equation (106)) remain valid for unconfined aquifers when working with a discharge potential proportional to h^2 . [Exercise 9](#) and [Exercise 10](#) illustrate the application of the Laplace equation in unconfined aquifers.

6. As outlined in Box 1, we can non-dimensionalize Equation (105) by introducing the dimensionless variables $h^* = h/h_0$, $t^* = t/T_{aqu}$, $x^* = x/L$, and $y^* = y/L$ resulting in Equation (112).

$$\frac{SL^2}{T_K T_{aqu}} \frac{\partial h^*}{\partial t^*} = \frac{\partial^2 h^*}{\partial x^{*2}} + \frac{\partial^2 h^*}{\partial y^{*2}} \quad (112)$$

This indicates a time scale of aquifer response T_{aqu} as shown by Equation (113).

$$T_{aqu} = \frac{SL^2}{T_K} \quad (113)$$

where:

L = horizontal aquifer length scale over which significant changes in h occur (L)

The similarity between Equation (113) and Equation (70) is due to the common diffusive character of the governing equations. The difference is that for the fluid flow discussed in Sections 3 and 5 momentum diffuses through shear stresses, while for flow in porous media hydraulic head diffuses through water fluxes. [Exercise 11](#) explores an analogy of this situation using a single reservoir model.

7. Depending on the type of aquifer (confined or not), typical values of S (Equation (102)) vary over orders of magnitude. Hence, aquifer response-time scale T_{aqu} (Equation (113)) may range from days to years, decades, and more, being an important descriptor of a watershed's baseflow dynamics. However, T_{aqu} is not representative of solute transport processes (e.g., contaminant plumes and travel times) because T_{aqu} is related to the propagation of hydraulic head (i.e., pressure) and not migration of solute particles or concentrations.
8. The time-scale of aquifer response and resulting hydraulic head distribution are illustrated by considering an unconfined aquifer under relatively pristine conditions (i.e., without groundwater extraction) between long parallel rivers of equal elevation without variability in the direction parallel to the rivers. If the

aquifer thickness below the river is much larger than the water table elevation above the rivers, then the aquifer transmissivity T_K may be assumed to be approximately constant and Equation (107) reduces to Equation (114).

$$\frac{\partial h}{\partial t} = \frac{1}{S} \left(q_{re} + T_K \frac{\partial^2 h}{\partial y^2} \right) \quad (114)$$

This has the same form as Equation (27) when substituting v for h , ρ for S , μ for T_K and $-\rho g \partial h / \partial s = -\rho g J$ for q_{re} , meaning that the hydraulic head in a simplified one-dimensional aquifer reacts to recharge in exactly the same way as flow velocity between two plates reacts to a driving force gradient. Thus, the solutions of Section 3.2 remain valid with the appropriate changes in variables such that Equation (31) gives Equation (115) after substituting $B = L$ for the half-width of the aquifer.

$$h_{max} = \frac{q_{re}}{2T_K} L^2 \quad (115)$$

This further implies that Figure 8 remains directly applicable if h/h_{max} is used on the abscissa, y/L on the ordinate, and t/T_{aqu} as the dimensionless time parameter. In this case, the half-width L of the aquifer is used as the relevant length scale because each half of the aquifer has the same response dynamics as the combination of both halves. Exercise 9 is a practical example of this dynamic and [Box 6](#) provides a digression on this dynamic related to a dimensionless parameter called the *water table ratio*.

9. The conservation of mass and momentum (or force balances) remains applicable to situations beyond the scenario of a single fluid in a fully saturated pore space as considered in this book. [Box 7](#) and [Box 8](#) provide mathematical derivations related to *flow in the unsaturated zone* and *flow of two immiscible fluids*, respectively. [Exercise 12](#), [Exercise 13](#), and [Exercise 14](#) present further practical applications of Darcy's law in combination with the principle of mass conservation related to methods for laboratory and in situ measurement of hydraulic conductivity.

8 Initial and Boundary Conditions

Sections 1 through 6 discuss the physical principles of force (or momentum) balances to arrive at Darcy's law as a constitutive relationship for flow through porous media. Section 7 uses this relationship in combination with the principle of continuity (i.e., conservation of mass) to derive governing equations of fluid flow, in particular, groundwater flow under a variety of simplified practical scenarios.

Applying these governing equations to solve for temporally and spatially variable distributions of hydraulic properties, heads, and fluxes, requires two more critical elements, namely (1) initial conditions and (2) boundary conditions. Initial conditions ↗ determine the state of a system (e.g., the spatial distribution of hydraulic heads) at the beginning of a period of interest, while boundary conditions ↗ define the system behavior along its spatial delimitation. Thus, based on a known initial state over the domain of interest and a known behavior along the spatial boundaries of that domain, a governing partial differential equation may be solved for the spatio-temporal dynamics of hydraulic heads or fluxes, for example.

The requirement and implementation of initial conditions is further illustrated in Box 2 as well as Exercise 3 and Exercise 10. For the relatively simple dynamic problems (i.e., mostly linear with a single steady state) considered here, the influence of initial conditions disappears over the characteristic system response-time scale as reflected by Figure 3, Figure 5, Figure 8, and Figure 10, as well as in Exercise 10. If initial conditions are uncertain or completely unknown, a model initialization—also known as a warm-up or spin-up—may be necessary. Model initialization consists of running the model for a period of several response-time scales before results are considered to be independent of possibly erroneous initial conditions and, thus, relevant for interpretation.

As to boundary conditions, there are different types with the three most important ones in groundwater science being (1) a specified head or Dirichlet boundary, (2) a specified flux or Neumann boundary, and (3) a weighted average of (1) and (2) known as a Robin boundary, with a special case of the Robin boundary known as the general head, or head-dependent flux, boundary.

A specified head boundary is mathematically defined by a function f as shown by Equation (116) for head h along a boundary of coordinates x_b and over time t .

$$h = f(x_b, t) \quad (116)$$

That is, the head may vary in a known fashion both along the boundary and in time. Numerically, in a finite difference framework, this is implemented by extending the grid cells of the modeling domain by a single line of cells around its circumference and assigning known values to the cells (e.g., as discussed in Exercise 10).

The mathematical formulation of a specified flux boundary is shown by Equation (117).

$$\frac{\partial h}{\partial n} = f(x_b, t) \quad (117)$$

where:

n = the coordinate normal to the boundary (L; typically directed outward)

Equation (117) represents the hydraulic gradient normal to the orientation of the boundary, which by Darcy's law is proportional to the fluid flux across the boundary. This means that a known flux entering or leaving the domain across its boundary may be implemented by this condition (hence the name). Like Equation (116), this may be achieved in a numerical finite difference scheme by imposing the prescribed gradient of Equation (117) between the added boundary cells and cells at the edge of the model domain. In many practical applications, this type of boundary condition is used to represent an impermeable (or no-flow) boundary, where $\partial h/\partial n = 0$ and the boundary cells are assigned the same head values as the limiting domain cells to assure this condition.

The Robin boundary condition is a weighted sum of the specified head and specified flux conditions resulting in Equation (118).

$$C_1 h + C_2 \frac{\partial h}{\partial n} = f(x_b, t) \quad (118)$$

This equation again collapses to Equation (116) and (117) for $C_2 = 0$ and $C_1 = 0$, respectively. Assuming that f is proportional to C_1 (i.e., $f(x_b, t) = C_1 h_b$), the Robin boundary condition may be reformulated as shown by Equation (119) where hydraulic conductivity K is substituted for C_2 , such that q_b represents the boundary flux into the domain.

$$q_b = K \frac{\partial h}{\partial n} = C_1 (h_b - h) \quad (119)$$

Equation (119) is a special case of the more general Robin condition and is also known as a *general head* or *head-dependent flux boundary*. It corresponds to the physical scenario of a specified head distribution h_b immediately outside the model domain which are connected to the model by a hydraulic conductance C_1 to admit a boundary flux q_b as a function of the head difference. For very small values of C_1 , the boundary becomes increasingly impermeable resulting in the no-flow condition $q_b = 0$. In the opposite case of very large values of C_1 , the boundary becomes increasingly permeable such that heads within the model are equal to the boundary heads, yielding the specified head condition of $h = h_b$ (e.g., as used in Exercise 10). Intermediate values of C_1 are often used along rivers that are directly connected to the saturated zone of an aquifer, where C_1 accounts for a smaller hydraulic conductivity of the riverbed material with respect to the aquifer (e.g., like the application of Darcy's law in Exercise 11).

In groundwater science, it is also common to encounter flow domains that are delimited by boundary segments over which different types of boundary conditions apply. These are called *mixed boundary conditions* and most typically consist of impermeable boundary segments in combination with one or more specified or general head segments. The specified head and specified flux conditions may also be applied separately and simultaneously to a domain boundary, which is referred to as *Cauchy condition*. This is different to the Robin or general head conditions of Equation (118) and Equation (119) in that boundary heads and fluxes are prescribed independently at each location of the boundary.

9 Wrap-up

This book begins with the first physical principles of classical mechanics as stipulated by Newton's laws of motion and fluid viscosity to explain Darcy's law as an empirical macro-scale relationship for groundwater movement in aquifers. We show how frictional effects of viscosity are due to shearing of a fluid and, hence, are dependent on flow velocity. This is fundamentally different from Coulomb friction for rigid bodies, which depends on the normal force across a contact surface and does not grow with velocity. Thus, for a given driving force, a rigid body under Coulomb friction (or a fluid parcel in the absence of any viscous effects) would continue accelerating at a constant rate, while a fluid approaches a steady-state flow regime, where viscous friction exactly balances the driving force. This is illustrated in detail for laminar (Poiseuille) flow between two flat plates and through a circular pipe. In both cases, the steady-state flow profiles are parabolic and frictional resistance is linearly proportional to the average flow velocity.

The approximate time it takes to establish a steady-state laminar velocity profile is derived and shown to be fundamental for assessing whether laminar flow conditions will prevail, or if turbulence will become a dominant factor. That is, the occurrence of laminar flow requires that the frictional effects of fluid viscosity act much faster than the chaotic impacts of inertial forces in order to approach an orderly flow profile. The relative magnitude of viscous and inertial forces is used to derive the Reynolds number as a fundamental dimensionless quantity to distinguish laminar from turbulent flow regimes. In typical groundwater situations, flow velocities are very low (e.g., centimeters per day) and average pore openings or fracture apertures are small (e.g., millimeters). Both factors contribute to the dominance of laminar flow conditions. The small openings also make the time required to achieve steady-state laminar flow profiles extremely small (e.g., seconds) compared to typical hydrogeological time scales of interest (e.g., days, years, or more).

The rapid establishment of steady-state laminar flow conditions and linear proportionality of frictional forces to flow velocity, lead to Darcy's law as a constitutive algebraic relationship for groundwater flow. We show this by simplifying the Navier-Stokes equation for the conditions of flow through porous media, where frictional effects are considered as a distributed body force on the fluid over a representative elementary volume (REV) of many grains/pores. For fluids of uniform density, the hydraulic head emerges as a convenient scalar variable for quantifying the combined flow-driving mechanisms of gravity and pressure. In particular, hydraulic head is identified as a flow-driving force potential per unit weight of fluid. Hydraulic conductivity emerges as a useful empirical parameter summarizing the flow-resisting effects of the porous medium on the viscous fluid. From an inverse perspective, we discuss how a moving viscous fluid exerts a seepage force onto the stationary porous medium with

impacts on the pore pressure distribution, its effective stress state, and mechanical stability (e.g., through liquefaction).

Due to the quasi-steady-state assumption for laminar flow development, Darcy's law for a given hydraulic gradient is an algebraic relationship and not a time-dependent differential equation. However, typical groundwater flow problems are transient (i.e., not steady-state) in the sense that driving mechanisms and/or boundary conditions may change with time. This generally results in variable flow fields and changes in groundwater storage due to fluctuations of hydraulic head. The law of mass conservation is utilized to describe these effects by constructing partial differential equations that represent the water balance at each location (or numerical grid cell) of an aquifer. We apply this principle to fully saturated zones of aquifers, while indicating several implications for particular conditions such as heterogeneity, anisotropy, and confinement. The same principles also govern the flow of water in the unsaturated zone where pore space is partially filled with air in addition to water; and they apply when two or more immiscible fluids occupy the pore space. In these cases, the effects of surface tension and resulting capillary forces need to be included.

Throughout the book, including its boxes and solved exercises, we construct and non-dimensionalize governing equations for order-of-magnitude analyses, in particular with respect to response-time scales. Dimensionless representations are not only useful for efficiently implementing solution methods and graphical representation of results but also for identifying common mathematical features of different problems. An example given here is the dynamics of laminar flow profiles between flat plates and that of hydraulic head in an aquifer between two parallel rivers. Another example is the functional identity of falling head laboratory tests, overdamped slug tests in wells, and first-order aquifer models, which are all described by the mechanics of a single dynamic reservoir but act at drastically different time scales. Thus, this book not only introduces the most important fundamentals of fluid mechanics for groundwater scientists but also identifies and facilitates understanding of some common aspects of different problems in groundwater science.

An enormous amount of further physical and mathematical detail pertaining to the topic of fluid mechanics are thoroughly discussed in the classical textbooks cited throughout. Research related to fluid mechanics associated with groundwater flow is ongoing. There is intensive continued interest in and research into the description and effects of flow turbulence and flow through natural, irregular, and poorly characterized, fracture networks. Recently, the effects of seepage forces due to baseflow exiting the subsurface have been found to be important factors for driving fluvial geomorphology — that is, the long-term evolution of surficial drainage networks and, hence, entire landscapes. From a marine perspective, it is known that waves induce seepage into and out of sedimentary seabeds with associated forces affecting the effective stress state. Such forces

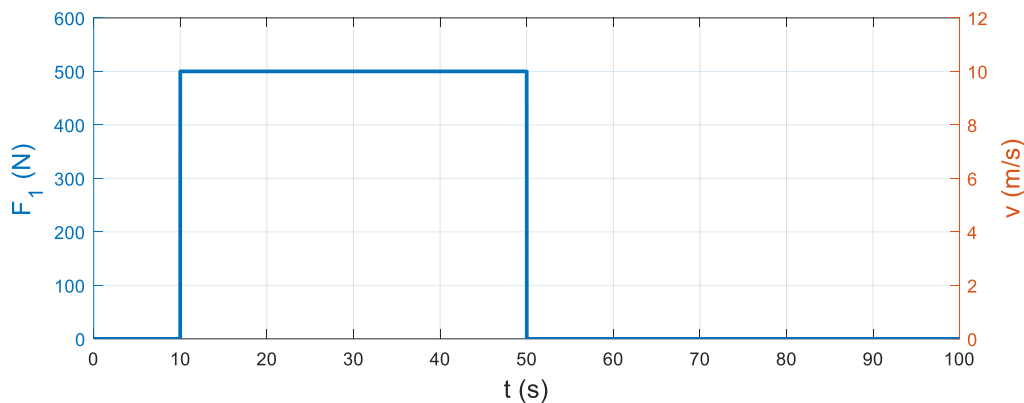
can be destabilizing and have recently been investigated as drivers for temporarily liquefying the seabed (leading to the sudden sinking and disappearance of heavy and possibly dangerous objects previously resting on top of the seabed), or for enhancing sediment entrainment into suspension with strong consequences for sediment transport and coastal morphology.

Scientific advances related to groundwater fluid mechanics improve our ability to understand and manage the relationship between humans and Earth's systems. Such advances require a sound understanding and description of the relevant forces and scales of fluid mechanics based on first principles.

10 Exercises

Exercise 1 - Accelerating Boat and Response-Time Scales

Imagine a resting boat of mass $m = 100$ kg on a quiet lake. When turning on the engine, the propeller provides a constant driving force $F_1 = 500$ N to accelerate the boat for 40 s as illustrated in the figure that accompanies this exercise. Assume the resisting drag force is strictly proportional to the boat's velocity v with a Stokes friction factor $f_{sto} = 50$ Ns/m.



Driving force F_1 on the boat as a function of time.

- Make a conceptual sketch of the problem indicating the driving and resisting forces on the boat.
- Write down the expression for the resisting force and interpret the Stokes friction factor based on its units.
- Calculate the final (steady-state or terminal) velocity v_∞ of the boat and the time scale T that it takes for reaching it.
- Add an approximate (hand-drawn) graph of v as a function of time t to the figure above. The velocity scale on the right can be used to show how the boat accelerates and subsequently slows down after the propeller is turned off.
- Next, imagine the boat is heavily loaded to a total mass of $m = 1000$ kg. Recalculate v_∞ and T and draw the respective graph of $v(t)$ on the chart. What do you observe related to these parameters and steady state?
- Finally, imagine the boat is light, with $m = 10$ kg and draw yet another graph of $v(t)$ for this situation. What do you observe related to steady state and to the quasi-steady-state assumption if the time scale of interest is on the order of tens of seconds like the period of acceleration? What if the time scale of interest was much smaller, such as fractions of a second?

[Solution to Exercise 1](#) ↴

[Return to where text linked to Exercise 1](#) ↲

Exercise 2 - Stokes Friction and Terminal Velocity of a Sinking Sphere

Consider a spherical sand grain of radius $R = 0.1$ mm and density $\rho_g = 2500$ kg/m³ that is released at the surface of a lake to sink. The water has a density $\rho_f = 1000$ kg/m³ and a dynamic viscosity of $\mu = 10^{-3}$ Ns/m².

- Determine the driving and resisting forces acting on the grain and draw a conceptual diagram of the problem.
- What is the terminal sinking velocity of the grain assuming that flow remains laminar?

[Solution to Exercise 2](#) ↴

[Return to where text linked to Exercise 2](#) ↲

Exercise 3 - Implementing the Euler Forward Method

Solve the partial differential in Equation (36) (with Equation (37) for T), describing the dynamics of fluid laminae between two parallel plates using the Euler forward method outlined in Box 2 and recreate the graphs shown in Figure 8. Implement the numerical solution in a software package of your choice such as MATLAB, Octave, Mathematica, R, Python, or any other software package.

[Solution to Exercise 3](#) ↴

[Return to where text linked to Exercise 3](#) ↲

Exercise 4 - Effective Hydraulic Conductivity of a Pipe and a Fracture

Based on the solutions presented in Section 3.2 and Section 3.3 for laminar flow between a) flat plates and b) along a circular pipe, determine the effective hydraulic conductivities for Darcy's law derived in Section 6.1.

[Solution to Exercise 4](#) ↴

[Return to where text linked to Exercise 4](#) ↲

Exercise 5 - Effective Hydraulic Conductivity of Layered Media

In general, hydrogeological conditions are heterogeneous – that is, properties such as hydraulic conductivity K vary in space. In relatively simple cases, some effective conductivity may be defined as a kind of upscaled property. Based on Equations (83) through (85) determine the effective hydraulic conductivities for the following two situations:

- a) Flow perpendicular to a layered medium with conductivity K_1 over a length L_1 , and with conductivity K_2 over the remaining length L_2 .
- b) Flow parallel to the layers of the same medium.

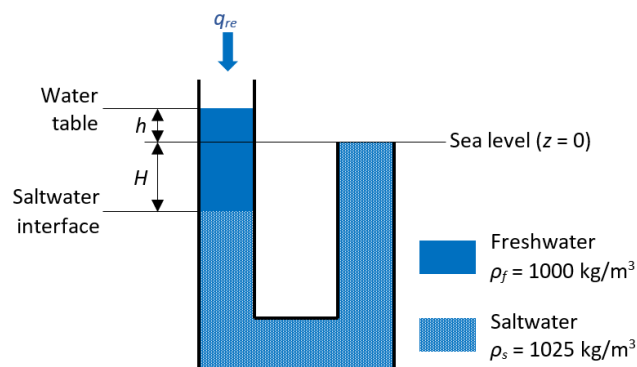
[Solution to Exercise 5](#) ↓

[Return to where text linked to Exercise 5](#) ↑

Exercise 6 - Freshwater-Saltwater Interaction and Ghyben-Herzberg Principle

Consider an unconfined coastal aquifer of porosity θ with a freshwater density of $\rho_f = 1000 \text{ kg/m}^3$ and a water table at elevation h above sea level. At depth H below sea level, the freshwater is underlain by a saltwater body with a higher density of $\rho_s = 1025 \text{ kg/m}^3$, that is hydraulically connected to the ocean which has a constant head equal to the average sea level. The figure that accompanies this exercise shows a simplified conceptual model of this problem in the form of a U-tube with a sharp freshwater-saltwater interface. This concept is also presented in the GW-Project book *Variable-Density Groundwater Flow* (Post & Simmons, 2022) and, for coastal aquifers in particular, by Jiao and Post (2019).

- Under steady-state conditions, establish the force balance at the saltwater interface and determine the water table elevation h as well as the interface depth H with respect to the sea level.
- After a freshwater recharge q_{re} (as volume per area) has occurred, and again under steady-state conditions, what are the changes Δh and ΔH in h and H , respectively? Determine the effective storage coefficient (also known as storativity) defined as the change in freshwater storage volume per unit surface area and unit change in freshwater head, that is, $S = q_{re}/\Delta h$, and discuss the finding. The result will include specific yield for the change in storage due to water table fluctuations as for a typical unconfined aquifer, but also another contribution due to changes in saltwater interface elevation.
- Express the changes Δh and ΔH in water table and interface elevations as a function of sea level rise Δz .
- How does the previous solution for sea level rise change if h is kept at a constant elevation, which may be due to a very effective surface drainage network on top of the aquifer? Discuss possible implications.



Conceptual sketch of a U-tube containing lighter freshwater and denser saltwater separated by a sharp interface.

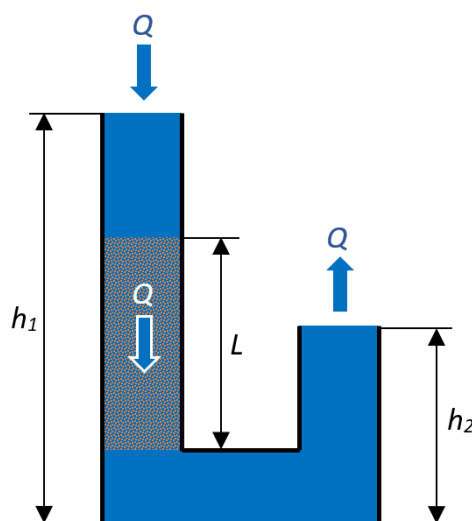
[Solution to Exercise 6](#) ↓

[Return to where text linked to Exercise 6](#) ↑

Exercise 7 - Constant Head K Tests and Seepage Force

A cylindrical sand column of length $L = 10$ cm and diameter $D = 5$ cm is exposed to constant hydraulic heads $h_1 = 30$ cm and $h_2 = 28$ cm as shown schematically in the figure that accompanies this exercise. During the experiment, flow through the column is measured as $Q = 10$ mL/min.

- Estimate the hydraulic conductivity K of the sand from this constant head test using Equation (85). What is the value of the hydraulic gradient J along the column?
- Based on Equation (74), express the frictional seepage force F_f that the sand exerts on the flowing water (frictional forces are illustrated Figure 13). How does this relate to h_1 and h_2 ?



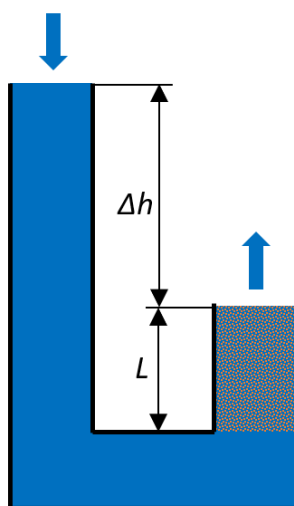
Conceptual sketch of constant head K test.

[Solution to Exercise 7](#) ↴

[Return to where text linked to Exercise 7](#) ↴

Exercise 8 - Liquefaction and Quicksand Formation

As a direct modification of Exercise 7, consider water of density $\rho_f = 1 \text{ g/mL}$ with a sand column of length $L = 10 \text{ cm}$ and porosity $\theta = 0.25$ located in the rising limb of a constant head test as shown in the figure that accompanies this exercise. Using the discussion provided in Box 3, and assuming $\Delta h = 10 \text{ cm}$, what is the minimum density of the sand grains required to avoid quicksand conditions? Quicksand conditions occur when the sand loses its bearing capacity due to upward seepage forces that effectively float the sand grains, annulling the vertical effective stress.



Conceptual sketch of a sand column exposed to an upward seepage force.

[Solution to Exercise 8](#) ↴

[Return to where text linked to Exercise 8](#) ↲

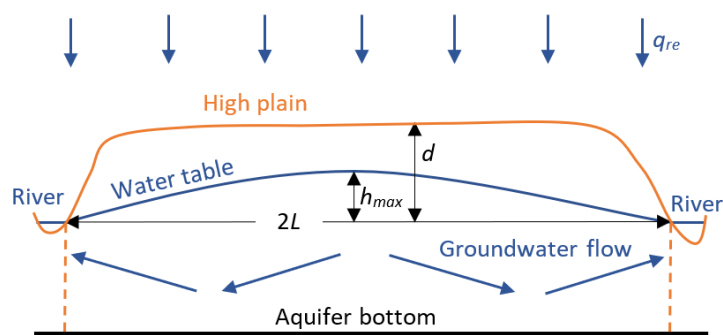
Exercise 9 - Unconfined Aquifer and Drought

The conceptual sketch in the figure that accompanies this exercise is similar to the figures shown in Box 6 and Exercise 10. Here we consider an unconfined aquifer between two parallel rivers at approximately equal elevations that are separated by a higher planar region of relative elevation $d = 50$ m above the rivers over a distance $2L = 10$ km. Pumping test data were used to estimate the aquifer transmissivity to be $T_K = 10^{-3}$ m²/s with a storage coefficient of $S = 0.2$. Average recharge q_{re} is estimated to be 100 mm/yr.

Assuming further that the saturated zone of the aquifer is approximately 100 m thick on average, we may attempt to redraw the figure below with identical scales in the horizontal and vertical directions (i.e., without vertical exaggeration as generally applied and also used below). Doing this with a scale of 1:10,000 would yield an aquifer thickness of 1 cm with a width of 1 m in the sketch, showing that groundwater flow has to be essentially horizontal in the overwhelming part of the aquifer, even knowing that the rivers do not fully penetrate down to the aquifer bottom. Mathematically, hence, we take the simplifying assumption of fully penetrating rivers at the aquifer boundaries, as indicated by the dashed vertical lines in the figure.

Based on these assumptions and using Equations (113) and (115), determine the following:

- What is the depth of the water table below ground surface near the center of the high plain, and is it justified to assume an approximately constant saturated aquifer thickness?
- If a drought sets in causing absence of any significant recharge, what would be the approximate time frame over which the aquifer may sustain baseflow to the rivers? How would this differ if $2L$ is only 1 km?



Conceptual sketch of unconfined aquifer between two rivers (dashed vertical lines represent idealized boundary conditions of fully penetrating rivers).

A more general treatment of an unconfined aquifer with variable thickness is provided by Cuthbert and others (2019) and is explored in Exercise 10.

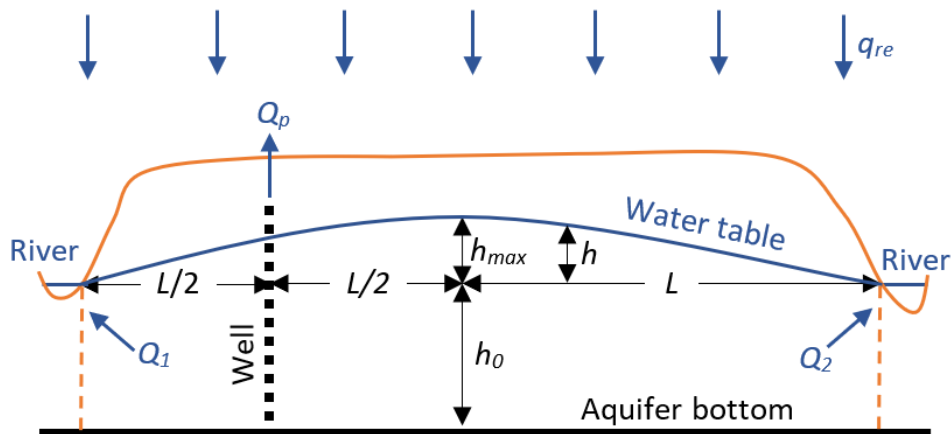
[Solution to Exercise 9 ↴](#)

[Return to where text linked to Exercise 9 ↲](#)

Exercise 10 - A Dynamic Aquifer Model

As illustrated in the figure that accompanies this exercise, consider again the one-dimensional aquifer model of Exercise 9 with $2L = 1$ km and a thickness of $h_0 = 10$ m below the river elevations, while $T_K = 10^{-3} \text{ m}^2/\text{s}$ as. Generalize the code of Exercise 3 to accommodate the following details.

- Using Equation (107), include the possibilities of a seasonally variable (sinusoidal) recharge and a constant pumping rate Q_p from a well at a distance $L/2$ from a river. Given the one-dimensional nature of the system, strictly speaking, this would be a line of wells parallel to the rivers with one well per unit distance perpendicular to the plane of the drawing, each pumping at Q_p . Plot the maximum water table elevation between the rivers and also plot the baseflow discharge Q_1 and Q_2 into each river as a function of time and discuss the results.
- Using Equation (110), compare the results from (a) that uses the approximation of a constant value of T_K to the more accurate implementation for unconfined aquifers, where T_K is spatially variable as $T_K = K(h + h_0)$.



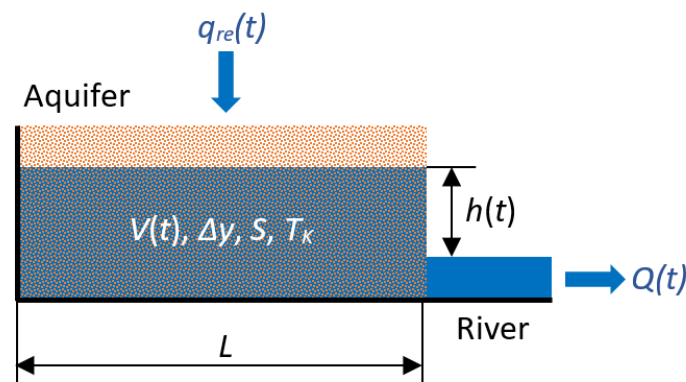
Conceptual sketch of unconfined aquifer with a pumping well between two rivers (dashed vertical lines represent idealized boundary conditions of fully penetrating rivers).

[Solution to Exercise 10](#) ↴

[Return to where text linked to Exercise 10](#) ↲

Exercise 11 - Reduced-Order Aquifer Models

The propagation of recharge into groundwater storage and river baseflow of hydrological catchments including aquifers is sometimes described in a simplified form by a single or a small number of coupled reservoirs, which can behave in linear or non-linear ways (e.g., Kirchner, 2009). In the simplest case of a single (i.e., first-order) linear reservoir as illustrated in the figure that accompanies this exercise, the aquifer response is mathematically equivalent to that of a falling head test, or an overdamped slug test, as discussed in Exercise 12 and Exercise 13. The only differences are the storage coefficient—which is smaller than one—and the forcing signal—which is no longer a single pulse of water being added or removed but rather a time-variable sequence of recharge pulses depending on the climatic conditions. If multiple reservoirs are coupled to each other (i.e., hydraulically interacting by exchanging water), the order of the model increases. In the extreme case of an infinite number of infinitesimally small reservoirs that are coupled with one another in a regular pattern, the model becomes equivalent to the partial differential equations derived in connection with Figure 18.



Conceptual sketch of a single reservoir aquifer model receiving recharge q_{re} and providing baseflow Q to a river.

In the unconfined aquifer model represented as a single reservoir presented in the figure shown here, q_{re} is recharge in length per time, Q is groundwater discharge to the river (baseflow) in volume per time, L is the length of the aquifer measured from the river, Δy is aquifer length along the river (in the third dimension), S is the storage coefficient, T_K is transmissivity, and h is the driving head difference between the river stage which is assumed to be constant, and the mean water table elevation in the aquifer. It is also assumed that Darcy's law is approximately valid in the form $Q = \Delta y T_K h / L$.

- Establish the governing differential equations relating h and Q to q_{re} and determine the time scale T_{aqu} of aquifer response.
- Relate T_{aqu} from the single (first-order) reservoir model here to the expression of T_{aqu} from the spatially distributed (infinite-order) reservoir model considered in Exercise 9 and briefly interpret the outcome.

- c) What happens to T_{aqu} if $V = V_0(h/h_0)^a$ and/or $Q = Q_0(h/h_0)^b$ are no longer linear functions of h , where $Q_0 = \Delta y T_{K,0} h_0 / L_0$ and $V_0 = \Delta y S_0 L_0 h_0$ are reference values of Q and V for $h = h_0$? This non-linearity may be introduced, for example, because S (due to changes of drainable porosity with water table elevation), T_K (due to changes in saturated aquifer thickness and/or hydraulic conductivity with depth), and/or L (due to a growing surface drainage network as the aquifer fills) depend on V and, hence, on h .

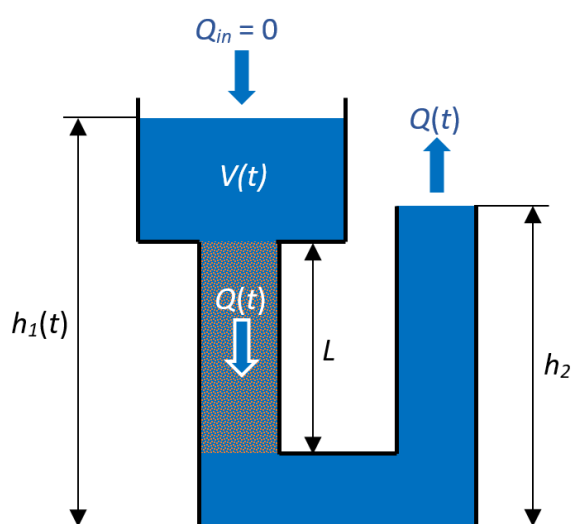
[Solution to Exercise 11](#) ↓

[Return to where text linked to Exercise 11](#) ↑

Exercise 12 - Falling Head K Test

A falling head hydraulic conductivity test is schematically illustrated in the figure that accompanies this exercise. This test differs from a constant head test (e.g., Exercise 7) in that no additional water is added to maintain a constant flow rate through the cylindrical test column, which here is of length $L = 10$ cm and diameter $D = 5$ cm. Instead, a reservoir of surface area $A_{res} = 100$ cm² and falling water level $h_1(t)$ provides a decreasing rate of flow $Q(t)$ to the exit at a constant elevation h_2 .

- Use the principle of continuity of flow illustrated in Figure 16 in combination with Darcy's law to derive the functional relationship and response-time scale of $h_1(t)$.
- Estimate the hydraulic conductivity K of the sand column given an observation that it took 14 minutes for h_1 to decrease by $(h_1 - h_2)/2$, that is, exactly half-way between its initial and final values.



Conceptual sketch of a falling head K test.

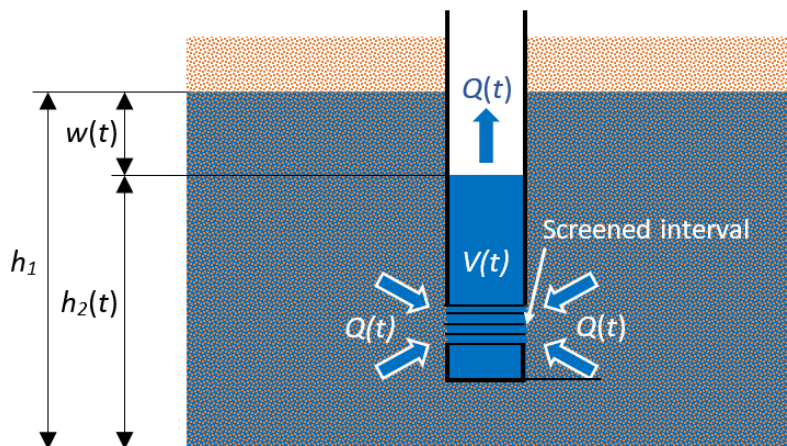
[Solution to Exercise 12](#) ↴

[Return to where text linked to Exercise 12](#) ↲

Exercise 13 - Slug Tests

Slug tests are like the falling head tests as explored in Exercise 12 except they are performed at a well in the field instead of a cylindrical sample of aquifer material in the laboratory. The same underlying principle is applied, that is: a known volume of water is added to the well over a short period (i.e., as a *slug*) followed by observation of the recovery process in which hydraulic head in the well declines (i.e., *falling head*) to the initial equilibrium level with the aquifer.

As illustrated in the figure that accompanies this exercise, slug tests may also be *rising head* tests when a known volume of water is rapidly withdrawn from the well and subsequent upward recovery of the water level is observed. The fundamental difference between these tests and typical pump tests is that the water extraction is sudden and of a relatively small volume compared to the aquifer volume, in contrast to continuous pumping that withdraws significant amounts of groundwater from aquifer storage.



Conceptual sketch of a rising head slug test where a known volume of water was quickly withdrawn from a well.

Under these conditions, the initial hydraulic head h_1 is the constant boundary condition in the aquifer and Darcy's law may be applied in a generalized form as shown here.

$$Q = -F_s K w$$

where:

$w(t) = h_2(t) - h_1$ = the dynamic water level deviation (L; positive upward) inside the well driving discharge Q into or out of the well

F_s = a shape factor (L), which accounts for the non-uniform shape of the flow field in the aquifer near the well screen

The shape factor must be known from existing equations (e.g., Hvorslev, 1951) and it mainly depends on the well screen geometry (e.g., length and diameter). It may also

account for anisotropy in K if the anisotropy ratio is known a priori, and assumes an immediate response of a locally homogeneous aquifer (i.e., transience and heterogeneity in the aquifer are neglected).

In analogy to Exercise 12, derive the dynamic solution and time scale for the water level recovery $w(t)$ in the well of cross-sectional areal A_{well} .

[Solution to Exercise 13](#) ↴

[Return to where text linked to Exercise 13](#) ↲

Exercise 14 - Oscillatory Slug Test and Well Friction

Exercise 13 is based on a mass balance and neglects effects of inertia and friction inside the well. However, for deep wells in conductive aquifers, the weight of the water column inside the well and the velocity at which it moves may generate significant forces. In extreme cases, this may lead to oscillation of the water column after the slug is initiated such that a momentum balance is required in addition to the mass balance of Exercise 13 in order to model and/or interpret the response. In deep and narrow wells, pipe friction inside the well casing also becomes more important.

For a control volume as illustrated by the dashed red rectangle in the figure that accompanies this exercise and when neglecting the mass of air being displaced as well as using atmospheric pressure as the (zero) reference pressure, the force balance ↗ can be written as shown here.

$$-F_g - F_f + F_p + v_{rel} \frac{dm}{dt} = m \frac{dv_{mean}}{dt}$$

where:

$F_g = \rho g L A_{well}$ = force of gravity acting on the water column of density ρ , length L , and cross-sectional area A_{well} (MLT^{-2})

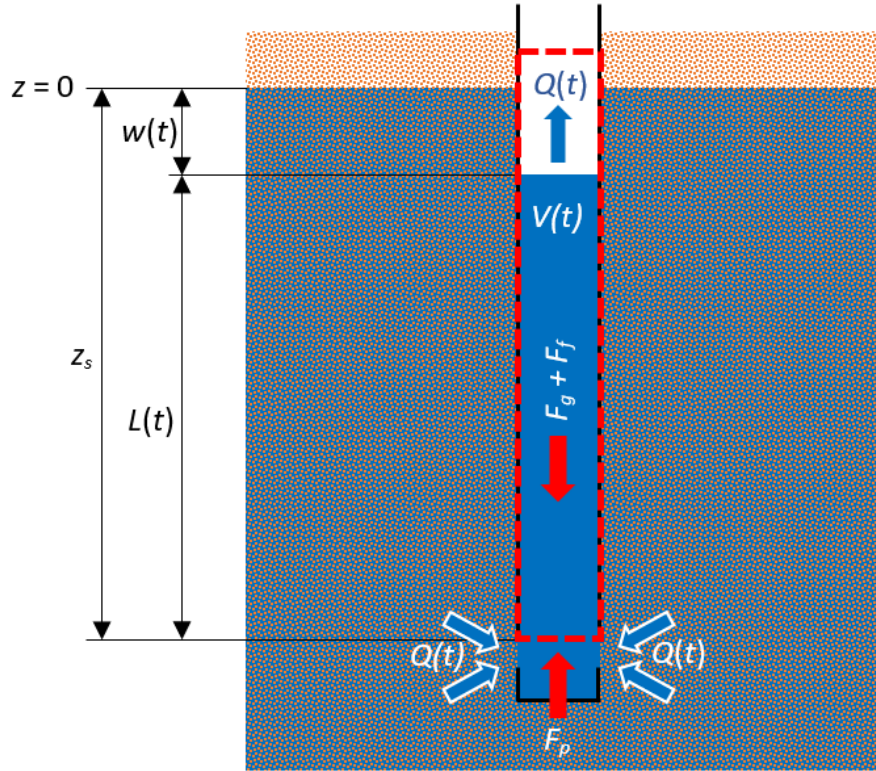
F_f = frictional force of the water against the well casing (MLT^{-2})

F_p = pressure force acting on the bottom of the water column (MLT^{-2})

v_{rel} = relative velocity of water entering or leaving the control volume from the bottom with respect to the mean velocity v_{mean} of the water column inside the well (LT^{-1})

$m = \rho L A_{well}$ = mass of the water column (M)

t = time (T)



Conceptual sketch of a slug test in a well indicating the control volume (red dashed rectangle) for the force (momentum) balance inside the well when effects of inertia and well friction become relevant.

This equation differs from Equation (4), which is valid for a body of constant mass ($dm/dt = 0$), whereas the mass of water inside the control volume varies with time in the case presented here. However, as the water enters or leaves the bottom of the control volume at the same velocity v_{mean} as the water column inside the well, we find $v_{rel} = 0$ such that the expression can be simplified to the following.

$$-F_g - F_f + F_p = m \frac{dv_{mean}}{dt}$$

In this expression m may vary with time, while F_g , F_f and F_p appear as the driving and resisting forces (on the volume of the entire water column inside the well), as discussed in Section 2. The negative signs are used because we define both v_{mean} and the water level deviation w inside the well as positive upward such that $v_{mean} = dw/dt$.

From Equation (46), we further know that in the laminar flow regime, the frictional force per unit volume $\rho g J = 8\mu v_{mean}/R^2$, where μ is the dynamic viscosity of the water and R is the inner well radius. Thus, the total frictional force on the water column results as follows.

$$F_f = \rho g J L A_{well} = \frac{8\mu L A_{well}}{R^2} \frac{dw}{dt}$$

Furthermore,

- defining the elevation datum $z = 0$ at the water table in the aquifer (i.e., the water table acts as a constant head boundary with a head = 0), and
- using
 - $Q = -KF_s h_s$ from Darcy's law, where K is the hydraulic conductivity of the aquifer,
 - F_s as a shape factor as introduced in Exercise 13, and,
 - $h_s = -z_s + p_s/(\rho g)$ as the hydraulic head inside the well screen at depth z_s and at pressure p_s ,
- then,

$$F_p = p_s A_{well} = \rho g(z_s + h_s) A_{well} = \rho g \left(z_s - \frac{Q}{KF_s} \right) A_{well}$$

With Q defined as

$$Q = A_{well} \frac{dw}{dt}$$

this becomes

$$F_p = \rho g \left(z_s - \frac{A_{well}}{KF_s} \frac{dw}{dt} \right) A_{well}$$

showing that F_p equals the hydrostatic force at depth z_s (a positive value) minus the frictional loss inside the aquifer due to flow Q to the well. During oscillatory slug tests, Q changes sign such that F_p fluctuates about its hydrostatic value.

Using $L = z_s + w$ and substituting for the remaining variables in the expression presented at the start of this exercise (and repeated here), we find the following equation.

$$-F_g - F_f + F_p = m \frac{dv_{mean}}{dt}$$

$$-\rho g(z_s + w) A_{well} - \frac{8\mu(z_s + w) A_{well}}{R^2} \frac{dw}{dt} + \rho g \left(z_s - \frac{A_{well}}{KF_s} \frac{dw}{dt} \right) A_{well} = \rho(z_s + w) A_{well} \frac{d^2 w}{dt^2}$$

Next, we divide by ρA_{well} and cancel the term gz_s on the left-hand side.

$$-gw - \frac{8\mu(z_s + w)}{\rho R^2} \frac{dw}{dt} - \frac{g A_{well}}{KF_s} \frac{dw}{dt} = (z_s + w) \frac{d^2 w}{dt^2}$$

Thus, we obtain a non-linear second-order ordinary differential equation in w . However, since typically $z_s \gg w$, so we may use the approximation $z_s + w \approx z_s$ to arrive at the following as a linear approximation, where we also substituted $A_{well} = R^2 \pi$ and rearranged terms.

$$z_s \frac{d^2 w}{dt^2} + \left(\frac{8\mu z_s}{\rho R^2} + \frac{g R^2 \pi}{KF_s} \right) \frac{dw}{dt} + gw = 0$$

This is the governing equation of a damped oscillation, analogous to a mass-spring-friction system ([harmonic oscillator ↗](#); [damping ↗](#)).

- a) Non-dimensionalize the governing equation using an initial slug displacement w_0 and determine an inertial response-time scale T_w .
- b) Ideally, for estimating K , a slug test must be most sensitive to frictional (Darcy flow) losses in the aquifer as opposed to frictional (pipe flow) losses inside the well. Derive a dimensionless number d_K to evaluate this condition.
- c) Derive another dimensionless number d_f to evaluate the relative importance of inertia (causing oscillation) and friction (causing damping). Compute or hand-draw solutions of w for small, intermediate, and large values of this number. Under which conditions does the current solution collapse to the solution of Exercise 13?
- d) When deriving the frictional force F_f inside the well, we used Equation (46), which assumes a (quasi) steady-state laminar flow profile. Use Equation (49) to estimate a minimum response-time scale T_w for w at which this assumption is justified.

[Solution to Exercise 14](#) ↓

[Return to where text linked to Exercise 14](#) ↑

11 Boxes

Box 1 - Order-of-Magnitude Analysis

Section 2.3 shows how a simple dynamic problem can be solved in terms of $v(t)$ —that is, velocity as a function of time—and how this solution can be represented and applied very efficiently using *non-dimensional variables*. However, a problem is often too complex to find a straightforward analytical solution and an *order-of-magnitude analysis* of the governing equation may provide some reduced, but important, insight about a system's dynamic behavior.

Order-of-magnitude analysis consists of non-dimensionalizing the governing equation (rather than its solution) to reduce the number of relevant parameters, comparing the magnitudes of different contributing mechanisms, and obtaining an estimate of a *response-time scale*, if one exists. Thus, even if a problem is to be solved numerically, an order-of-magnitude analysis may be extremely useful to reduce the parameter space, to possibly eliminate irrelevant terms of the governing equation, and to get an a priori idea about minimum required simulation times for observing significant responses.

For our example of an accelerating body opposed by a drag force, we arrived at Equation (14) (reproduced here as Equation Box 1-1) as the governing equation of the system in terms of body velocity v .

$$\frac{dv}{dt} = \frac{1}{m}(F_1 - vf_{sto}) \quad (\text{Equation Box 1-1})$$

We call v a *state variable* of the system because it describes the situation (state) of body movement at any point in time. Here, v is the only state variable of the problem, and it can be easily converted into location $x(t)$ by Equation (1) through integration over time. Equation Box 1-1 is called a *governing equation* because it expresses the change dv/dt in the state of the body as a function of all driving and resisting forces.

Along these lines, we further distinguish between *variables*, which may change over time (here: v , F_1 , and t itself), and *parameters*, which describe properties that remain constant over time (here: m and f_{sto}).

Before starting with the order-of-magnitude analysis, it is often informative to check for *possible steady states* of the system, which occur when all variables reach constant values and no longer change with time (i.e., $F_1 = \text{constant}$ and $v = v_\infty$). Mathematically, this implies $dv/dt = 0$ in Equation Box 1-1 and allows expressing v_∞ as shown in Equation Box 1-2.

$$v_\infty = \frac{F_1}{f_{sto}} \quad (\text{Equation Box 1-2})$$

To rewrite Equation (14) (shown here as Equation Box 1-1) in normalized form, we adopt the dimensionless variables $v^* = (v - v_0)/(v_\infty - v_0)$ as the relative change in velocity from initial to terminal values, and $t^* = t/T$ (implying $dt = Tdt^*$), where T is a time scale to

be defined. Using these expressions for v and t , while substituting F_1 from Equation Box 1-2 into Equation Box 1-1 gives Equation Box 1-3.

$$\frac{m}{f_{sto}T} \frac{dv^*}{dt^*} = 1 - v^* \quad (\text{Equation Box 1-3})$$

The velocities v_0 and v_∞ are contained in v^* but otherwise dropped out. From the definition of v^* , we know that the value of v^* must be on the order-of-magnitude of one, because v varies between v_0 and v_∞ . By the [rules of scale analysis](#)[↗], the order-of-magnitude of a sum or difference is equal to the largest order-of-magnitude of the elements to be added or subtracted. This indicates that the order-of-magnitude of the right-hand side of Equation Box 1-3 is one.

For Equation Box 1-3 to be true, the order-of-magnitude of its left-hand side must also be one. To achieve this, we express T as shown in Equation Box 1-4.

$$T = \frac{m}{f_{sto}} \quad (\text{Equation Box 1-4})$$

In this case, the leading coefficient on the left-hand side of Equation Box 1-3 becomes one, such that dv^*/dt^* must be on the order of one. The latter means that significant changes in v are to be expected over one dimensionless-time interval, corresponding to the dimensional time scale of T from Equation Box 1-4. Thus, T is the approximate time (in terms of order-of-magnitude or scale, such as seconds, hour, or years), after which a *significant change in velocity* will occur between the initial and terminal (steady-state) values.

Terminal velocity v_∞ from Equation Box 1-2 and response-time scale T from Equation Box 1-4 are identical to the results of Equations (18) and (20), respectively. However, the solution here was obtained without explicitly solving the governing ordinary differential equation. In combination, v_∞ and T provide the two most important system-response characteristics for this simple example, which are the steady state for a given forcing, and the time scale it will take to approach this steady state. This is a significant shortcut, but it is not always applicable as illustrated by the example of Coulomb friction (Section 2.3), where neither steady state nor a corresponding time scale exist. Exercise 11 provides a further example of when a unique response-time scale does not exist.

[Return to where text linked to Box 1](#)[↗]

Box 2 - A Simple Numerical Solution Method

Perhaps the simplest numerical method for solving an ordinary or partial differential equation is the *Euler forward method*, which is based on the approximation of finite differences⁷. In practice, many complex solution methods are available that are more stable and faster. However, due to its simplicity, easy transferability to other types of governing equations, and intuitive connection to how differential equations are generally derived, we provide an example of how it can be applied to generate the solutions of Equation (36) that are shown in Figure 8, which is also implemented in Exercise 3.

Substituting Equation (37) into Equation (36) results in the non-dimensional governing equation shown in Equation Box 2-1.

$$\frac{\partial v^*}{\partial t^*} = 2 + \frac{\partial^2 v^*}{\partial n^{*2}} \quad (\text{Equation Box 2-1})$$

The asterisk terms, $v^* = v/v_{max}$, $t^* = t/T$, and $n^* = n/B$ are dimensionless variables and the asterisks are omitted from the variables for the remainder of this box for brevity. From the definition of the differential operator, we have Equation Box 2-2.

$$\frac{\partial v}{\partial t} \approx \frac{v_{i+1} - v_i}{\Delta t} \quad (\text{Equation Box 2-2})$$

Here, Δt is the finite time interval between steps i and $i + 1$, over which velocity changes from v_i to v_{i+1} . Similarly, we can write Equation Box 2-3.

$$\frac{\partial v}{\partial n} \approx \frac{v_{j+1} - v_j}{\Delta n} \quad (\text{Equation Box 2-3})$$

Here, Δy is the finite distance between grid locations (fluid laminae) j and $j + 1$, over which velocity changes from v_j to v_{j+1} . This is applied in the inverse direction, as done when deriving the partial differential Equation (26) from Equation (25), for example. Since the second derivative is simply the derivative of the first derivative, Equation Box 2-3 can be applied again to arrive at Equation Box 2-4.

$$\frac{\partial^2 v}{\partial n^2} \approx \frac{\left. \frac{\partial v}{\partial n} \right|_{j+1} - \left. \frac{\partial v}{\partial n} \right|_j}{\Delta n} \approx \frac{\frac{v_{j+1} - v_j}{\Delta n} - \frac{v_j - v_{j-1}}{\Delta n}}{\Delta n} = \frac{v_{j+1} - 2v_j + v_{j-1}}{\Delta n^2} \quad (\text{Equation Box 2-4})$$

Substituting Equation Box 2-2 and Equation Box 2-4 into Equation Box 2-1, while recognizing that v_{ij} is both a function of time (index i) and space (index j), we arrive at Equation Box 2-5.

$$\frac{v_{i+1,j} - v_{i,j}}{\Delta t} = 2 + \frac{v_{i,j+1} - 2v_{i,j} + v_{i,j-1}}{\Delta n^2} \quad (\text{Equation Box 2-5})$$

This allows for expressing Equation Box 2-6 as follows.

$$v_{i+1,j} = v_{i,j} + \left(2 + \frac{v_{i,j+1} - 2v_{i,j} + v_{i,j-1}}{\Delta n^2} \right) \Delta t \quad (\text{Equation Box 2-6})$$

The method is called *Euler forward* or *explicit* method because Equation Box 2-6 computes the velocity at a location j for a subsequent time step $i + 1$ (left-hand side) from

known velocities at a previous time step i (right-hand side). Thus, it is necessary to define *initial conditions* for the first time-step at $i = 1$. For example, $v_{1,j} = 0$ for all locations j when starting from rest. If the spatial (here one-dimensional) grid has N_j elements (i.e., $j = 1, 2, \dots, N_j$), then *boundary conditions* may be simply applied by assigning appropriate values to additional boundary elements at $j = 0$ and $j = N_j + 1$. For the no-slip condition at stationary boundaries, this is $v_{i,0} = v_{i,N_j+1} = 0$ for all time steps i .

[Return to where text linked to Box 2](#) ↑

Box 3 - Effective Stress, Seepage Force and Quicksand Formation

The effective stress σ' in an unconsolidated porous medium is the average compressive pressure over a bulk cross-sectional area (i.e., including grains and voids) that purely acts on the solid matrix made up by the grain skeleton. As such, it determines the *deformational state of the medium* (e.g., degree of compression), which is of particular importance for confined aquifers where groundwater pumping leads to a reduction in groundwater pore pressure. Such a reduction redistributes the heavy weight of the overlying confining layer onto the aquifer's matrix, thus increasing the effective stress and compressing the matrix. Under extreme conditions, the compression may be large enough to cause *critical subsidence* (lowering) of the land surface. This is discussed in the GW-Project book Land Subsidence and its Mitigation σ' by Gambolati & Teatini (2021).

Moreover, a moving fluid affects the pore pressure distribution and effective stress state of a porous medium through the *frictional seepage force* F_f per unit volume of fluid as introduced in Equation (73). We begin by considering a dry sand with grain density ρ_g and porosity θ . The vertical (compressive) effective stress σ' in such a sand column is described by Equation Box 3-1.

$$\sigma' = -(1 - \theta)\rho_g g z \quad (\text{Equation Box 3-1})$$

where:

g = acceleration of gravity (LT^{-2})

z = vertical coordinate defined as positive upward from the sand surface (L)

The minus sign is added to make compressional effective stress positive, because tensile stress cannot exist in an unconsolidated sediment, thus there is no need to incorporate the possibility of an opposite sign for stress. The relationship represents the apparent pressure over an area on a horizontal plane through the sand (including grain and void spaces) at elevation z due to the dry weight of the sand above z . For fully saturated wet sand with a fluid of density ρ_f the effective weight of the sand grains is reduced by the effects of hydrostatic forces (*buoyancy*) and, assuming the sand is saturated up to its surface or above, the effective stress becomes Equation Box 3-2.

$$\sigma' = -(1 - \theta)(\rho_g - \rho_f)g z \quad (\text{Equation Box 3-2})$$

The effective weight $(1 - \theta)(\rho_g - \rho_f)g$ of the saturated sand is the force of gravity minus buoyancy per unit bulk volume under hydrostatic conditions.

In contrast, when there is movement (seepage) of the fluid through the pore space at a uniform Darcy flux q , for example, then additional hydrodynamic forces begin to act on the grain skeleton. From Equation (73) and Equation (74), the frictional force per unit fluid volume in terms of hydraulic gradient J is equal to Equation Box 3-3.

$$F_f = \frac{dp}{ds} + \rho_f g \frac{dz}{ds} = J\rho_f g \quad (\text{Equation Box 3-3})$$

Similar to Figure 13, but for exactly vertical flow in the upward direction, the corresponding force balance on the fluid is illustrated in Figure Box 3-1. The forces of gravity $F_{g,f}$ and friction F_f act downward on the fluid volume, while pressures p_1 and p_2 apply on the porous part $\Delta A\theta$ of the surface area.

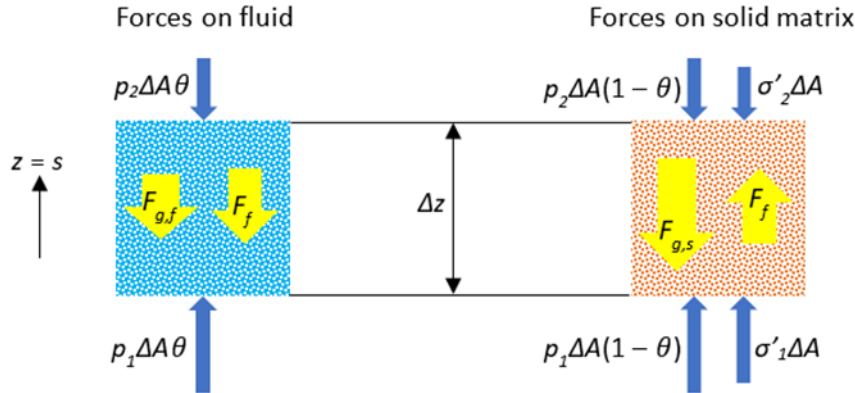


Figure Box 3-1 - Forces acting on a pore fluid (left) and corresponding porous solid matrix (right) due to gravity F_g , pressure p , friction F_f and effective stress σ' for flow direction s vertically upward in a domain of size $\Delta A\Delta z$ and porosity θ . Blue and yellow arrows are surface and body forces, respectively.

Figure Box 3-1 also represents the corresponding force balance on the solid matrix, where F_f is upward in flow direction and against gravity $F_{g,s}$. Moreover, fluid pore pressures p_1 and p_2 act on the solid part $\Delta A(1 - \theta)$ of the surface area and there is an additional contribution of effective stresses σ'_1 and σ'_2 , which are defined with respect to the total surface area ΔA . Based on this, we may write Equation Box 3-4.

$$(\sigma'_2 - \sigma'_1)\Delta A = F_f - F_{g,s} - (p_2 - p_1)(1 - \theta)\Delta A \quad (\text{Equation Box 3-4})$$

We know $F_{g,s} = \Delta A\Delta z(1 - \theta)\rho_g g$ and $p_2 - p_1 = \Delta z\rho_f g(J - 1)$ from the second equality in Equation Box 3-3 with $\Delta z = \Delta s$. Also, after multiplication by fluid volume and inverting the sign (direction of force), $F_f = -\Delta A\Delta z\theta J\rho_f g$. Substituting these items, dividing by the bulk volume $\Delta A\Delta z$ and simplifying leads to Equation Box 3-5 describing the increase of vertical effective stress in the downward direction in a saturated porous medium with vertical fluid flow driven by a hydraulic gradient J .

$$\frac{\sigma'_1 - \sigma'_2}{\Delta z} = [(1 - \theta)(\rho_g - \rho_f) + J\rho_f]g \quad (\text{Equation Box 3-5})$$

For $J = 0$, Equation Box 3-5 reduces to the hydrostatic scenario of Equation Box 3-2. The hydrodynamic component $J\rho_f g$ corresponds exactly to Equation Box 3-3 with the important difference that in Equation Box 3-5 it represents a force per unit bulk volume. The reason for this is explained by Equation Box 3-4, showing that the hydrodynamic impact of $J \neq 0$

on effective stress is two-fold: 1) it causes friction F_f as a distributed body force over the fluid volume, and 2) it modifies the difference in pore pressure $p_2 - p_1$ acting on the solid matrix surface. When considering that the solid matrix is saturated up to its surface where $z = 0$, then $\sigma'_2 = 0$ and $\Delta z = -z$, such that Equation Box 3-5 becomes Equation Box 3-6 as the direct generalization of Equation Box 3-2.

$$\sigma' = -[(1 - \theta)(\rho_g - \rho_f) + J\rho_f]gz \quad (\text{Equation Box 3-6})$$

Equation Box 3-5 and Equation Box 3-6 show that σ' becomes larger (more compressive) with depth when J is positive (i.e., downward flow). With coordinate z being positive upward, as adopted here, a positive J means that hydraulic heads are larger at the top and decrease in the downward direction, such that flux q is downward. This intuitively explains the compressive or stabilizing effect that the fluid seepage force exerts on the solid matrix when flux is downward. However, Equation Box 3-6 also indicates that for negative values of J (i.e., upward flux q), seepage forces decrease the compressive effective stress and may *destabilize the porous matrix*. Once the effective stress vanishes, there is no contact pressure between sand grains and, hence, no frictional resistance against shear between grains. Thus, the grains behave as if they were floating in the fluid and the solid matrix is said to be fluidized or liquefied, resulting in what is commonly known as *quicksand*. Mathematically, this is described by setting the bracketed term in Equation Box 3-5 to zero, yielding a *critical hydraulic gradient* J_{cr} for liquefaction as shown by Equation Box 3-7.

$$J_{cr} = -(1 - \theta) \left(\frac{\rho_g}{\rho_f} - 1 \right) \quad (\text{Equation Box 3-7})$$

For a given hydraulic conductivity K , this may be reformulated into a *critical Darcy flux* $q_{cr} = -J_{cr}K$ as shown by Equation Box 3-8.

$$q_{cr} = K(1 - \theta) \left(\frac{\rho_g}{\rho_f} - 1 \right) \quad (\text{Equation Box 3-8})$$

In summary, an analogous force balance that leads to Darcy's law in Section 6, when accounting for frictional losses in groundwater flow, may also lead to a condition of soil liquefaction, such as quicksand formation. The friction force exerted on the fluid when it flows through a stationary matrix must be balanced by a drag force that the liquid exerts on the solid.

In the simple example of vertical flow considered here, this drag force can act in a stabilizing or destabilizing way. Moreover, the frictional effects cause a concurrent redistribution of pore pressures, which further adds to the stabilizing or destabilizing influence of friction. Complete destabilization occurs when the vertical effective stress becomes zero. For the hypothetical case of equal densities (e.g., *water grains* in liquid water), we know $\rho_g = \rho_f$ and Equation Box 3-8 yields $q_{cr} = 0$, thus correctly indicating a state of inherent liquefaction, even without any destabilizing flow.

J_{cr} and q_{cr} increase with relative grain density ρ_g/ρ_f and q_{cr} also increases with increased K as the resistance to flow decreases. As porosity θ approaches one, the critical values approach zero; however, when θ approaches zero, then $J_{cr} = 1 - \rho_g/\rho_f$. This may not be intuitively obvious at first, but substitution for J into the second equality of Equation Box 3-3 for a depth Δz results in an absolute value of $p = \rho_g g \Delta z$, which exactly corresponds to the pressure under a vertical prism of density ρ_g . In this case, the contribution of friction vanishes because $\theta = 0$, and the redistribution of pressure acting on the solid body surface is solely responsible for floating. To facilitate understanding of this, imagine a heavy solid piston resting on top of a fluid within a closed cylinder where the fluid cannot by-pass the piston, so it does not sink, but it exerts pressure on the fluid below the piston.

The composite effect of frictional forces and concurrent pore pressure redistribution opens an interesting perspective on the question of “what is the critical density of an object that is much larger than the typical grain size of a liquefied sediment, that will cause the object to sink?” From the foregoing discussion, it is clear that typical sediment grains of density ρ_g and size L effectively float at the critical liquefaction limit. For objects much larger than typical sediment grains, however, Equation (77) suggests that the frictional contribution is much smaller, while the overall pore pressure redistribution remains fixed by the ambient hydraulic gradient. In the extreme case of a vanishing frictional contribution, we may reevaluate Equation Box 3-4 with $F_f = 0$ to arrive at Equation Box 3-8 and Equation Box 3-9.

$$\frac{\sigma'_1 - \sigma'_2}{\Delta z} = (1 - \theta)[\rho_g + \rho_f(J - 1)]g \quad \text{(Equation Box 3-8)}$$

$$\frac{\sigma'_1 - \sigma'_2}{\Delta z} = (1 - \theta)[\rho_g - \rho_{sat}]g \quad \text{(Equation Box 3-9)}$$

Here, J_{cr} from Equation Box 3-7 was substituted for J and ρ_{sat} represents the bulk density of the saturated sediment as shown in Equation Box 3-10.

$$\rho_{sat} = \theta\rho_f + (1 - \theta)\rho_g \quad \text{(Equation Box 3-10)}$$

Setting Equation Box 3-9 to zero shows that the critical limit for floating or sinking of a large object is $\rho_g = \rho_{sat}$. This suggests that the liquefied sediment acts with a force of buoyancy equal to that of an equivalent homogeneous fluid with the same density ρ_{sat} .

For objects much smaller than the typical sediment grain size, Equation (77) indicates the opposite scenario of increased frictional effects and larger mobilizing forces (e.g., the transport of fine sediment grains in sea beds exposed to wave-induced pressure variations). Overall, this suggests a size-dependence for sinking, floating, or rising of objects in a liquefied sediment, in the sense that larger objects of similar grain density may

sink at the same time as small objects such as fine sediments can be transported upwards to the surface.

Many of these issues are the subject of ongoing research. The possibility of destabilizing effects illustrates the importance of hydrodynamics for soil mechanics and engineering practice, which was recognized a century ago by Terzaghi (1925). On the theoretical level, the mutual fluid-solid interaction in terms of stresses and deformations is studied in the field of poroelasticity, which was pioneered by Biot (1941) while investigating soil consolidation. Comprehensive summaries of wave-induced liquefaction in sedimentary seabeds and its effects on structural stability are discussed by Jeng (2013, 2018).

[Back to where text linked to Box 3↑](#)

Box 4 - Anisotropy and Notational Conventions

Using Cartesian coordinates in all three spatial dimensions, and when hydraulic conductivity is anisotropic with the principal axes not aligned with the x , y , and z -directions, Darcy's law as derived in Section 6 is as shown by Equation Box 4-1.

$$\begin{aligned} q_x &= - \left(K_{xx} \frac{\partial h}{\partial x} + K_{xy} \frac{\partial h}{\partial y} + K_{xz} \frac{\partial h}{\partial z} \right) \\ q_y &= - \left(K_{yx} \frac{\partial h}{\partial x} + K_{yy} \frac{\partial h}{\partial y} + K_{yz} \frac{\partial h}{\partial z} \right) \\ q_z &= - \left(K_{zx} \frac{\partial h}{\partial x} + K_{zy} \frac{\partial h}{\partial y} + K_{zz} \frac{\partial h}{\partial z} \right) \end{aligned} \quad \text{(Equation Box 4-1)}$$

where:

q_i = spatial components of Darcy flux (LT^{-1})

h = hydraulic head (L)

K_{ij} = elements of the (symmetric) *hydraulic conductivity tensor* K (LT^{-1}) with subscripts i and j representing x , y , and z

The hydraulic conductivity tensor K can be written in matrix form as shown by Equation Box 4-2.

$$K = \begin{bmatrix} K_{xx} & K_{xy} & K_{xz} \\ K_{yx} & K_{yy} & K_{yz} \\ K_{zx} & K_{zy} & K_{zz} \end{bmatrix} \quad \text{(Equation Box 4-2)}$$

Equation Box 4-1 shows that, in general, a flux component in one spatial dimension also receives contributions due to the head gradient in the other two dimensions. This effect disappears when the principal directions of anisotropy are aligned with the coordinate axes because then $K_{ij} = 0$ for $i \neq j$, such that only K_{xx} , K_{yy} and K_{zz} remain different from zero. This is discussed in Section 6.4 for two dimensions.

However, Equation Box 4-1 is quite lengthy and may be written in a shorter form using matrix multiplication and *vector notation* as shown by Equation Box 4-3.

$$\vec{q} = \begin{bmatrix} q_x \\ q_y \\ q_z \end{bmatrix} = - \begin{bmatrix} K_{xx} & K_{xy} & K_{xz} \\ K_{yx} & K_{yy} & K_{yz} \\ K_{zx} & K_{zy} & K_{zz} \end{bmatrix} \cdot \begin{bmatrix} \frac{\partial h}{\partial x} \\ \frac{\partial h}{\partial y} \\ \frac{\partial h}{\partial z} \end{bmatrix} = -K \cdot \vec{\nabla} h \quad \text{(Equation Box 4-3)}$$

The arrow above q (i.e., \vec{q}) indicates that it is a vector, as opposed to scalar (e.g., h). In the final expression, the *gradient operator* $\vec{\nabla}$ is defined as shown by Equation Box 4-4.

$$\vec{\nabla}h = \text{grad } h = \begin{bmatrix} \frac{\partial h}{\partial x} \\ \frac{\partial h}{\partial y} \\ \frac{\partial h}{\partial z} \end{bmatrix} \quad (\text{Equation Box 4-4})$$

The arrow (e.g., $\vec{\nabla}$) is not always used but is included here to emphasize that the result is a vector.

Equation Box 4-1 and Equation Box 4-3 may also be written in summation form as shown by Equation Box 4-5 with $x_1 = x$, $x_2 = y$, and $x_3 = z$.

$$q_i = - \sum_{j=1}^3 K_{ij} \frac{\partial h}{\partial x_j} = -K_{ij} \frac{\partial h}{\partial x_j} \quad (\text{Equation Box 4-5})$$

The final expression uses the Einstein summation convention⁷, where although the summation sign is dropped, summation is presumed to be implicit over the repeated subscript (here j from 1 to 3 because i only appears once on the right-hand side and persists as an index on the left-hand side in q_i).

The law of continuity (mass conservation) for fluids of constant density as discussed in Section 7 leads to the *divergence operator* $\nabla \cdot$ applied to the Darcy fluxes. For three dimensions, this is shown by Equation Box 4-6.

$$\nabla \cdot \vec{q} = \text{div } \vec{q} = \frac{\partial q_x}{\partial x} + \frac{\partial q_y}{\partial y} + \frac{\partial q_z}{\partial z} = \sum_{i=1}^3 \frac{\partial q_i}{\partial x_i} = \frac{\partial q_i}{\partial x_i} \quad (\text{Equation Box 4-6})$$

Here, the final expression again adopts Einstein's summation convention over the repeated subscript i . Substituting Equation Box 4-1, Equation Box 4-3, or Equation Box 4-5 for the fluxes q_i in Equation Box 4-6 results in Equation Box 4-7.

$$\begin{aligned} \text{div}(-K \cdot \text{grad } h) &= \nabla \cdot (-K \cdot \vec{\nabla}h) = \\ &= -\frac{\partial}{\partial x} \left(K_{xx} \frac{\partial h}{\partial x} + K_{xy} \frac{\partial h}{\partial y} + K_{xz} \frac{\partial h}{\partial z} \right) \\ &\quad -\frac{\partial}{\partial y} \left(K_{yx} \frac{\partial h}{\partial x} + K_{yy} \frac{\partial h}{\partial y} + K_{yz} \frac{\partial h}{\partial z} \right) \\ &\quad -\frac{\partial}{\partial z} \left(K_{zx} \frac{\partial h}{\partial x} + K_{zy} \frac{\partial h}{\partial y} + K_{zz} \frac{\partial h}{\partial z} \right) \\ &= - \sum_{i=1}^3 \frac{\partial}{\partial x_i} \sum_{j=1}^3 K_{ij} \frac{\partial h}{\partial x_j} = -\frac{\partial}{\partial x_i} \left(K_{ij} \frac{\partial h}{\partial x_j} \right) \end{aligned} \quad (\text{Equation Box 4-7})$$

The final expression again invokes the Einstein summation convention: first, inside the parentheses over repeated subscript j as in Equation Box 4-5 and, subsequently, for the

outside derivative over the repeated subscript i in the resulting term $\partial q_i / \partial x_i$ as in Equation Box 4-6. If hydraulic conductivity is isotropic and uniform in space, and if no external sources or sinks affect the mass balance such that Equation Box 4-7 is equal to zero, we arrive at Equation Box 4-8.

$$\operatorname{div}(\operatorname{grad} h) = \nabla \cdot (\vec{\nabla} h) = \nabla^2 h = \Delta h = \frac{\partial^2 h}{\partial x^2} + \frac{\partial^2 h}{\partial y^2} + \frac{\partial^2 h}{\partial z^2} = 0 \quad (\text{Equation Box 4-8})$$

Where $\nabla^2 = \Delta$ is the Laplace operator as shown in Equation (106) for two dimensions.

[Back to where text linked to Box 4↑](#)

Box 5 - The Radial Flow Problem

Analogous to Section 7 for Cartesian coordinates, we apply Darcy's law and the principle of mass conservation to a situation of purely radial flow in a horizontal plane as illustrated in Figure Box 5-1.

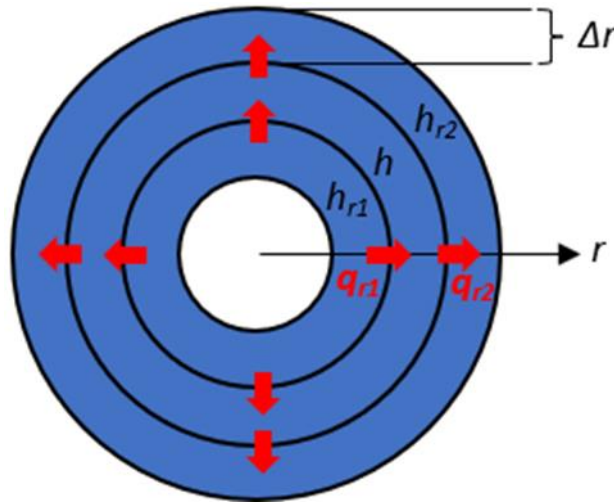


Figure Box 5-1 - Three interacting annular reservoirs of thickness Δr in the horizontal plane at hydraulic heads h and exchanging fluxes q (red arrows).

As in Equation (99), we start with the mass balance for the center ring of inner radius r as shown by Equation Box 5-1.

$$\frac{\Delta V}{\Delta t} = 2\pi\Delta z r q_{r1} - 2\pi\Delta z (r + \Delta r) q_{r2} \quad (\text{Equation Box 5-1})$$

In this equation, Δz is again the height of the reservoirs in the third dimension (i.e., in this case the vertical direction). The volumetric change ΔV may be related to respective changes Δh in head as shown by Equation Box 5-2.

$$\Delta V = S\Delta h\pi[(r + \Delta r)^2 - r^2] \approx 2\pi r S\Delta h\Delta r \quad (\text{Equation Box 5-2})$$

where:

S = the storage coefficient (dimensionless)

The approximation is justified by neglecting Δr^2 as being very small.

Substitution of Equation Box 5-2 into Equation Box 5-1 with subsequent division by $2\pi r\Delta r$ leads to Equation Box 5-3.

$$S \frac{\Delta h}{\Delta t} = \frac{\Delta z}{r} \frac{r q_{r1} - (r + \Delta r) q_{r2}}{\Delta r} \quad (\text{Equation Box 5-3})$$

This equation becomes Equation Box 5-4 in differential form.

$$S \frac{\partial h}{\partial t} = - \frac{\Delta z}{r} \frac{\partial (r q)}{\partial r} \quad (\text{Equation Box 5-4})$$

Substituting Darcy's law $q = -K\partial h/\partial r$ then gives Equation Box 5-5 with $T_K = K\Delta z$ representing the uniform hydraulic transmissivity of an aquifer.

$$S \frac{\partial h}{\partial t} = \frac{T_K}{r} \frac{\partial}{\partial r} \left(r \frac{\partial h}{\partial r} \right) \quad (\text{Equation Box 5-5})$$

Differentiating the term in parentheses by parts allows writing an equivalent solution as shown by Equation Box 5-6.

$$\frac{S}{T_K} \frac{\partial h}{\partial t} = \frac{\partial^2 h}{\partial r^2} + \frac{1}{r} \frac{\partial h}{\partial r} \quad (\text{Equation Box 5-6})$$

Equation Box 5-6 in radial coordinates is one-dimensional in contrast to the two-dimensional form of the corresponding Equation (105) for Cartesian coordinates. In this case, flow is one-dimensional, varying only in the radial direction r . The last term in Equation Box 5-6 corrects for the diverging (or converging) stream lines of a radial flow field. For very large distances from the origin of the radial coordinate system, the factor $1/r$ becomes very small, and the correction term vanishes, such that Equation Box 5-6 collapses to a one-dimensional form of Equation (105).

Similar remarks to those made in Section 7 are also pertinent here, but we only emphasize the case of a circular aquifer (e.g., an idealized island in a freshwater lake) receiving spatially uniform recharge q_{re} (LT^{-1}) per unit surface area. Since Equation Box 5-5 is already written in the same dimensions of q_{re} , it may be added as an additional source (positive) term on the right-hand side. After division by S , we find Equation Box 5-7.

$$\frac{\partial h}{\partial t} = \frac{1}{S} \left[q_{re} + \frac{T_K}{r} \frac{\partial}{\partial r} \left(r \frac{\partial h}{\partial r} \right) \right] \quad (\text{Equation Box 5-7})$$

This is identical to Equation (41) if we substitute v for h , ρ for S , μ for T_K , and $\rho g \partial h / \partial s = -\rho g J$ for q_{re} . Consequently, the results of Section 3.3 are again directly applicable (e.g., Equation (43) and Figure 10).

Of particular interest in practice is the situation of groundwater pumping from an aquifer at a well. If the well screen spans the entire thickness of a relatively homogeneous and confined aquifer, then flow may be considered radial and Equation Box 5-5 is valid. At steady-state $\partial h / \partial t = 0$ such that we obtain Equation Box 5-8.

$$\frac{\partial}{\partial r} \left(r \frac{\partial h}{\partial r} \right) = 0 \quad (\text{Equation Box 5-8})$$

Then, integrating once, followed by division by r , gives Equation Box 5-9 where C_1 is an integration constant.

$$\frac{\partial h}{\partial r} = \frac{C_1}{r} \quad (\text{Equation Box 5-9})$$

Integrating once more yields Equation Box 5-10 with a second integration constant C_2 .

$$h = C_1 \ln r + C_2 \quad (\text{Equation Box 5-10})$$

This is a degenerate form of the solution to Equation (42)—but the logarithmic term is crucial now.

The pumping rate Q_p (L^3T^{-1}) to the well may be expressed by Darcy's law as $Q_p = 2\pi r T_K \partial h / \partial r$ such that Equation Box 5-9 delivers $C_1 = Q_p / (2\pi T_K)$, with the negative sign omitted to indicate that we take Q_p as positive for groundwater extraction. Next, imposing a head h_0 at a distance r_0 from the well, Equation Box 5-10 gives $C_2 = h_0 - C_1 \ln r_0$. Substituting the expressions for C_1 and C_2 into Equation Box 5-10 results in Equation Box 5-11.

$$h = h_0 + \frac{Q_p}{2\pi T_K} \ln \frac{r}{r_0} \quad (\text{Equation Box 5-11})$$

This is known as the Thiem (1906) solution for steady-state radial flow in a confined aquifer of uniform thickness.

[Back to where text linked to Box 5](#) ↑

Box 6 - The Water Table Ratio

As noted in remark 8 of Section 7 and as illustrated in Figure Box 6-1, consider a one-dimensional aquifer delimited by two parallel rivers separated by a distance $2L$. If the topographic elevations d of the landscape above the rivers are larger than $h_{max} = (q_{re}L^2)/(2T_K)$ as specified by Equation (115), then *topography does not interfere with water table elevation*, rather the water table elevation is controlled by recharge. However, when d is smaller than h_{max} the water table is sufficiently high to generate surface drainage along elevated valleys. This causes local depressions in the water table as shown in Figure Box 6-2 such that the water table elevation profile becomes *increasingly controlled by and mimics the topographic elevation profile*.

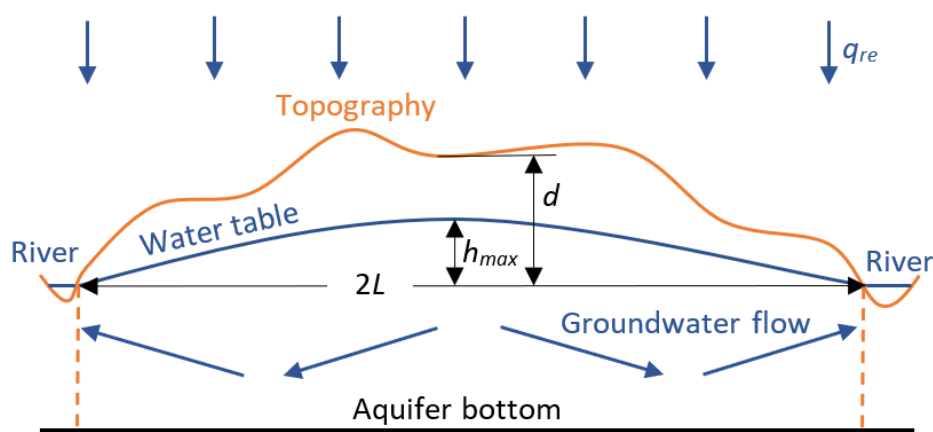


Figure Box 6-1 – One-dimensional aquifer of average transmissivity T_K between two rivers receiving baseflow from the aquifer (dashed vertical lines represent idealized boundary conditions of fully penetrating rivers). The water table is controlled by recharge because the water table ratio $W = h_{max}/d$ is small, and topography does not interfere.

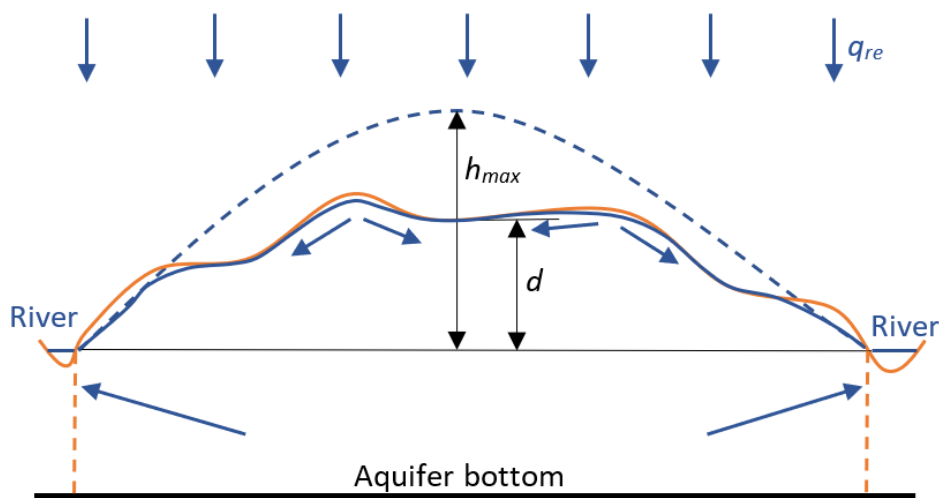


Figure Box 6-2 – One-dimensional aquifer of average transmissivity T_K between two rivers receiving baseflow from the aquifer (dashed vertical lines represent idealized boundary conditions of fully penetrating rivers). The water table is controlled by topography because the water table ratio $W = h_{max}/d$ is large and changes in recharge only affect surface runoff at local depressions.

Other GW-Project books address the relationship between topography and groundwater flow such as [Graphical Construction of Groundwater Flow Nets](#) (Poeter & Hsieh, 2021) and [Groundwater in our Water Cycle](#) (Poeter et al., 2020). In addition, the book [Groundwater - Surface Water Exchange](#) (Woessner, 2020) discusses general aspects of aquifer-river interaction.

A dimensionless parameter called the *water table ratio* W is defined as shown by Equation Box 6-1. It distinguishes between recharge-controlled and topography-controlled groundwater systems (Haitjema & Mitchell Bruker, 2005; Cuthbert et al., 2019).

$$W = \frac{h_{max}}{d} = \frac{q_{re}L^2}{2T_K d} \quad (\text{Equation Box 6-1})$$

Alternatively, the water table ratio may be regarded as a *measure of the "fullness" of an aquifer*, in the sense of how filled it is with water. This can be a useful parameter not only in arid climates, but also in regions where active surface drainage networks may change dynamically (e.g., in basins with discontinuous baseflow contributions and ephemeral streams). If we consider $T_{aqu} = SL^2/T_K$ from Equation (113) as the *time scale for an aquifer to significantly drain* down to the river elevation in the absence of recharge, and $T_{fill} = dS/q_{re}$ as the *time scale for an aquifer to completely fill* in the absence of discharge (i.e., zero baseflow to the rivers), then we find what is expressed in Equation Box 6-2.

$$W_{fullness} = \frac{T_{aqu}}{T_{fill}} = \frac{q_{re}L^2}{T_K d} \quad (\text{Equation Box 6-2})$$

This is the same as Equation Box 6-1 in terms of order-of-magnitude, because the different factor of 2 is of order one; it originates from the particular one-dimensional aquifer geometry illustrated in Figure Box 6-1 and Figure Box 6-2.

[Back to where text linked to Box 6](#) ↑

Box 7 - Unsaturated Flow and Richards Equation

The mass balance of Equation (104) assumes saturated conditions where the entire pore space is filled with water and changes in storage only occur due to elastic deformation and/or fluctuations in water table elevation. Under unsaturated conditions in the so-called *vadose zone*, the pore space is only partially filled with water, while air occupies the remaining volume. Water may be stored or released by changes in the water (or in this context also called moisture) content θ_w (dimensionless), which expresses the fraction of a medium's bulk volume that is filled with water.

Consequently, θ_w may range from zero (or some minimum residual value) up to the value of its total porosity. Moreover, saturated groundwater flow is predominantly horizontal (especially on a regional scale), while water transport in unsaturated porous media is mostly vertically downward through the vadose zone. This is represented in Figure Box 7-1 where the vertical axis on the page represents the z -direction whereas in previous illustrations it has represented the y -direction. Consequently, the mass balance of Equation (99) is rewritten as shown by Equation Box 7-1 where y is the third dimension not shown in Figure Box 7-1.

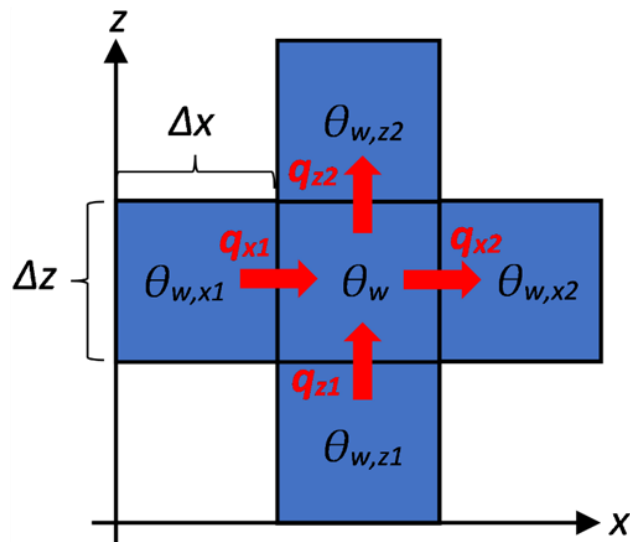


Figure Box 7-1 - Five interacting unsaturated reservoirs of size $\Delta x \Delta z$ in the vertical plane at water contents θ_w and exchanging fluxes q (red arrows).

$$\frac{\Delta V}{\Delta t} = (q_{x1} - q_{x2})\Delta y \Delta z + (q_{z1} - q_{z2})\Delta x \Delta y \quad (\text{Equation Box 7-1})$$

Volumetric change for unsaturated conditions is represented by changes in water content as shown in Equation Box 7-2 rather than by changes in head coupled with a storage parameter as shown in Equation (100).

$$\Delta V = \Delta \theta_w \Delta x \Delta y \Delta z \quad (\text{Equation Box 7-2})$$

Substituting Equation Box 7-2 into Equation Box 7-1 and dividing by $\Delta x \Delta y \Delta z$ yields Equation Box 7-3.

$$\frac{\Delta \theta_w}{\Delta t} = \frac{q_{x1} - q_{x2}}{\Delta x} + \frac{q_{z1} - q_{z2}}{\Delta z} \quad (\text{Equation Box 7-3})$$

The differential form of Equation Box 7-3 is Equation Box 7-4.

$$\frac{\partial \theta_w}{\partial t} = - \left(\frac{\partial q_x}{\partial x} + \frac{\partial q_z}{\partial z} \right) \quad (\text{Equation Box 7-4})$$

Positive values of $\partial q_x / \partial x$ and $\partial q_z / \partial z$ decrease the water content θ_w because a positive value indicates that flux increases in the direction of the respective coordinate such that the outfluxes q_{x2} and q_{z2} in Figure Box 7-1 are larger than the influxes q_{x1} and q_{z1} .

Besides the difference between saturated and unsaturated flow with respect to storage changes as indicated by Equation Box 7-2, another important difference is that under unsaturated conditions the *effects of wettability and surface tension cause capillary suction*, which can be described by negative pressures as opposed to positive (compressive) pressures in the saturated zone below the water table. When water content is lower, pressure is lower (i.e., a larger negative value).

In the same way as Equation (73) is derived from the force balance in Figure 13 for a saturated medium of porosity n , the force balance remains valid for unsaturated conditions of water content $\theta_w < n$. However, an additional phenomenon occurs for unsaturated flow that significantly complicates the problem. That is, hydraulic conductivity K is dependent on water content. When water content is lower, hydraulic conductivity is lower. Thus, hydraulic conductivity K is a function of water pressure p_w with lower values of K at lower pressure.

In short, as p_w becomes more negative (i.e., stronger capillary suction), K approaches zero. To account for this, we rewrite Equation (80) as shown by Equation Box 7-5 with an explicit emphasis on the dependences of p_w and K on θ_w .

$$q = -K(\theta_w) \frac{d \left(\frac{p_w(\theta_w)}{\rho g} + z \right)}{ds} \quad (\text{Equation Box 7-5})$$

Because of these dependences, it is no longer useful to define a combined hydraulic head as in Equation (74). However, for $ds = dx$ we differentiate along the x -direction, leading to Equation Box 7-6 because $dz/dx = 0$ (elevation does not change in the horizontal direction).

$$q_x = -K(\theta_w) \frac{dh_m(\theta_w)}{dx} \quad (\text{Equation Box 7-6})$$

For $ds = dz$, differentiation is along the z -direction, yielding Equation Box 7-7 because $dz/dz = 1$.

$$q_z = -K(\theta_w) \left(\frac{dh_m(\theta_w)}{dz} + 1 \right) \quad (\text{Equation Box 7-7})$$

In both Equation Box 7-6 and Equation Box 7-7, we use the matrix head h_m (L) defined as shown by Equation Box 7-8.

$$h_m = \frac{p_w}{\rho g} \quad (\text{Equation Box 7-8})$$

In contrast to the hydraulic head for saturated flow in Equation (74), h_m is purely a function of matrix (water) pressure p_w and does not depend on elevation z . It may also be regarded as a *matrix potential* because it is a scalar variable whose gradient (spatial derivative) is proportional to a flow driving force due to differences in matrix pressures. This is shown directly in Equation Box 7-6 in the horizontal direction, but can also be discerned for the vertical direction by ignoring the contribution of gravity (elevation change) embedded in the final term “+1” in Equation Box 7-7. The contribution of gravity to q_z is negative overall because the vertical coordinate z is defined as positive upward and the force of gravity is downward.

Substituting Equations Box 7-6 and Box 7-7 into Equation Box 7-4 gives Equation Box 7-9.

$$\frac{\partial \theta_w}{\partial t} = \frac{\partial}{\partial x} \left(K(\theta_w) \frac{dh_m(\theta_w)}{dx} \right) + \frac{\partial}{\partial z} \left(K(\theta_w) \frac{dh_m(\theta_w)}{dz} \right) + \frac{\partial K(\theta_w)}{\partial z} \quad (\text{Equation Box 7-9})$$

This is known as Richards equation⁷ written in terms of θ_w here, for which functional relationships to K and h_m need to be known for a given soil type (Richards, 1931). Alternatively, a reformulation in terms of h_m results in Equation Box 7-10 where the soil moisture capacity $C_m = \partial \theta_w / \partial h_m$ is a function of h_m and expresses the change in water stored for a unit change in matrix head.

$$C_m(h_m) \frac{\partial h_m}{\partial t} = \frac{\partial}{\partial x} \left(K(h_m) \frac{dh_m}{dx} \right) + \frac{\partial}{\partial z} \left(K(h_m) \frac{dh_m}{dz} \right) + \frac{\partial K(h_m)}{\partial z} \quad (\text{Equation Box 7-10})$$

Soil moisture capacity C_m has a role analogous to that of specific storage S_s for saturated conditions. This is discussed in remark 7 of Section 7 of this book and by Bear (1972).

In the same way as shown by Equation (107), Equations Box 7-9 and Box 7-10 can be generalized by including respective source and/or sink terms. For example, a source term can represent recharge by rainfall at the soil surface. A sink term can represent water consumption by plant roots as a function of both depth and available moisture (and energy) in the soil zone. The latter is difficult to quantify, but if appropriate simplifications are applied, the water balance of the soil zone may be used as the fundamental mechanism for quantifying deep percolation across the vadose zone of an aquifer toward the water table. In the vadose zone, sources and sinks are unlikely to act, but significant delay (time lags) and smoothing of a recharge signal between the soil zone and the saturated aquifer zone may occur. This implies that responses of the water table—and, hence, river baseflow—

climatic drivers may be significantly affected by the unsaturated moisture transport in the vadose zone.

[Back to where text linked to Box 7 ↗](#)

Box 8 - Multi-Phase Flow

In Box 7, we considered the pore space to be partially filled with water and air but did not explicitly account for air pressure. It was assumed to be constant (atmospheric) and not affected by changes in water content or air fluxes. As a generalization to this scenario, we now consider another fluid to be present in the pore space instead of air. If the fluid is *immiscible with water*, it will remain as a separate phase leading to a multiple-phase (in this case two phases: water and the other immiscible fluid) flow problem. This is relevant for petroleum engineering and for contamination of groundwater by non-aqueous phase liquids (NAPLs) such as toxic petroleum derivatives (e.g., gasoline) and many others.

To account for a second fluid phase, we denote the volumetric water content by θ_w , while we introduce θ_n for the volumetric NAPL content. If air is absent and the pore space is completely saturated, then the sum of both must equal the porosity θ as shown by Equation Box 8-1.

$$\theta = \theta_w + \theta_n \quad (\text{Equation Box 8-1})$$

The different wettability of water and NAPL with respect to the porous matrix induces pore scale curvature of the water-NAPL interface. As with water and air, the combination of this curvature and the surface tension between the fluids generates a *capillary pressure difference* p_c between the pressures p_w and p_n in the water and NAPL phases, respectively, which is shown in Equation Box 8-2.

$$p_c = p_n - p_w \quad (\text{Equation Box 8-2})$$

Typically, water is the wetting phase such that it preferentially covers the porous matrix surface leading to interface curvatures that bend into the water phase. Thus, surface tension acts to compress the NAPL phase and increase p_n with respect to p_w . This yields positive values of p_c from Equation Box 8-2. For the unsaturated air-water problem of Box 7, we may set $p_n = 0$ such that negative values of p_w give positive values of capillary pressure p_c .

Assuming incompressibility of both fluids (i.e., invariable fluid densities), the volumetric flow balances of the water and NAPL content become analogous to that of Equation Box 7-4 as shown by Equation Box 8-3 and Equation Box 8-4.

$$\frac{\partial \theta_w}{\partial t} = - \left(\frac{\partial q_{w,x}}{\partial x} + \frac{\partial q_{w,z}}{\partial z} \right) \quad (\text{Equation Box 8-3})$$

$$\frac{\partial \theta_n}{\partial t} = - \left(\frac{\partial q_{n,x}}{\partial x} + \frac{\partial q_{n,z}}{\partial z} \right) \quad (\text{Equation Box 8-4})$$

Similar to Equation Box 7-5, Equations (80) and (81) may be used to express the water and NAPL fluxes as shown by Equations Box 8-5 through Equation Box 8-8 where

μ_w and μ_n are the dynamic viscosities, while ρ_w and ρ_n are the densities of water and NAPL, respectively.

$$q_{w,x} = -\frac{kk_{r,w}}{\mu_w} \frac{d(p_w + \rho_w gz)}{dx} \quad (\text{Equation Box 8-5})$$

$$q_{w,z} = -\frac{kk_{r,w}}{\mu_w} \frac{d(p_w + \rho_w gz)}{dz} \quad (\text{Equation Box 8-6})$$

$$q_{n,x} = -\frac{kk_{r,n}}{\mu_n} \frac{d(p_n + \rho_n gz)}{dx} \quad (\text{Equation Box 8-7})$$

$$q_{n,z} = -\frac{kk_{r,n}}{\mu_n} \frac{d(p_n + \rho_n gz)}{dz} \quad (\text{Equation Box 8-8})$$

The intrinsic permeability k (L^2) is a property of the porous medium, which is reduced by *relative permeability factors* $k_{r,w}$ and $k_{r,n}$ (dimensionless) to arrive at effective values for each fluid phase as a function of their respective volumetric contents. Equations Box 8-5 through 8-8 may be substituted into Equations Box 8-3 and 8-4 to arrive at Equations Box 8-9 and 8-10.

$$\frac{\partial \theta_w}{\partial t} = \frac{1}{\mu_w} \left\{ \frac{\partial}{\partial x} \left[kk_{r,w} \frac{d(p_w + \rho_w gz)}{dx} \right] + \frac{\partial}{\partial z} \left[kk_{r,w} \frac{d(p_w + \rho_w gz)}{dz} \right] \right\} \quad (\text{Equation Box 8-9})$$

$$\frac{\partial \theta_n}{\partial t} = \frac{1}{\mu_n} \left\{ \frac{\partial}{\partial x} \left[kk_{r,n} \frac{d(p_n + \rho_n gz)}{dx} \right] + \frac{\partial}{\partial z} \left[kk_{r,n} \frac{d(p_n + \rho_n gz)}{dz} \right] \right\} \quad (\text{Equation Box 8-10})$$

As written here, μ_w and μ_n are assumed to be constant (taken out of the derivatives), while k may vary in space. These parameters and the constant fluid densities need to be known a priori. Moreover, appropriate relationships need to be used to define $k_{r,w}$ and $k_{r,n}$ as functions of θ_w and θ_n , respectively. Thus, Equation Box 8-9 and Equation Box 8-10 become a *coupled system of two partial differential equations* in the four unknown variables θ_w , θ_n , p_w , and p_n .

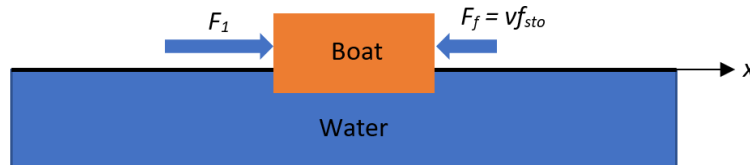
The remaining information in the form of two additional equations for solving the problem (typically by some numerical method) is given by Equations Box 8-1 and 8-2, where porosity θ is a known parameter, while capillary pressure p_c is a function of θ_w and an appropriate functional relationship has to be applied. If air is still present as a third gaseous phase in addition to water and NAPL, then the same principles as outlined here and in Box 7 remain valid, with many further details given in Kueper and Frind (1991), and the classical textbooks by Corey (1994) and Dullien (1979).

[Back to where the text linked to Box 8 ↑](#)

11 Exercise Solutions

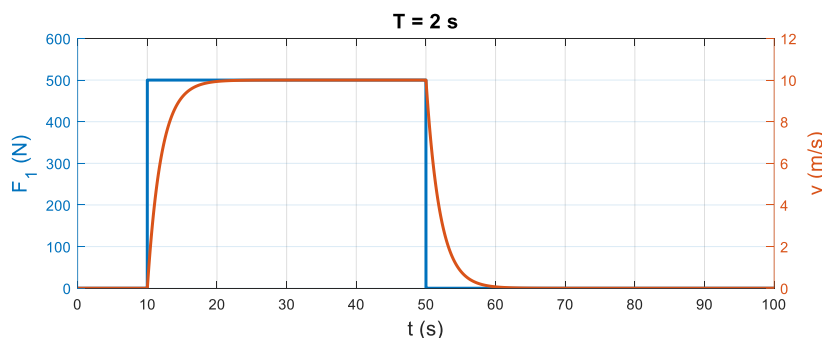
Solution Exercise 1 - Accelerating Boat and Response-Time Scales

- a) The following figure is a conceptual sketch of the forces acting on a boat, based on Figure 4, where the resisting force $F_f = v f_{sto}$. The friction factor f_{sto} has units of Ns/m, which is Newtons per meter/second. Thus, it indicates the increase of the drag force in N (here, 50) that acts on the boat as its velocity increases by 1 m/s.



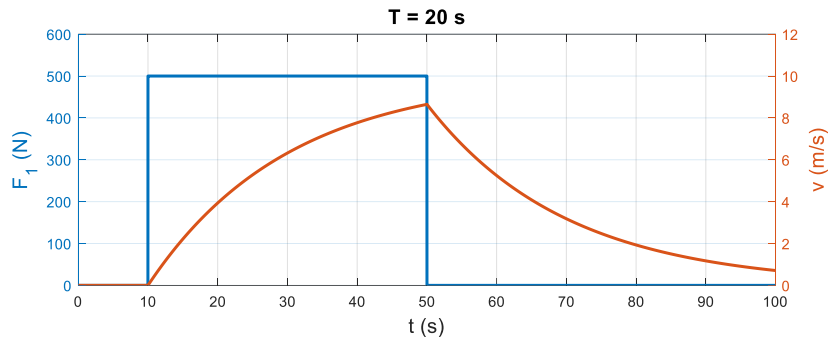
Conceptual sketch of driving and resisting forces acting on the boat.

- b) From Equation (18), we know that $v_{\infty} = F_1/f_{sto} = 500/50 = 10$ m/s. The final velocity does not depend on boat mass m , because $F_1 = F_f$ at steady state when inertial forces are absent. From Equation (20), we know that $T = m/f_{sto} = 100/50 = 2$ s. This is independent of the driving force F_1 .
- c) The time scale T indicates the time required for the boat to closely approach its final velocity. From Section 2.3, and as shown in the following graph of boat velocity (*Boat velocity v in response to driving force F_1 for $m = 100$ kg resulting in $T = 2$ s*), v will increase by an exponential function such that after a time T (i.e., 2 s, which is at 12 s on the x -axis) approximately 65 percent of the difference between initial and final velocity is reached. After a time $3T$ (i.e., 6 s, which is at 16 s on the x -axis), the velocity is approximately 95 percent, and after $5T$ (i.e., 10 s, which is at 20 s on the x -axis) v practically matches v_{∞} (although theoretically the approach is asymptotic so reaching the final velocity takes infinite time). When the propeller stops driving the boat at $t = 50$ s, the exact opposite progression of velocity with time occurs, that is $T = 2$ s remains unaffected, while $v_{\infty} = F_1/f_{sto}$ is now zero because $F_1 = 0$.



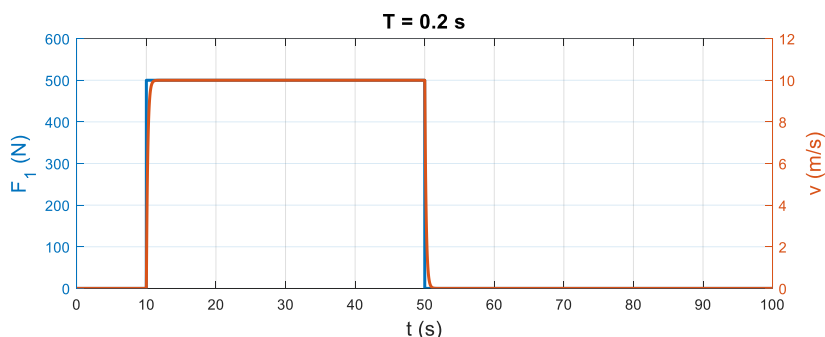
Boat velocity v in response to driving force F_1 for $m = 100$ kg resulting in $T = 2$ s.

- d) For a boat that is ten times heavier (i.e., of mass $m = 1000$ kg), the response-time scale is ten times larger (i.e., $T = 20$ s), while v_∞ remains the same. T is of the same order-of-magnitude (tens of seconds) as the 40-second period during which the force is applied so the transient phase of acceleration is too long for the boat to reach steady-state velocity, as illustrated in the next graph (*Boat velocity v in response to driving force F_1 for $m = 1000$ kg resulting in $T = 20$ s*).



Boat velocity v in response to driving force F_1 for $m = 1000$ kg resulting in $T = 20$ s.

- e) In contrast, as shown in the following figure (*Boat velocity v in response to driving force F_1 for $m = 10$ kg resulting in $T = 0.2$ s*), a boat of $m = 10$ kg reaches steady-state relatively quickly, because $T = 0.2$ s. This is much smaller than the time scale of interest of tens of seconds such that the quasi-steady-state assumption of $v \approx v_\infty$ is very reasonable. Intuitively, this means that the simple solution $v = F_1/f_{sto}$ is a good approximation of the exact exponential solution as reflected by the graph below. However, if we zoom into a time window between $t = 10$ and 11 s then the time scale of interest is reduced to the sub-second scale, which is on the same order-of-magnitude as T . The resulting zoomed-in view would be like the chart above for $T = 20$ s. In this case, the transient part of the response cannot be neglected, and the quasi-steady-state assumption would imply significant errors.



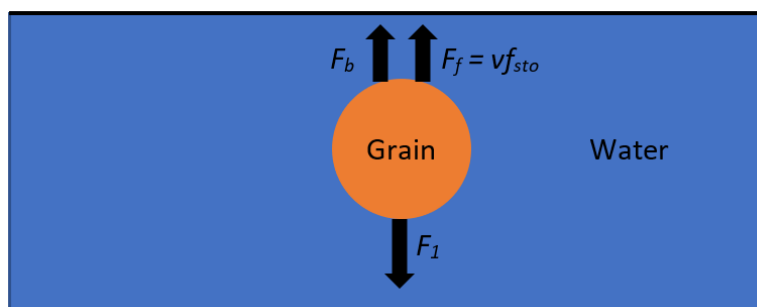
Boat velocity v in response to driving force F_1 for $m = 10$ kg resulting in $T = 0.2$ s.

[Return to Exercise 1](#) ↗

[Return to where text linked to Exercise 1](#) ↗

Solution Exercise 2 - Stokes Friction and Terminal Velocity of a Sinking Sphere

- a) As illustrated in the figure below of a sinking, spherical sand grain, the downward driving force on the grain is due to gravity and equal to $F_1 = V\rho_g g = 1.03 \times 10^{-7}$ N; where $\rho_g = 2500 \text{ kg/m}^3$, $g = 9.81 \text{ m/s}^2$ is the acceleration of gravity, and $V = 4\pi R^3/3 = 4.19 \times 10^{-12} \text{ m}^3$ is the volume of the grain given that $R = 0.1 \text{ mm} = 0.0001 \text{ m}$. The resisting upward forces on the grain are due to viscous friction $F_f = f_{sto}v_\infty = 6\pi R\mu v_\infty$ (Equation (23)) and buoyancy $F_b = V\rho_f g = 4.11 \times 10^{-8}$ N.



Conceptual sketch of a sand grain sinking at a constant velocity with driving and resisting forces.

- b) At the terminal sinking velocity, inertial forces are absent (no more acceleration and $dv/dt = 0$ in Equation (14), for example). Thus, the force balance on the grain becomes $F_1 = F_b + F_f$ and substituting values from the previous paragraph allows for calculation of v_∞ as the terminal sinking velocity.

$$v_\infty = \frac{2g(\rho_g - \rho_f)R^2}{9\mu} = \frac{2\left(9.81 \frac{\text{m}}{\text{s}^2}\right)\left(2500 \frac{\text{kg}}{\text{m}^3} - 1000 \frac{\text{kg}}{\text{m}^3}\right)(0.0001 \text{ m})^2}{9\left(0.001 \frac{\text{kg}}{\text{ms}}\right)} = 0.0327 \frac{\text{m}}{\text{s}} \text{ or } 3.27 \frac{\text{cm}}{\text{s}}$$

By reformulating this equation to isolate μ , the viscosity of a liquid may be estimated from measuring the sinking velocity v_∞ of a spherical particle in a laboratory experiment.

[Return to Exercise 2](#) ↗

[Return to where text linked to Exercise 2](#) ↗

Solution Exercise 3 - Implementing the Euler Forward Method

Below is a code implementation in [MATLAB](#) or [Octave](#) with a single loop in time over index i and a vector of velocities v over locations n . The time step dt needs to be small enough for a stable solution. In particular, we apply the stability criterion of Von Neumann requiring that $dt \leq \alpha dn^2/2$, where $\alpha = 1$ is the coefficient of the second derivative in Equation (36) and a coefficient of 0.8 is added in the code as a *safety margin* from the stability limit. The result of the code with the parameter values as indicated is shown in the figure that follows the code. Numerical instability can be observed by raising α to values greater than one. [The MATLAB code shown below is provided in a zip file on the web page for this book](#).

```

dn = 0.05;           % dimensionless grid size in n-direction (-)
dt = 0.8 * (dn^2)/2; % dimensionless time step (-)
tmax = 0.1;         % dimensionless simulation time (-)

t = 0:dt:tmax; % vector of dimensionless time (-)
n = -1:dn:1;   % vector of dimensionless n-coordinates (-)

v = zeros(size(n)); % initial condition for dimensionless velocity (-)

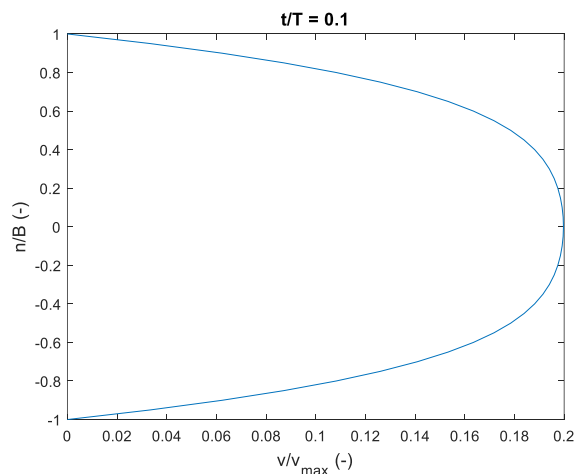
for i = 1:numel(t) % loop in time for repeated application of Equation Box 2-6

    v(2:end-1) = v(2:end-1) + (2 + (v(1:end-2) - 2*v(2:end-1) + v(3:end)) / dn^2) * dt;
    % v(1) and v(end) always remain at zero here
    % to implement the no-slip boundary condition

end

figure
plot(v,n)
xlabel('v/v_{max} (-)')
ylabel('n/B (-)')
title(['t/T = ', num2str(tmax)])

```



Dimensionless solution of the laminar flow problem between two flat plates from numerical computation by the Euler forward method for $t/T = 0.1$.

[Return to Exercise 3](#) ↑

[Return to where text linked to Exercise 3](#) ↑

Solution Exercise 4 - Effective Hydraulic Conductivity of a Fracture and a Pipe

a) One form of Darcy's law is expressed by Equation (85) as follows.

$$Q = -AK \frac{\Delta h}{\Delta L}$$

where:

Q = flow rate (volumetric discharge) (L^3T^{-1})

A = cross-sectional area transverse to flow direction (L^2)

K = hydraulic conductivity (LT^{-1})

Δh = change in hydraulic head (L) over distance ΔL (L) in the flow direction

For comparison, Equation (32) gives the flow rate between two flat plates per unit transverse width of flow in the third dimension as follows.

$$Q_{plates} = -\frac{2\rho g}{3\mu} B^3 J$$

where:

Q_{plates} = flow rate between plates per unit transverse width (L^2T^{-1})

$J = \Delta h/\Delta L$ = hydraulic gradient (-)

B = half-width between the plates (L)

μ = dynamic viscosity of the fluid ($ML^{-1}T^{-1}$)

While the dimensions of Q are volume per time (L^3T^{-1}), those of Q_{plates} are volume per time per unit transverse width (L^2T^{-1}). By using $A = 2B$ as the flow cross-sectional area per unit transverse width, the two equations become dimensionally consistent, and when using an effective hydraulic conductivity K_{plates} (LT^{-1}) we can equate them to arrive at the following.

$$-2BK_{plates} = -\frac{2\rho g}{3\mu} B^3$$

$$K_{plates} = \frac{\rho g B^2}{3\mu}$$

b) For flow in a circular pipe of radius R , Equation (45) gives the following.

$$Q_{pipe} = -\frac{\rho g \pi}{8\mu} R^4 J$$

where:

Q_{pipe} = flow rate along pipe (L^3T^{-1})

R = pipe radius (L)

By equating the right-hand sides of Equation (45) and Equation (85), which are already of identical dimensions (L^3T^{-1}), and using an effective hydraulic conductivity K_{pipe} (LT^{-1}) we find the following.

$$-AK_{pipe} \frac{\Delta h}{\Delta L} = -\frac{\rho g \pi}{8\mu} R^4 J$$

By writing A as πR^2 , and again canceling J with $\Delta h/\Delta L$, we arrive at the following.

$$K_{pipe} = \frac{\rho g R^2}{8\mu}$$

This is smaller than K_{plates} for $R = B$ because there is more viscous friction due to the presence of the pipe wall in all transverse directions. The effective conductivity K_{pipe} is directly related to the friction factor used for laminar flow in pipe hydraulics.

[Return to Exercise 4](#) ↑

[Return to where text linked to Exercise 4](#) ↑

Solution Exercise 5 - Effective Hydraulic Conductivity of Layered Media

- a) In the case of flow perpendicular to the layers, we use Equation (84) to express the hydraulic resistance R_K over both layers for some arbitrary cross-sectional area A as shown here.

$$R_K = \int_0^{L_1} \frac{1}{AK_1} ds + \int_{L_1}^{L_1+L_2} \frac{1}{AK_2} ds = \frac{1}{A} \left(\frac{L_1}{K_1} + \frac{L_2}{K_2} \right)$$

For an equivalent, but homogeneous, medium of effective conductivity $K_{eff-perpendicular}$, the resistance R_K is as follows.

$$R_K = \int_0^{L_1+L_2} \frac{1}{AK_{eff-perpendicular}} ds = \frac{L_1 + L_2}{AK_{eff-perpendicular}}$$

We want an expression using $K_{eff-perpendicular}$ to produce the same discharge as an expression for the heterogeneous medium given the same head gradient. Hence, we equate the two equations and solve for $K_{eff-perpendicular}$.

$$\frac{1}{A} \left(\frac{L_1}{K_1} + \frac{L_2}{K_2} \right) = \frac{L_1+L_2}{AK_{eff-perpendicular}}$$

Rearranging, we obtain.

$$K_{eff-perpendicular} = \frac{L_1 + L_2}{\frac{L_1}{K_1} + \frac{L_2}{K_2}}$$

In this case the effective hydraulic conductivity is the flow length-weighted harmonic average of K_1 and K_2 .

- b) In the case of flow parallel to the layers, we may use Equation (84) to find the total discharge along both layers of arbitrary width Δy as follows.

$$Q = Q_1 + Q_2 = -\Delta y L_1 K_1 \frac{\Delta h}{L} - \Delta y L_2 K_2 \frac{\Delta h}{L}$$

For a single homogeneous medium of effective conductivity $K_{eff-parallel}$, the discharge is as follows.

$$Q = -\Delta y (L_1 + L_2) K_{eff-parallel} \frac{\Delta h}{L}$$

We want an expression using $K_{eff-parallel}$ to produce the same discharge as an expression for the heterogeneous medium given the same head gradient. Hence, we equate the two expressions and solve for $K_{eff-parallel}$.

$$-\Delta y (L_1 + L_2) K_{eff-parallel} \frac{\Delta h}{L} = -\Delta y L_1 K_1 \frac{\Delta h}{L} - \Delta y L_2 K_2 \frac{\Delta h}{L}$$

Cancelling the gradient and Δy terms, and multiplying both sides by -1 we obtain the following.

$$(L_1 + L_2)K_{eff-parallel} = L_1K_1 + L_2K_2$$

Rearranging produces the following expression for $K_{eff-parallel}$.

$$K_{eff-parallel} = \frac{L_1K_1 + L_2K_2}{L_1 + L_2}$$

In this case the effective hydraulic conductivity is the layer thickness-weighted arithmetic average of K_1 and K_2 .

[Return to Exercise 5](#) ↑

[Return to where text linked to Exercise 5](#) ↑

Solution Exercise 6 - Freshwater-Saltwater Interaction and Ghyben-Herzberg Principle

- a) At the saltwater interface and at steady-state, the pressure of the freshwater column is equal to $(h + H)\rho_f g$, while the pressure on the saltwater side is $H\rho_s g$. Both pressures must be the same resulting in the following.

$$(h + H)\rho_f g = H\rho_s g$$

$$\frac{1}{H}(h + H)\rho_f = \rho_s$$

$$\frac{\rho_f h}{H} + \rho_f = \rho_s$$

$$\frac{\rho_f h}{H} = \rho_s - \rho_f$$

$$\frac{\rho_f h}{\rho_s - \rho_f} = H$$

$$H = \frac{\rho_f}{\rho_s - \rho_f} h = 40h$$

which is known as the Ghyben-Herzberg principle⁷, and shows that most ((40/41)100 percent \approx 98 percent) of the freshwater in a coastal aquifer that is hydraulically connected to the ocean resides below the sea level (Post et al., 2018).

- b) After receiving recharge q_{re} , both the water table and the interface elevations change, leading to a new steady-state equilibrium as shown here.

$$H + \Delta H = 40(h + \Delta h)$$

Because $H = 40h$ as shown in part (a) of this solution, it cancels out, leaving only the changes as follows.

$$\Delta H = 40\Delta h$$

The recharge enters only the pore space and not the portion of the aquifer volume occupied by the solid matrix. Thus, the height of the column of water will increase more than the depth of recharge. The total height of the column will increase by an amount equal to the volume of recharge per unit area divided by the porosity. Thus, $(\Delta h + \Delta H) = q_{re}/\theta$ and knowing $\Delta H = 40\Delta h$, Δh and ΔH are as shown here.

$$\Delta h = \frac{q_{re}}{41\theta}$$

$$\Delta H = \frac{40q_{re}}{41\theta}$$

The effective storage coefficient S , defined as the change in fresh-water storage volume per unit area and per unit change in fresh-water head (i.e., water table elevation). Hence, we divide the volume of added water per unit area q_{re} by the change in water table elevation Δh so the effective storage coefficient results as shown here.

$$S = \frac{q_{re}}{\Delta h} = 41\theta$$

This is much larger (41 times!) than the specific yield S_y , equal to drainable porosity θ . It may even be larger than one, even for small values of θ , which is more than the storativity of an open container (e.g., a lake with $\theta = 1$) without any solid matrix components that the water cannot occupy. This effect is due to the “hidden” freshwater storage caused by the much larger movement ΔH of the saltwater interface. Fitts (2013) presents this well. This steady-state evaluation of the head relationships at a freshwater-saltwater interface does not account for the resistance to freshwater and saltwater flow that typically slows down the response of ΔH with respect to that of Δh after recharge events. As a consequence, the discrepancy may be delayed and attenuated in a field setting during transient stages.

- c) With a sea level rise of Δz , nothing changes except the elevation reference datum. That is, both h and H rise by the same amount Δz with respect to the initial sea level. However, if h cannot rise because the water table is already very close to the land surface and its elevation remains limited by surface drainage elements such as springs and stream networks receiving baseflow from the aquifer, then the change Δh of water table elevation with respect to the new sea level is exactly $\Delta h = -\Delta z$. This is because h does not change, while z rises, so the distance of the water table above the sea level decreases by Δz . Since $\Delta H = 40\Delta h$ as shown in part (a) of this solution, this further leads to $\Delta H = -40\Delta z$, meaning that the total thickness of the freshwater lens is reduced by 41 times the amount of sea level rise. This implies that a large amount of fresh groundwater is lost from aquifer storage by outflow at the ground surface through coastal springs and stream baseflow, for example.

[Return to Exercise 6](#) ↗

[Return to where text linked to Exercise 6](#) ↗

Solution Exercise 7 - Constant Head K Tests and Seepage Force

- a) Equation (85) is rearranged to solve for K using $A = D^2\pi/4 = 19.64 \text{ cm}^2$, $\Delta L = 10 \text{ cm}$, and $\Delta h = h_2 - h_1 = -2 \text{ cm}$.

$$K = -\frac{QL}{A\Delta h} = -\frac{10 \frac{\text{cm}^3}{\text{min}} 10 \text{ cm}}{19.64 \text{ cm}^2 (-2 \text{ cm})} = 2.55 \frac{\text{cm}}{\text{min}} \frac{1 \text{ m}}{100 \text{ cm}} \frac{1 \text{ min}}{60 \text{ sec}} = 4.2 \times 10^{-4} \frac{\text{m}}{\text{sec}}$$

The hydraulic gradient is $J = \Delta h / \Delta L = -0.2$. Typically, only the absolute (i.e., positive) value 0.2 is reported.

- b) Equation (74) expresses the frictional force per unit volume as follows.

$$\frac{F_f}{\rho g} = \frac{d\left(\frac{p}{\rho g} + z\right)}{ds} = \frac{dh}{ds} = J$$

Shortening and multiplying by ρg yields the following.

$$F_f = \rho g J$$

To calculate the frictional seepage force on the sand column we multiply F_f by the volume of fluid in the column. The volume of fluid is the volume of the sand column $V = \Delta LA$ multiplied by the porosity θ . Also, $\Delta h / \Delta L$ is substituted for J , and ΔL cancels out.

$$F_f \theta V = F_f \theta \Delta LA = \rho g J \theta \Delta LA = \rho g \frac{\Delta h}{\Delta L} \theta \Delta LA = \rho g \Delta h \theta A$$

Thus, the total frictional force $F_f \theta V$ on the sand column is exactly equal to the pressure force $\rho g \Delta h$ acting on the porous cross-sectional area θA due to the water column of height Δh between h_1 and h_2 , which is responsible for driving flow.

[Return to Exercise 7](#) ↑

[Return to where text linked to Exercise 7](#) ↑

Solution Exercise 8 - Liquefaction and Quicksand Formation

Equation Box 3-7 expresses the critical hydraulic gradient for liquefaction of a sand with grain density ρ_g . In this exercise, the hydraulic gradient $J = -\Delta h/L = -10/10 = -1$, where the negative sign reflects upward flow. Equation Box 3-7 is shown here.

$$J_{cr} = -(1 - \theta) \left(\frac{\rho_g}{\rho_f} - 1 \right)$$

Equation Box 3-7 can be reformulated to determine a critical sand grain density $\rho_{g,cr}$ for a given gradient J .

$$\rho_{g,cr} = \rho_f \left(1 - \frac{J}{1 - \theta} \right)$$

$$\rho_{g,cr} = 1 \frac{\text{g}}{\text{cm}^3} \left(1 - \frac{-1}{1 - 0.25} \right) = \left(1 + \frac{4}{3} \right) \frac{\text{g}}{\text{cm}^3} = 2.33 \frac{\text{g}}{\text{cm}^3}$$

This is slightly less than the typical density of quartz which is 2.65 g/cm^3 , meaning that the quartz sand would not fully liquefy but would have a drastically reduced bearing capacity and drastically reduced threshold for entrainment of sediment into suspension.

[Return to Exercise 8](#) ↑

[Return to where text linked to Exercise 8](#) ↑

Solution Exercise 9 - Unconfined Aquifer and Drought

a) Equation (115) is used to calculate h_{max} .

$$h_{max} = \frac{q_{re}}{2T_K} L^2$$

Substitution of the system parameters with all values converted to units of meters and years produces a maximum head of 40 m.

$$h_{max} = \frac{q_{re} L^2}{2T_K} = \frac{100 \frac{\text{mm}}{\text{yr}} 0.001 \frac{\text{m}}{\text{mm}} \left(5 \text{ km} \frac{1000 \text{ m}}{\text{km}}\right)^2}{2 \left(1 \times 10^{-3} \frac{\text{m}}{\text{sec}} \frac{3600 \text{ sec}}{\text{hr}} \frac{24 \text{ hr}}{\text{day}} \frac{365 \text{ day}}{\text{year}}\right)} \approx 40 \text{ m}$$

This elevation appears to be quite significant with respect to 100 m of aquifer thickness. However, if aquifer thickness represents some average elevation of the water table above the aquifer bottom, then this corresponds to approximately ± 20 percent, which is well within the usual margins of uncertainty for aquifer thickness and certainly hydraulic conductivity. Thus, we consider the approximate assumption of a constant transmissivity as appropriate. With the high plain at an elevation of $d = 50$ m above the rivers, the result indicates that the water table is approximately 10 m below ground surface near the center of the high plain.

b) When a drought starts—during which recharge is effectively zero—the aquifer will sustain baseflow to the rivers at the cost of declining groundwater levels. The steady-state situation for zero recharge is that all groundwater stored above the river elevation has depleted (i.e., $h_{max} = 0$) and baseflow stops sustaining river discharge. The time scale T_{aqu} for h_{max} to significantly change from 40 m to zero may be estimated by Equation (113), giving:

$$T_{aqu} = \frac{SL^2}{T_K} = \frac{0.2 \left(5 \text{ km} \frac{1000 \text{ m}}{\text{km}}\right)^2}{1 \times 10^{-3} \frac{\text{m}}{\text{sec}} \frac{3600 \text{ sec}}{\text{hr}} \frac{24 \text{ hr}}{\text{day}} \frac{365 \text{ day}}{\text{year}}} \approx 160 \text{ yr}$$

The result is on the order of $10^2 = 100$ years and shows that the rivers will continue to receive baseflow even if the drought were to last a few years.

If the size of the aquifer is decreased by 10 times to a distance of 1 km between the rivers, then the time scale for sustaining river baseflow decreases by a factor of 100 as shown here because L is squared in the equation for T_{aqu} .

$$T_{aqu} = \frac{SL^2}{T_K} = \frac{0.2 \left(0.5 \text{ km} \frac{1000 \text{ m}}{\text{km}}\right)^2}{1 \times 10^{-3} \frac{\text{m}}{\text{sec}} \frac{3600 \text{ sec}}{\text{hr}} \frac{24 \text{ hr}}{\text{day}} \frac{365 \text{ day}}{\text{year}}} \approx 1.6 \text{ yr}$$

This is on the order of $10^0 = 1$ years and shows that even seasonal droughts may significantly impact baseflow to the rivers. A closely related discussion is provided in the GW-Project book [Groundwater - Surface Water Exchange](#)[↗] (Woessner, 2020).

[Return to Exercise 9](#)[↗]

[Return to where text linked to Exercise 9](#)[↗]

Solution Exercise 10 - A Dynamic Aquifer Model

a) In this exercise, we compare three methods of solving this problem with decreasing degrees of approximation. In Method 1, recharge is included through the positive term q_{re} in Equation (107)—the recharge is spatially uniform but varies with time. Pumping is included through the negative q_{ex} term, which is temporally constant, but spatially variable in that it occurs only on the line of wells. Specifically, $q_{ex} = 0$ everywhere, except at $y = L/2$, where $q_{ex} = Q_p$ in dimensions of discharge per unit river length.

In this one-dimensional example, the pumping corresponds to a line sink rather than a point well. This is less realistic in practice, but still useful for the conceptual illustration and mathematical implementation of primary interest here. The baseflow contributions (per unit river length) can be directly found from Darcy's law as shown here.

$$Q_1 = T_K \left. \frac{\partial h}{\partial y} \right|_{y=-L}$$

$$Q_2 = -T_K \left. \frac{\partial h}{\partial y} \right|_{y=L}$$

b) In Method 2, we include the variable thickness of the saturated zone by assuming conductivity K is constant and accommodating h_0 in the last term of Equation (110). Subsequently, using the product rule of differentiation, knowing $\partial h_0 / \partial y = 0$, and neglecting $(\partial h / \partial y)^2$ for being the square of a typically small head gradient, we arrive at the following expression.

$$\frac{\partial}{\partial y} \left[K(h + h_0) \frac{\partial h}{\partial y} \right] = K \left[\left(\frac{\partial h}{\partial y} \right)^2 + (h + h_0) \frac{\partial^2 h}{\partial y^2} \right] \approx K(h + h_0) \frac{\partial^2 h}{\partial y^2}$$

Method 3 is an alternative solution that does not depend on the approximation of Method 2 and instead adopts $h_{tot} = h + h_0$, such that the expression can be written as $K/2 \partial^2 h_{tot} / \partial y^2$ similar to Equation (111). Here is an example code implemented in [MATLAB](#) or [Octave](#). [The MATLAB code shown below is provided in a zip file on the web page for this book](#).

```
L = 500;           % aquifer half-width (m)
S = 0.2;          % storage coefficient (-)
TK = 1e-3 * 3600*24*365; % hydraulic transmissivity (m^2/yr)
h0 = 10;          % aquifer thickness (m)
qre = 0.1;        % spatially uniform recharge (m/yr)
seas = 0;         % seasonality in recharge from 0 (constant) to 1 (between 0 and 2*Qre)
Qp = 0;           % pumping rate at y = L/2 (m^3/yr and per m parallel to rivers)

K = TK / h0;
Taq = S * L^2 / TK; % time scale (yr)
hmax = qre * L^2 / (2*TK); % maximum water table elevation (m)

dt = 0.001;      % time step (yr); see Exercise 3 for stability criterion
t = 0:dt:5;      % time vector (yr)

dy = 0.05 * L;  % grid size in y-direction (m)
y = -L:dy:L;    % vector of y-coordinates (m)

h = zeros(size(y)); % initial condition for hydraulic head (Method 1)
```

```

hu = zeros(size(y));           % initial condition for hydraulic head (Method 2)
hdf = h0 * ones(size(y));     % initial condition for hydraulic head (Method 3)
qex = Qp/dy * ones(size(y));  % auxiliary pumping rate vector (m/yr) accounting for dy
p = zeros(size(y));
p(round(0.5*L/dy)) = 1;        % location of pumping at y = L/2
qex = qex .* p;               % pumping rate vector (m/yr)

figure('position',[100 200 1000 250])
subplot(1,3,1)
hold on, box on
xlabel('L (m)'), ylabel('h (m)')

for i = 1:numel(t)

    if mod(2*t(i),1) == 0      % plot two graphs per year
        plot(y,h)
    end

    qret(i) = qre * (1 + seas*sin(2*pi*t(i))); % seasonally variable recharge of mean Qre
    TKu = TK/h0 * (h0 + h(2:end-1));          % variable "unconfined" transmissivity

    h(2:end-1) = h(2:end-1) + ...             % Method 1
        (qret(i) + TK*(h(1:end-2) - 2*h(2:end-1) + h(3:end))/dy^2 - qex(2:end-1))*dt/S;
    hu(2:end-1) = hu(2:end-1) + ...           % Method 2
        (qret(i) + TKu.*(hu(1:end-2) - 2*hu(2:end-1) + hu(3:end))/dy^2 - qex(2:end-1))*dt/S;
    hdf(2:end-1) = hdf(2:end-1) + ...         % Method 3
        (qret(i)+K/2.*(hdf(1:end-2).^2-2*hdf(2:end-1).^2+hdf(3:end).^2)/dy^2-qex(2:end-1))*dt/S;

    hmaxt(i) = max(h);                       % results for constant TK - Method 1
    Q1t(i) = TK * (h(2) - h(1)) / dy;
    Q2t(i) = TK * (h(end-1) - h(end)) / dy;

    hmaxtu(i) = max(hu);                     % results for TK = K(h + h0) - Method 2
    Q1tu(i) = TKu(1) * (hu(2) - hu(1)) / dy;
    Q2tu(i) = TKu(end) * (hu(end-1) - hu(end)) / dy;

    hmaxtdf(i) = max(hdf);                   % results for hdf^2 - Method 3
    Q1tdf(i) = TK * (hdf(2) - hdf(1)) / dy;
    Q2tdf(i) = TK * (hdf(end-1) - hdf(end)) / dy;

end

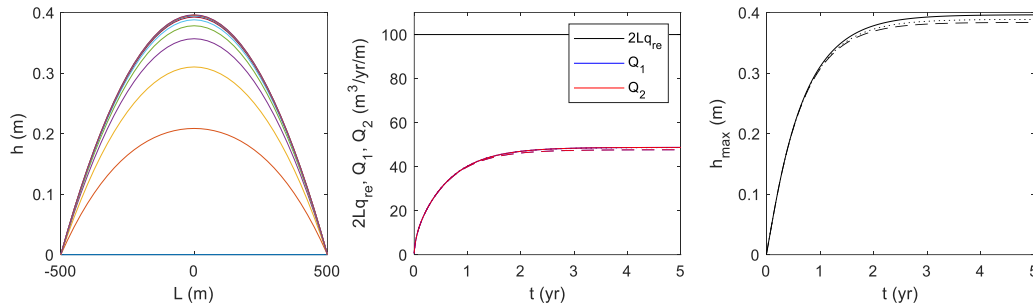
subplot(1,3,2)
hold on, box on
plot(t,2*L*qret,'k-')
plot(t,Q1t,'b-')
plot(t,Q2t,'r-')
plot(t,Q1tu,'b--')
plot(t,Q2tu,'r--')
plot(t,Q1tdf,'b:')
plot(t,Q2tdf,'r:')
legend('2Lq_{re}','Q_1','Q_2')
xlabel('t (yr)'), ylabel('2Lq_{re}, Q_1, Q_2 (m^3/yr/m)')

subplot(1,3,3)
hold on, box on
plot(t,hmaxt,'k-')
plot(t,hmaxtu,'k--')
plot(t,hmaxtdf-h0,'k:')
xlabel('t (yr)'), ylabel('h_{max} (m)')

```

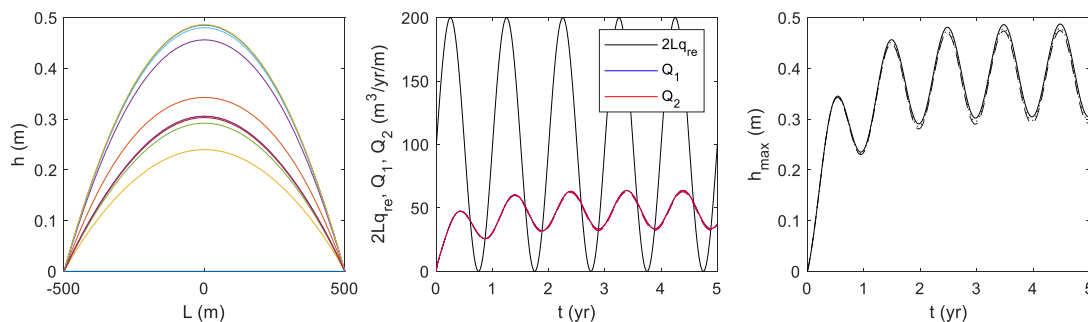
The following figure represents the base case of constant q_{re} and no pumping ($Q_p = 0$) with three charts generated by running the code as given. Time ranges from static initial conditions at time zero to five years when the system is stabilized as shown by the head distribution reaching its maximum in the left panel. For the center and right panel, Methods 1, 2 and 3 are represented by the continuous, dashed, and dotted lines, respectively. In the left panel, h develops as discussed in Section 3.2 and Section 7—by

approaching a parabolic shape toward steady state. The different colors of the graphs represent this temporal evolution every six months. The center panel shows that the total amount of recharge $2Lq_{re}$ is divided evenly between both rivers (blue line covered by red line). The right panel represents the respective growth in the maximum head h_{max} . Both the center and right panels correctly indicate a response-time scale on the order of years. In the center and right panels, the differences between methods in this situation are relatively small and barely visible with results of the most precise method (i.e., Method 3) falling between the simpler methods.



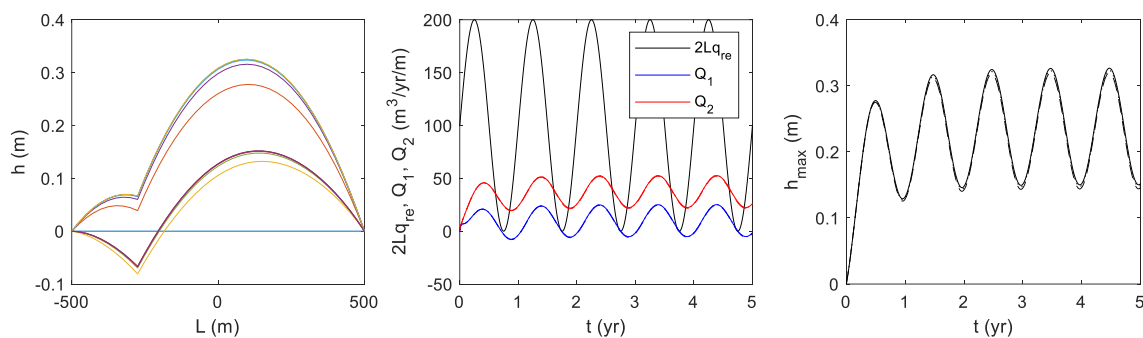
Numerical simulation results without pumping and no climatic seasonality. Methods 1, 2, and 3 are represented in the center and right graphs by the continuous, dashed, and dotted lines, respectively.

The charts in the next figure (*Numerical simulation results without pumping, but with climatic seasonality*) are generated from the code provided in this exercise solution by setting the variable “seas” (for seasonality) from 0 to 1. The recharge variation is shown by the black line in the center panel. In the same center panel, amplitudes of the baseflow discharges are significantly attenuated (smaller) and lag behind the seasonal recharge signal. This is because recharge does not flow directly to the rivers, rather it is temporarily stored in the aquifer resulting in a delay and lower amplitude. Once the cyclic equilibrium is established, the area under the recharge and discharge curves for an annual period are the same. Again, the center and right panels indicate a response-time scale on the order of years, and differences between methods in this situation are relatively small with results of the most precise method (i.e., Method 3) falling between the simpler methods.



Numerical simulation results without pumping, but with climatic seasonality. Methods 1, 2, and 3 are represented in the center and right graphs by the continuous, dashed, and dotted lines, respectively.

For the panels of the next figure (*Numerical simulation results with pumping and climatic seasonality*), Q_p is changed in the code from 0 to 50 m³/yr/m. This breaks the spatial symmetry by creating drawdown at $L = -250$ m. The left panel shows that the pumping is strong enough to reverse the hydraulic gradient next to the left river during parts of the year when recharge is low. This is further indicated by negative values of Q_1 in the center panel during periods when the river on the left is a losing stream. Again, the center and right panels indicate a response-time scale on the order of years, and differences between methods in this situation are relatively small with results of the most precise method (i.e., Method 3) falling between the simpler methods.



Numerical simulation results with pumping and climatic seasonality. Methods 1, 2, and 3 are represented in the center and right graphs by the continuous, dashed, and dotted lines, respectively.

This situation is closely related to discussions in the GW-Project books *Groundwater - Surface Water Exchange* ↗ (Woessner, 2020) and *Groundwater Resources Development: Effects and Sustainability* ↗ (Konikow & Bredehoeft, 2020).

[Return to Exercise 10](#) ↗

[Return to where text linked to Exercise 10](#) ↗

Solution Exercise 11 - Reduced-Order Aquifer Models

a) We start with the equation of continuity, as shown here.

$$\frac{dV}{dt} = Q_{in} - Q_{out} = \Delta y L q_{re} - Q \quad (\text{Equation Solution Exercise 11-1})$$

Substituting $dV = \Delta y L S dh$ and Darcy's law for Q , and dividing by $\Delta y L$, then Equation Solution Exercise 11-1 becomes Equation Solution Exercise 11-2 as the governing differential equation in terms of h .

$$S \frac{dh}{dt} = q_{re} - \frac{T_K h}{L^2} \quad (\text{Equation Solution Exercise 11-2})$$

Expressing h as $QL/(\Delta y T_K)$ from Darcy's law and then substituting Equation Solution Exercise 11-2 leads to Equation Solution Exercise (11-3) as the governing differential equation in terms of Q .

$$\frac{SL}{\Delta y T_K} \frac{dQ}{dt} = q_{re} - \frac{Q}{\Delta y L} \quad (\text{Equation Solution Exercise 11-3})$$

In river baseflow analysis (e.g., Brutsaert, 2005), where measurements of Q are available over time, this equation is used during recession events (i.e., when $q_{re} = 0$) in the form of Equation Solution Exercise 11-4. Data points of $-dQ/dt$ on the y -axis are plotted against those of Q on the x -axis and the recession rate constant $T_K/(SL^2)$ is estimated from the slope of the respective linear regression fit.

$$-\frac{dQ}{dt} = \frac{T_K}{SL^2} Q \quad (\text{Equation Solution Exercise 11-4})$$

To assess the aquifer response-time scale T_{aqu} , we eliminate the forcing effects in Equation Solution Exercise 11-2 by setting $q_{re} = 0$ and non-dimensionalize the remaining equation by adopting the dimensionless variables $h^* = h/h_0$ and $t^* = t/T_{aqu}$. Here, h_0 can be an average aquifer reference head above the river stage and cancels out, yielding Equation Solution Exercise 11-5. By imposing a unit order-of-magnitude to the leading coefficient on the left-hand side (as presented in Box 1), this further results in T_{aqu} as expressed by Equation Solution Exercise 11-6.

$$\frac{SL^2}{T_K T_{aqu}} \frac{dh^*}{dt^*} = h^* \quad (\text{Equation Solution Exercise 11-5})$$

$$T_{aqu} = \frac{SL^2}{T_K} \quad (\text{Equation Solution Exercise 11-6})$$

Equation Solution Exercise 11-6 is exactly the reciprocal of the recession rate constant found in Equation Solution Exercise 11-4 and the same as T_{aqu} obtained in Exercise 9 from the infinite-order model. This demonstrates that the single reservoir model represents a valid and much simpler *first-order approximation* in that it reproduces the correct time scales of change; however, it is not the exact mathematical response function. Given the typical levels of uncertainty related to hydrogeological investigations, such approximations are valid and extremely useful tools. In a more

intuitive way, we may also use Equation Solution Exercise 11-1 with $q_{re} = 0$ in its difference form as in Solution Exercise Equation 11-7.

$$\frac{\Delta V}{\Delta t} = -Q = -\frac{\Delta y T_K h}{L} \quad (\text{Equation Solution Exercise 11-7})$$

Adopting $\Delta V = -S\Delta y L h$ as the drainable volume of water in the aquifer and $\Delta t = T_{aqu}$ as the time scale of full aquifer drainage, we arrive at Equation Solution Exercise 11-8.

$$\frac{S\Delta y L h}{T_{aqu}} = \frac{\Delta y T_K h}{L} \quad (\text{Equation Solution Exercise 11-8})$$

Rearranging we have Equation Solution Exercise 11-9 as the same response-time scale, independent of h .

$$T_{aqu} = \frac{\Delta V}{Q} = \frac{SL^2}{T_K} \quad (\text{Equation Solution Exercise 11-9})$$

- b) Substituting the power functions $V = V_0(h/h_0)^a$ and $Q = Q_0(h/h_0)^b$ into Equation Solution Exercise 11-1 with $q_{re} = 0$ yields Equation Solution Exercise 11-10.

$$V_0 \frac{d\left(\frac{h}{h_0}\right)^a}{dt} = -Q_0 \left(\frac{h}{h_0}\right)^b \quad (\text{Equation Solution Exercise 11-10})$$

Non-dimensionalization using $h^* = h/h_0$ and $t^* = t/T_{aqu}$ as above, results in Equation Solution Exercise 11-11.

$$\frac{V_0}{Q_0 T_{aqu}} \frac{dh^{*a}}{dt^*} = -h^{*b} \quad (\text{Equation Solution Exercise 11-11})$$

Since both h^* and t^* are of unit order magnitude (i.e., $\approx 10^0$) due to the normalization, h^{*a} and h^{*b} are also of unit order magnitude. After setting the leading coefficient to one and substituting for V_0 and Q_0 , this gives Equation Solution Exercise 11-12.

$$T_{aqu} = \frac{V_0}{Q_0} = \frac{S_0 L_0^2}{T_{K,0}} \quad (\text{Equation Solution Exercise 11-12})$$

This shows that T_{aqu} is in general not a constant anymore, because S_0 , L_0 and/or $T_{K,0}$ vary with the chosen reference head h_0 . Consequently, a single characteristic response-time scale no longer exists in this non-linear case (e.g., Kirchner, 2009).

[Return to Exercise 11](#) ↑

[Return to where text linked to Exercise 11](#) ↑

Solution Exercise 12 - Falling Head K Test

- a) The differential form of Equation (98), with V denoting the volume of water in the falling head reservoir, is shown here.

$$\frac{dV}{dt} = Q_{in} - Q_{out}$$

In this expression, $Q_{in} = 0$, $Q_{out} = KA_{col}(h_1 - h_2)/L$ from Darcy's law (with A_{col} being the cross-sectional area of the test column), and $dV = A_{res}dh_1$ is the change of water volume in the reservoir in terms of change dh_1 in water level. Substitution of these items yields the following.

$$A_{res} \frac{dh_1}{dt} = -KA_{col} \frac{h_1 - h_2}{L}$$

Next, we separate variables and integrate.

$$\int \frac{dh_1}{h_1 - h_2} = -\frac{KA_{col}}{LA_{res}} \int dt$$

$$\ln(h_1 - h_2) = -\frac{KA_{col}}{LA_{res}} t + C_1$$

In this expression, C_1 is an integration constant, which is determined from the initial condition that $h_1 = h_0$ at $t = 0$, giving the following.

$$C_1 = \ln(h_0 - h_2)$$

Substituting for C_1 in the solution above and combining the logarithmic terms leads to the following.

$$\ln \frac{h_1 - h_2}{h_0 - h_2} = -\frac{KA_{col}}{LA_{res}} t \quad \text{(Equation Solution Exercise 12-1)}$$

$$h_1(t) = h_2 + (h_0 - h_2)e^{-\frac{t}{T}}$$

In this case, $T = LA_{res}/(KA_{col})$ is the hydraulic response-time scale, over which h_1 declines exponentially from its initial value h_0 toward its final value h_2 . By Darcy's law, this means that Q declines from an initial maximum value toward zero. If an observation of h_1 at a time t is available, then Equation Solution Exercise 12-1 can be reformulated into the following.

$$K = \frac{LA_{res}}{tA_{col}} \ln \frac{h_0 - h_2}{h_1 - h_2}$$

- b) To evaluate K , we substitute the provided falling head test data $L = 10$ cm, $D = 5$ cm, $A_{res} = 100$ cm², $t = 14$ min and $h_1 - h_2 = 0.5(h_0 - h_2)$, that is, h_1 is exactly half-way between its initial and final values.

$$K = \frac{10 \text{ cm } 100 \text{ cm}^2}{14 \text{ min } \pi (2.5 \text{ cm})^2} \frac{1 \text{ m}}{100 \text{ cm}} \frac{1 \text{ min}}{60 \text{ sec}} \ln \frac{1}{0.5} = 0.00042 \frac{\text{m}}{\text{sec}}$$

In practice, multiple measurements of $h_1(t)$ are made and, again based on Equation Solution Exercise 12-1, K can be estimated more robustly as the negative slope of a linear regression relationship $y = -Kx$ where $y = \ln[(h_1 - h_2)/(h_0 - h_2)]$ and $x = tA_{col}/(LA_{res})$.

[Return to Exercise 12](#) ↑

[Return to where text linked to Exercise 12](#) ↑

Solution Exercise 13 - Slug Tests

After withdrawing the initial slug, no more water is added or withdrawn from the top of the well and the only flow entering or leaving the well is discharge Q through the well screen. Consequently, the water balance in terms of volume V inside the well is as shown here.

$$\frac{dV}{dt} = Q$$

Discharge Q is taken positive for flow entering the well (i.e., increasing V). By definition of the problem, the following are true (i.e., with h_1 being the initial head before the slug is withdrawn and also the constant head in the aquifer; and h_2 , the head in the well at a later time). Given that h_1 is constant, $dw = dh_2$.

$$w = h_2 - h_1$$

$$dV = A_{\text{well}} dh_2 = A_{\text{well}} dw$$

$$A_{\text{well}} \frac{dw}{dt} = Q$$

We substitute for Q from Darcy's law in Exercise 13 (i.e., $Q = -F_s K w$) to obtain the following, then separate variables and integrate over w and time t .

$$A_{\text{well}} \frac{dw}{dt} = -F_s K w$$

$$\int \frac{dw}{w} = -\frac{F_s K}{A_{\text{well}}} \int dt$$

$$\ln(w) = -\frac{F_s K}{A_{\text{well}}} t + C_1$$

Using the initial condition that $w = w_0$ at $t = 0$, we find the integration constant $C_1 = \ln(w_0)$ and the solution is as follows.

$$\ln \frac{w}{w_0} = -\frac{F_s K}{A_{\text{well}}} t$$

$$w(t) = w_0 e^{-\frac{t}{T}}$$

From this, the hydraulic response-time scale T , over which w approaches zero, is as follows.

$$T = \frac{A_{\text{well}}}{F_s K}$$

We observe that A_{well} takes the role of A_{res} from Exercise 12. This solution applies to both falling and rising head tests, when w is allowed to be positive and negative, respectively. The initial slug disturbance of magnitude w_0 equilibrates toward its steady-state value of zero at an exponentially decreasing rate. Knowing w/w_0 at a certain time $t > 0$ allows estimating hydraulic conductivity K from the following.

$$K = \frac{A_{well}}{tF_s} \ln \frac{w}{w_0}$$

Similar to the falling head laboratory test discussed in Exercise 12, the calculated K value will be more representative if a sequence of measurements of $w(t)$ are collected. The solution above is repeated here.

$$\ln \frac{w}{w_0} = - \frac{F_s K}{A_{well}} t$$

Given this solution, the negative slope of a linear regression relationship $y = -Kx$, with $y = \ln(w/w_0)$ and $x = tF_s/A_{well}$ can be used to estimate K .

[Return to Exercise 13](#) ↑

[Return to where text linked to Exercise 13](#) ↑

Solution Exercise 14 - Oscillatory Slug Test and Well Friction

- a) We introduce the dimensionless variables $w^* = w/w_0$, $t^* = t/T_w$ and substitute into the final equation presented in Exercise 14 (replicated here). Dividing by g (to bring the final term on the left-hand side to unit order-of-magnitude) yields Equation Solution Exercise 14-1, where w_0 dropped out.

$$z_s \frac{d^2 w}{dt^2} + \left(\frac{8\mu z_s}{\rho R^2} + \frac{gR^2\pi}{KF_s} \right) \frac{dw}{dt} + gw = 0$$

$$\frac{z_s}{gT_w^2} \frac{d^2 w^*}{dt^{*2}} + \left(\frac{8\mu z_s}{\rho g R^2} + \frac{R^2\pi}{KF_s} \right) \frac{1}{T_w} \frac{dw^*}{dt^*} + w^* = 0 \quad (\text{Equation Solution Exercise 14-1})$$

We recognize

- the leading term containing the acceleration $d^2 w^*/dt^{*2}$ as the inertial (oscillation) term,
- the second term containing the velocity dw^*/dt^* as the frictional (damping) term, and,
- the third term, representing elevation w^* , accounting for gravity.

For determining an inertial response-time scale, the frictional term is considered negligible such that the leading coefficient of the first term delivers Equation Solution Exercise 14-2.

$$T_w = \sqrt{\frac{z_s}{g}} \quad (\text{Equation Solution Exercise 14-2})$$

Thus, we arrive at the non-dimensional governing equation as follows.

$$\frac{d^2 w^*}{dt^{*2}} + \left(\frac{8\mu}{\rho R^2} \sqrt{\frac{z_s}{g}} + \frac{R^2\pi}{KF_s} \sqrt{\frac{g}{z_s}} \right) \frac{dw^*}{dt^*} + w^* = 0 \quad (\text{Equation Solution Exercise 14-3})$$

Equation Solution Exercise 14-3 is analogous to Butler (2002), but without specification of different effective inertial and frictional lengths inside the well (both equal to z_s here for simplicity).

- b) We recall from the derivation above that the first term within the parentheses of Equation Solution Exercise 14-3 represents the well friction losses due to viscosity $\mu > 0$, while the second term within the parentheses represents the frictional losses in the aquifer due to Darcy's law and $K < \infty$. Consequently, dividing the second term by the first results in a dimensionless number d_K with large sensitivity to K for $d_K \gg 1$ and the opposite otherwise as shown in Equation Solution Exercise 14-4.

$$d_K = \frac{R^4 \rho g \pi}{8 z_s K F_s \mu} \quad (\text{Equation Solution Exercise 14-4})$$

This is analogous to van der Kamp (1976), with the exception that we consider an instantaneous aquifer response here for simplicity. Assuming example values of $R \approx 10^{-2}$ m, $\mu/\rho \approx 10^{-6}$ m²/s, $g \approx 10^1$ m/s², $8 \approx 10^1$, $z_s \approx 10^1$ m, $K \approx 10^{-6}$ m/s and $F_s \approx 10^0$ m, yields $d_K \approx 10^3$ indicating favorable conditions for conducting a slug test. However, the test may deteriorate if z_s and/or K are larger than assumed. Also favorable is the large sensitivity to the fourth power of well radius R , which is typically several centimeters.

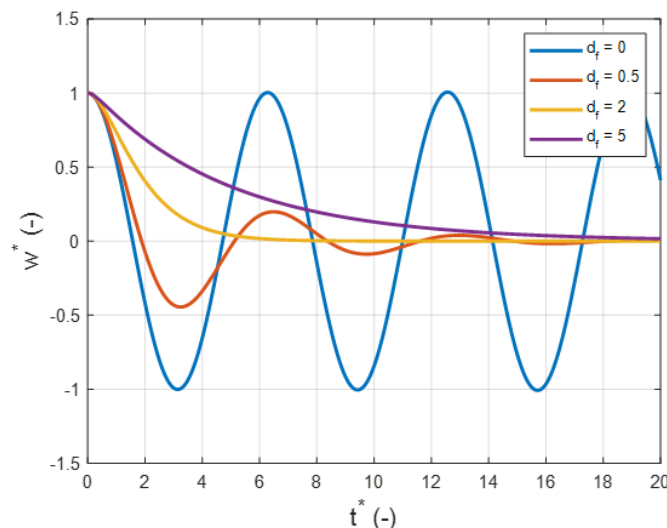
- c) As observed before, the non-dimensional governing Equation Solution Exercise 14-3 accounts for effects of inertia through the acceleration term $d^2 w^*/dt^{*2}$, which is of unit order. Effects of friction in both the aquifer and well are accounted for in the velocity term proportional to dw^*/dt^* , which is also normalized to unit order-of-magnitude. Thus, the relative importance of friction over inertia can be expressed by the dimensionless coefficient as shown in Solution Exercise Equation 14-5.

$$d_f = \frac{8\mu}{\rho R^2} \sqrt{\frac{z_s}{g}} + \frac{R^2 \pi}{K F_s} \sqrt{\frac{g}{z_s}} \quad (\text{Equation Solution Exercise 14-5})$$

Equation Solution Exercise 14-5 can be incorporated in Equation Solution Exercise 14-3 to arrive at Equation Solution Exercise 14-6.

$$\frac{d^2 w^*}{dt^{*2}} + d_f \frac{dw^*}{dt^*} + w^* = 0 \quad (\text{Equation Solution Exercise 14-6})$$

The results of evaluating Equation Solution Exercise 14-6 for different values of d_f are shown in the following figure (*Under and overdamped solutions of Equation Solution Exercise 14-6 for different values of d_f*).



Under and overdamped solutions of Equation Solution Exercise 14-6 for different values of d_f .

For $d_f = 0$, there is no damping by friction and the result is a perfectly sinusoidal oscillation. As d_f grows, the oscillations are increasingly attenuated and above some limiting value of d_f the oscillations completely disappear. For very large values of d_f , the solution approaches the exponential form found in Exercise 13. Mathematically, this can be determined by eliminating the effects of inertia from the equation in Exercise 14 (shown below as Equation Solution Exercise14-7) by setting both m and dm/dt to zero, while substituting for F_g , F_f (if relevant) and F_p as before.

$$-F_g - F_f + F_p + v_{rel} \frac{dm}{dt} = m \frac{dv_{mean}}{dt} \quad (\text{Equation Solution Exercise 14-7})$$

In the absence of inertia, the definition of T_w in Equation Solution Exercise 14-1 becomes meaningless. Instead, a frictional response-time scale may be defined by neglecting the inertial term in Equation Solution Exercise 14-1, which leads back to the solution of Exercise 13.

One way to interpret an oscillatory slug test is to determine the value of d_f in Equation Solution Exercise 14-6, which gives the best fit to the observations of normalized displacement $w^* = w/w_0$ as a function of normalized time $t^* = t/T_w$. Hydraulic conductivity K may then be estimated by inverting Equation Solution Exercise 14-5 to solve for K with all other parameters known. This is the fundamental principle for the interpretation of oscillatory slug tests, but many variants and complicating factors exist in practice. Butler (2020) provides more information in his comprehensive textbook on slug tests.

When neglecting frictional losses inside the well, the non-dimensional damping factor d_f from Equation Solution Exercise 14-5 becomes Equation Solution Exercise 14-8.

$$d_f = \frac{R^2 \pi}{KF_s} \sqrt{\frac{g}{z_s}} = \frac{R^2 \pi}{KF_s T_w} \quad (\text{Equation Solution Exercise 14-8})$$

This confirms that conditions for oscillatory slug responses are most favorable in deep high-conductivity formations, where large z_s (large mass of water inside well) and large K (high flow velocity) lead to a strong influence of inertia and correspondingly small values of d_f . This expression further illustrates that oscillations can only happen at a time scale T_w above some minimum threshold. Otherwise, d_f would be too large resulting in an overdamped (non-oscillating) response.

- d) From the oscillating solutions for w^* presented in the figure included in this solution exercise (*Under and overdamped solutions of Equation Solution Exercise 14-6 for different values of d_f*), we observe that the flow velocity inside the well fluctuates between zero and its maximum absolute value over a time scale on the order of $10^0 = 1$ dimensionless

time unit. This was to be expected from the normalization adopted and in dimensional time, it corresponds to T_w on the order of seconds (i.e., $T_w \approx 10^0$ s from Equation Solution Exercise 14-2, when using typical well depths z_s on the order of 10^1 to 10^2 m).

In contrast, Equation (49) with typical values of $R \approx 10^{-2}$ m and $\mu/\rho \approx 10^{-6}$ m²/s delivers an estimate of a time scale $T_{vis} \approx 10^2$ s for the laminar flow profile inside the well to develop. For the assumption of a fully developed laminar flow profile to hold, $T_{vis} \ll T_w$ would be required, which cannot be expected to be the case from this order-of-magnitude analysis. However, this is only a concern if frictional losses inside the well are not negligible (i.e., when d_K from Equation Solution Exercise 14-4 is not large enough).

In summary, frictional losses inside the well may be safely neglected, when $d_K \gg 1$ and the question of a fully developed flow profile does not even arise. If this condition is not met, then a response-time scale T_w of a slug test may be estimated from observed data. For oscillatory responses, this would be approximately a quarter or half period of fluctuation, while for overdamped responses this would be the time scale for w to return near zero.

A dimensionless number $T_w/T_{vis} \gg 1$ then indicates that the fully developed flow profile develops much faster than the flow velocity changes, and Equation (46) is appropriate, as assumed in this exercise. In the opposite case, when $T_w/T_{vis} \approx 1$ or smaller, this assumption is not justified and a more complex theoretical model (non-stationary flow profile) or experimental setup (e.g., including pressure measurements inside the well screen) are required, as discussed by Quinn et al. (2018).

[Return to Exercise 14](#) ↑

[Return to where text linked to Exercise 14](#) ↑

12 References

- Bear, J. (1972). *Dynamics of fluids in porous media*. Dover Publications.
- Biot, M. A. (1941). General theory of three-dimensional consolidation. *Journal of Applied Physics*, 26(2), 155–164. <https://doi.org/10.1063/1.1712886>.
- Bird, R. B., Stewart, W. E., & Lightfoot, E. N. (1960). *Transport phenomena*. Wiley.
- Brutsaert, W. (2005). *Hydrology: An introduction*. Cambridge University Press. <http://dx.doi.org/10.1017/CBO9780511808470>.
- Butler, J. J. (2002). A simple correction for slug test in small-diameter wells. *Groundwater*, 40(3), 303–307. <http://doi.org/10.1111/j.1745-6584.2002.tb02658.x>.
- Butler, J. J. (2020). *The design, performance, and analysis of slug tests* (2nd ed.). <http://doi.org/10.1201/9780367815509>.
- Cohen, A. J. B., & Cherry, J. A. (2020). *Conceptual and visual understanding of hydraulic head and groundwater flow*. The Groundwater Project. <https://gw-project.org/books/conceptual-and-visual-understanding-of-hydraulic-head-and-groundwater-flow/>.
- Corey, A. T. (1994). *Mechanics of immiscible fluids in porous media*. Water Resources Publications. <https://gw-project.org/books/mechanics-of-immiscible-fluids-in-porous-media/>.
- Cuthbert, M. O., Gleeson, T., Moosdorf, N., Befus, K. M., Scheider, A., Hartmann, J., & Lehner, B. (2019). Global patterns and dynamics of climate-groundwater interactions. *Nature Climate Change*, 9, 137–141. <https://www.nature.com/articles/s41558-018-0386-4>.
- Devlin, J. F. (2021). *Groundwater velocity*. The Groundwater Project. <https://gw-project.org/books/groundwater-velocity/>.
- Dullien, F. A. L. (1979). *Porous media: Fluid transport and pore structure*. Elsevier.
- Fitts, C. R. (2013). *Groundwater science* (2nd ed.). Elsevier.
- Forchheimer, P. (1901). Wasserbewegung durch den Boden [Water movement through the soil]. *Zeitschrift des Vereines deutscher Ingenieure*, 45(50), 1781–1788.
- Freeze, R. A., & Cherry, J. A. (1979). *Groundwater*. The Groundwater Project. <https://gw-project.org/books/groundwater/>.
- Gambolati, G. & Teatini, P. (2021). *Land subsidence and its mitigation*. The Groundwater Project. <https://gw-project.org/books/land-subsidence-and-its-mitigation/>.
- Haitjema, H. M., & Mitchell-Bruker, S. (2005). Are water tables a subdued replica of the topography? *Groundwater*, 43, 781–786. <https://doi.org/10.1111/j.1745-6584.2005.00090.x>.

- Hubbert, M. K. (1940). The theory of ground-water movement. *The Journal of Geology*, 48(8), part 1, 785–944. <https://www.jstor.org/stable/30057101>. ↗
- Hubbert, M. K. (1957). Darcy's law and the field equations of the flow of underground fluids. *Hydrogeological Science Journal*, 2(1), 23–59. <https://doi.org/10.2118/749-G>. ↗
- Hvorslev, M. J. (1951). Time lag and soil permeability in groundwater observations. *Bulletin of the U.S. Army Corps of Engineers, Waterways Experiment Station*, 36. https://www.csus.edu/indiv/h/hornert/geol_210_summer_2012/Week%203%20readings/Hvorslev%201951.pdf. ↗
- Jeng, D. S. (2013). *Porous models for wave-seabed interactions*. Springer.
- Jeng, D. S. (2018). *Mechanics of wave-seabed-structure interactions*. Cambridge University Press.
- Jiao, J. & Post, V. (2019). *Coastal hydrogeology*. Cambridge University Press. <https://doi.org/10.1017/9781139344142>. ↗
- Kirchner, J. W. (2009). Catchments as simple dynamical systems: Catchment characterization, rainfall-runoff modeling, and doing hydrology backward. *Water Resources Research*, 45(2). <https://doi.org/10.1029/2008WR006912>. ↗
- Konikow, L. F., & Bredehoeft, J. D. (2020). *Groundwater resources development: Effects and sustainability*. The Groundwater Project. <https://gw-project.org/books/groundwater-resource-development/>. ↗
- Kueper, B. H., & Frind, E. O. (1991). Two-phase flow in heterogeneous porous media: 1. Model development. *Water Resources Research*, 27(6), 1049–1057. <https://doi.org/10.1029/91WR00266>. ↗
- Poeter, E. P., & Hsieh, P. (2021). *Graphical construction of groundwater flow nets*. The Groundwater Project. <https://gw-project.org/books/graphical-construction-of-groundwater-flow-nets/>. ↗
- Poeter, E. P., Fan, Y., Cherry, J. A., Wood, W., & Mackay, D. (2020). *Groundwater in our water cycle*. The Groundwater Project. <https://gw-project.org/books/groundwater-in-our-water-cycle/>. ↗
- Post, V. E. A., Houben, G. J., & van Engelen, J. (2018). What is the Ghijben-Herzberg principle and who formulated it? *Hydrogeology Journal*, 26, 1801–1807. <https://doi.org/10.1007/s10040-018-1796-0>. ↗
- Post, V. E. A., & Simmons, C. T. (2022). *Variable-density groundwater flow*. The Groundwater Project. <https://gw-project.org/books/variable-density-groundwater-flow/>. ↗
- Quinn, P. M., Klammler, H., Cherry, J. A., & Parker, B. L. (2018). Insights from unsteady flow analysis of underdamped slug tests in fractured rock. *Water Resources Research*, 54, 5825–5840. <https://doi.org/10.1029/2018WR022874>. ↗

- Richards, L. A. (1931). Capillary conduction of liquids through porous mediums. *Physics*, 1(5), 318–333. <https://doi.org/10.1063/1.1745010>.
- Snow, D.T. (1969). Anisotropic permeability of fractured media. *Water Resources Research*, 5(6), 1273-1289. <https://doi.org/10.1029/WR005i006p01273>.
- Terzaghi, K. (1925). *Erdbaumechanik auf bodenphysikalischer Grundlage* [Earthwork mechanics based on soil physics]. Franz Deuticke, Vienna.
- Thiem, G. (1906). *Hydrologische Methoden* [Hydrological methods]. Gebhardt, Leipzig.
- van der Kamp, G. (1976). Determining aquifer transmissivity by means of well response tests: The underdamped case. *Water Resources Research*, 12(1), 71–77. <https://doi.org/10.1029/WR012i001p00071>.
- Wang, H. F. (2020). *Groundwater storage in confined aquifers*. The Groundwater Project. <https://gw-project.org/books/groundwater-storage-in-confined-aquifers/>.
- Woessner, W. W. (2020). *Groundwater - surface water exchange*. The Groundwater Project. <https://gw-project.org/books/groundwater-surface-water-exchange/>.
- Woessner, W. W., & Poeter, E. P. (2020). *Hydrogeologic properties of earth materials and principles of groundwater flow*. The Groundwater Project. <https://gw-project.org/books/hydrogeologic-properties-of-earth-materials-and-principles-of-groundwater-flow/>.

13 Basic Notations

a	=	acceleration (L^1T^{-2})
A	=	cross-sectional area transverse to flow direction (L^2)
B	=	half-width between flat plates (L)
C_1 and C_2	=	integration constants
C_m	=	soil moisture capacity (L^{-1})
d	=	topographic elevation (L)
d_K, d_f	=	slug test parameters (-)
E	=	kinetic energy ($M^1L^2T^{-2}$)
f_{col}	=	Coulomb friction factor (-)
f_{sto}	=	Stokes drag coefficient (MT^{-1})
F	=	force or force per volume in general ($M^1L^1T^{-2}$ or $M^1L^{-2}T^{-2}$)
F_S	=	well screen shape factor (L)
g	=	acceleration of gravity (L^1T^{-2})
h	=	hydraulic head (L)
J	=	hydraulic gradient (-)
J_{cr}	=	critical hydraulic gradient (-)
K	=	hydraulic conductivity (L^1T^{-1})
k	=	intrinsic permeability (L^2)
$k_{r,w}$ and $k_{r,n}$	=	relative permeability factors for water and NAPL (-)
L	=	length or length scale in general (L)
M	=	linear momentum ($M^1L^1T^{-1}$)
m	=	mass (M)
n	=	coordinate perpendicular to flow direction (L)

p	=	pressure ($M^1L^{-1}T^{-2}$)
p_c	=	capillary pressure difference ($M^1L^{-1}T^{-2}$)
q	=	specific discharge or Darcy flux (LT^{-1})
q_{re}	=	groundwater recharge (LT^{-1})
q_{ex}	=	groundwater extraction (LT^{-1})
Q	=	volumetric discharge or flow rate (L^3T^{-1})
Q_{in}	=	inflow (L^3T^{-1})
Q_{out}	=	outflow (L^3T^{-1})
r	=	radial coordinate (L)
R	=	radius of sphere or pipe (L)
R_K	=	hydraulic resistance (TL^{-2})
s	=	coordinate in flow direction (L)
S	=	storage coefficient (-)
S_s	=	specific storage (L^{-1})
S_y	=	specific yield or drainable porosity (-)
t	=	time (T)
T	=	response-time scale (T)
T_K	=	aquifer transmissivity (L^2/T)
v	=	velocity (L^1T^{-1})
w	=	water level deviation inside a well during a slug test (L)
W	=	water table ratio (-)
x, y, z	=	Cartesian coordinates (L)
Δh	=	change in hydraulic head over some distance (L)
Δt	=	time interval (T)

ΔV	=	change in fluid volume (L^3)
θ	=	porosity (-)
θ_w	=	fraction of a medium's bulk volume that is filled with water (-)
θ_n	=	fraction of a medium's bulk volume that is filled with NAPL (-)
μ	=	dynamic viscosity ($M^1L^{-1}T^{-1}$)
ρ	=	density (M^1L^{-3})
σ'	=	vertical effective stress in sediment ($M^1L^{-1}T^{-2}$)
τ	=	shear stress between adjacent fluid laminae ($M^1L^{-1}T^{-2}$)

14 About the Author



Harald Klammler received his diploma and doctoral degrees from Graz University of Technology, Austria, while spending significant exchange and research periods at the University of Granada, Spain, and the University of Florida, USA. For almost 20 years, he was a visiting scientist and professor in the USA and Brazil with scholarships from the Austrian Academy of Sciences, the Austrian Science Fund, and the Brazilian National Science Foundation. He now holds a permanent position at the Institute of Geosciences at the Federal University of Bahia, Brazil, where he teaches groundwater-related subjects. His research interests focus on the physical aspects of groundwater science including flow and transport at local scales but also other hydrological processes at the aquifer and catchment scales.

Please consider signing up to the GW-Project mailing list to stay informed about new book releases, events and ways to participate in the GW-Project. When you sign up for our email list it helps us build a global groundwater community. [Sign up](#)[↗].



Modifications to Original Release

Changes from the Original Version to Version 2

Original Version: November 21, 2023, Version 2: November 22, 2023

Page numbers refer to the original PDF.

page i, added Version 2

page 111-112, figure caption was moved from top of page 112 to bottom of page 111